2005:296 CIV

MASTER'S THESIS

UAV Tracking Device using 2.4 GHz Video Transmitter

Jonas Gustafsson
Fredrik Henriksson

Luleå University of Technology

MSc Programmes in Engineering

Department of Computer Science and Electrical Engineering
Division of EISLAB

2005:296 CIV - ISSN: 1402-1617 - ISRN: LTU-EX--05/296--SE

Abstract

The purpose of this thesis was to automatically track an Unmanned Aerial Vehicle (UAV), with an electronically steered antenna.

To make it possible to track the UAV during flights, a 2.4 GHz transmitter was mounted on the aircraft. Due to the regulations of transmitted signal power and the fact that a very powerful transmitter would consume to much power, a 10 mW transmitter was used during development. With such a weak transmitter a high gain antenna (a reflector antenna in this case) is required, in the receiver, to detect the transmitted signal at far distances. To be able to detect movement of the UAV, four small Yagi[1]-antennas are mounted around the focal point of the reflector disc antenna. The received signal strength in the four Yagi-antennas will vary depending on where the transmitter (UAV) is located relative to the tracking device. By comparing the strength of these signals using a microcontroller, the direction of the UAV can be computed and in turn the antenna can be made to track the UAV.

To detect the strength of the signals, four Linear Technology® 5534 power detector chips were used. These chips produce a linear DC voltage output corresponding to the received RF signal strength. The DC outputs of the power detectors are connected to the A/D inputs of the microcontroller (in this case a Microchip PIC16F877). The levels are evaluated, and the antenna motors are driven in the necessary direction.

A great deal of time was also spent on the mechanical design, as it had to be very strong but also collapsible to fit into a car trunk. All details were drafted in IronCAD®[2] before production in the ECSE[3] mechanical workshop.

The project was very successful; test flights were made on distances up to ~1km with good results. With minor adjustments in the power detectors, tracking of the UAV would be possible at even greater distances.

[1] Antenna made of several elements (described further in chapter 4.2)
[2] 3D CAD (http://www.ironcad.com)
[3] Department of Electrical and Computer System Engineering

Preface

This Master Thesis is the last part of our Master of Science program at Luleå University of Technology (LTU). The project was developed at the Department of Electrical and Computer Systems Engineering (ECSE) at Monash University in Melbourne, Australia.

LTU has collaboration with Monash University and every year students and staff from the Universities can go on exchange. The ECSE department has several on-going projects done by both staff and students. Our project was to develop and construct a tracking device to track UAVs using an onboard mounted video transmitter.

We would like to thank:

Our supervisor Mr. Stewart Jenvey, for helping us with antenna design problems and other helpful ideas regarding the project.

Mr. Sven Molin, for helping us organize our stay in Australia.

Mr. Anthony “Tony” Brosinsky and Mr. Morris C. Gay, for all the advices, mechanical expertise and help with the mechanical construction.

Mr. Ian Reynolds, for helping us with the PCB milling machine, and all the support when things had gone badly.

Mr. Ray Cooper, for component support.

Mr. Nathan Sneed at Soanar (http://www.soanar.com.au) in NSW for giving us samples of the Linear Technology 5534 power detecting chip.

MuRata, Netherlands, for supplying us with free chip filter samples and surface mount development kit.

Johansson Technology, for supplying us with free chip filters samples.

Content

1 Introduction

1.1 Background

The purpose of this assignment was to make a motor driven reflector antenna automatically track an UAV with an onboard mounted 2.4 GHz video transmitter. This was done for one reason, to be able to transmit the video signals from the UAV down to ground in real time. One possible task for an application like this would be to fly an UAV over dangerous areas like flooded areas and forest fires, and from a safe distance observe what the area looks like.

Until present, the people in the UAV group at Monash have tracked the plane by pointing the reflector antenna manually. This can be very difficult at longer distances, when the plane is hard to see with the bare eye.

Earlier, there have been experiments to steer the reflector antenna with GPS[4] coordinates of the plane. A drawback with that method is that the civil GPS system has limitation in accuracy, there is also a delay in time from the moment the UAV transmits its coordinates until the motors actually steers the antenna towards the given coordinates. So a new way of approach was needed.

1.2 Briefly about the system

Another approach to solve the problem of tracking UAV´s can be done as followed. To pick up the transmitted 2.4 GHz signal from the UAV, a high gain reflector antenna from Hills Industries was used.

When a reflector disc like this is aligned with a transmitter, the focal point will be located right in front of the antenna, but when the transmitter moves of out of line, the focal point will move in the opposite direction of the transmitter. This fact is used to track the UAV.

For each plane (horizontal and vertical), two small Yagi-antennas placed at a short distance from the theoretical focal point of the reflector antenna. Depending on the movement of the UAV, the signal strengths at the Yagi antennas will differ. Based on this the reflector disc can be steered to reduce these differences and hence make the disc point towards the UAV. When differences occur in the Yagi-antennas a microprocessor quickly responds by comparing these signals, and depending on the differences in signal strength, the microprocessor controls the motors to steer the reflector antenna to the right position. This means that the focal point always be located somewhere between the four detecting Yagis.

The interface between the Yagi antennas and the microprocessor A/D[5] inputs is a high-performance logarithmic RF[6] detector chip from Linear Technology, LT5534. This chip converts the RF signal strength into a DC level that is usable for the microprocessor. See Figure 1.1 for an overview of the system.

[4] Global Positioning System
[5] Analog to Digital conversion
[6] Radio Frequency, any frequency within the electromagnetic spectrum associated with radio wave propagation.

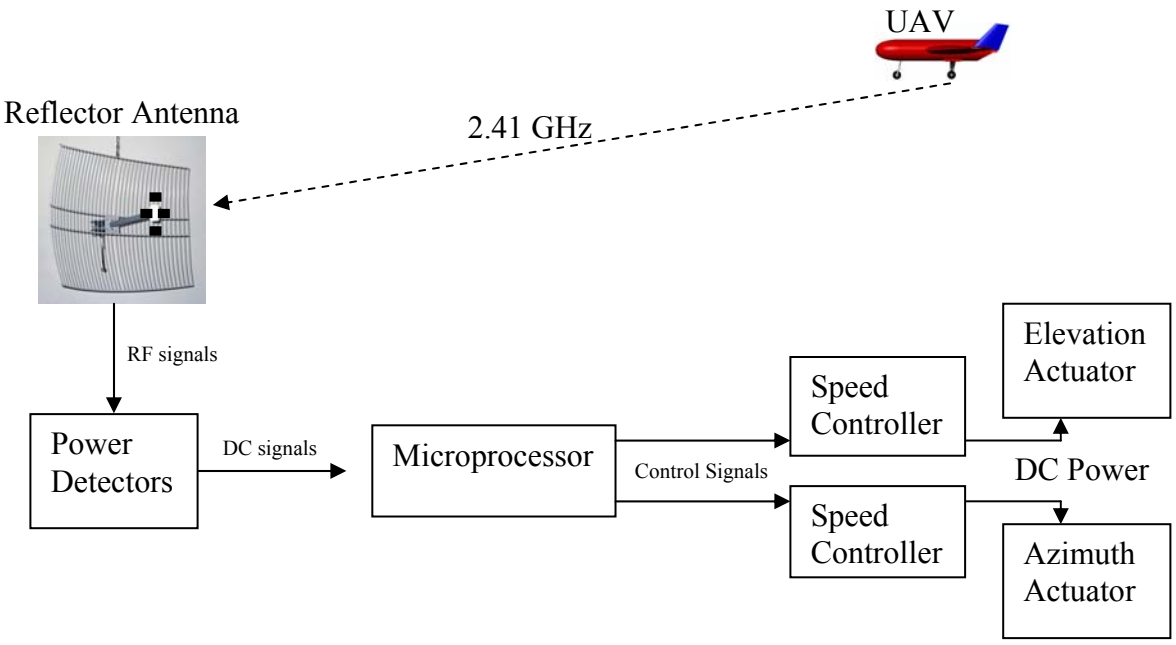

Figure 1.1: *System overview.*

2 Research

When we started our thesis work at Monash, the method of detecting the transmitted signal was not specified, the only part we new we were supposed to use were the Hills Industries reflector antenna. The other parts were up to us to choose.

2.1 Antennas

The use of Yagi antennas were not the only option, both Patch and Helix antennas were thought of and discussed with our supervisor Mr. Jenvey. After further investigation the use of patch antennas proved to be improper to use, as they would block too much of the incoming radiation and hence decrease the gain of the reflector antenna. Helix antennas were the backup option to choose if the Yagi antennas would not have worked out.

2.2 Power Detection

This was the part of the project that demanded the most research. In the beginning of the project, different ways of detecting and comparing RF signals were discussed with our supervisor. The outcome of the discussions was to look through different chip manufactures range of chips that might be useful to this application. This appeared to be a quite big task, as there is a lot of different manufactures with a lot of chips.

Over two weeks of time were spent on searching suitable detecting chips. Finally Analog Devices, Maxim and Linear Technology all seemed to have suitable power detector chips with a so called RSSI[7] output, for sale. All these companies were contacted and requested to send samples of their chips, this seemed to be a big problem, as no samples arrived. Finally we got in touch with Mr. Nathan Sneed at Soanar in NSW which is a retailer of Linear Technology. Mr. Sneed supplied us with two samples of the LT5534 power detector chip (see chapter 5.4 for more details) and the corresponding evaluation board. He also supplied us with 4 new samples for the final design in a later stage of the project.

2.3 Filters

A lot of web research was also done regarding filters and what type of filter to use. Several filter producing companies, like Toko, Murata and Johansson Technology were contacted regarding samples of 2.45 GHz bandpass filters. We managed to get filter samples from both MuRata (through their office in the Netherlands) and Johansson Technology, but no filters from ToKo were received.

2.4 Micro processor

The use of the PIC16F877 was not either determined at the start of the project, but as a processor and a development system were available, no further research was done to find a suitable processor.

[7] Received Signal Strength Indicator

3 Mechanical design

An existing mechanical construction from an earlier project was available and was from the beginning meant to be used in this project as well. But after some tests, the conclusion was that a new more rigid construction had to be built.

As the antenna of this system has to be capable to move with very small steps with high accuracy to keep track of the UAV at far distances, the mechanic solution has to be very solid to avoid glitching and slack.

Based on these facts we set up the design of our mechanic solution. The drawings for the different mechanical parts were drawn in IronCAD and then handed over to the ECSE mechanical workshop for manufacturing.

3.1 Design considerations

The specifications for the UAV tracking device has been set by the UAV group at Monash University. These were the main considerations that had to be taken in to calculation.

- **Speed**
  The system has to be able to track a UAV flying at 20 m/s at a distance of 100 m.
- **Resolution**
  The system has to be able to move with steps of 1 degree, to keep track of the UAV at long distance.
- **Portability**
  The system needs to fit in a regular car trunk for transportation.

With these considerations in mind together with a more or less non-existing budget, the mechanical design was not an easy task. A 3D model of the final assemble can be seen in Figure 3.1.

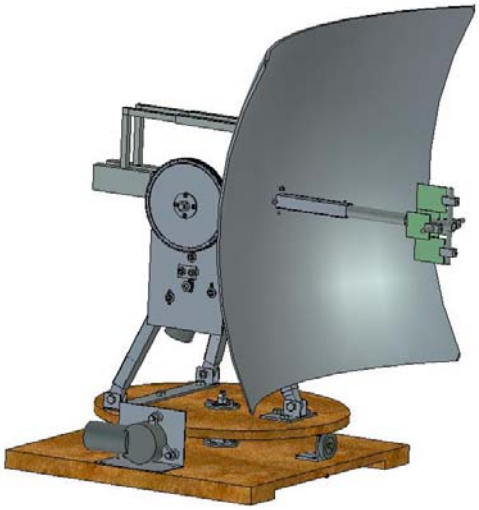

Figure 3.1: *Complete assemble.*

3.2 Mechanical parts

Here follows a description of the main parts, see appendix A1 for detailed drawings.

3.2.1 Horizontal Rotator

By adjusting the pressure on the centre bolt, the pressure on the support wheels and the drive wheel can be adjusted so the drive wheel won't slip. This method of transmission might not be the best in the long run, because rubber tends to lose the grip with time. A better way of doing it could be to mount a cogged circle under the wooden disc, and a small cogwheel on the motor, or use a belt drive similar to the transmission used in the vertical plane (described in section 3.2.3).

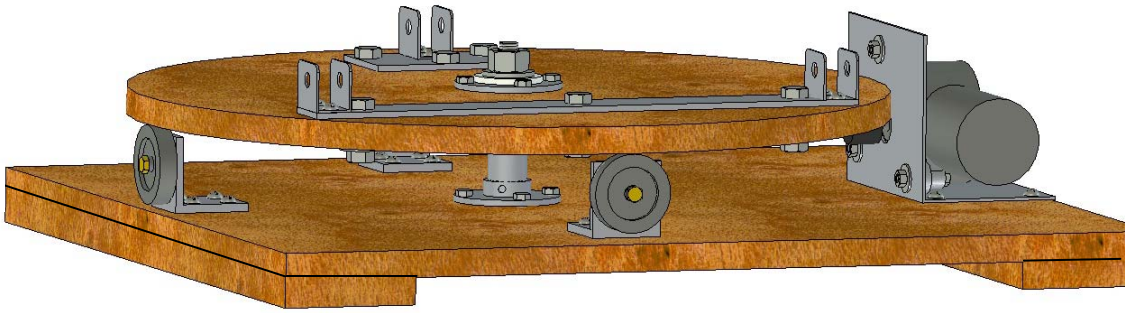

Figure 3.2: *Horizontal rotator.*

The bottom plate (base) is made of 18 mm thick particle board and is 560 x 600 mm^2. Two 10 mm holes, one in the centre of the base and one in centre of the rotating disc, were drilled for the ground, video and control cables that are needed to steer the horizontal motor and to get the video signal out. Four 8 mm holes were also drilled to hold the bolts for the middle support pole. Two 90 mm wide boards were attached along the shorter side of the main board to get some spacing for the cables coming out of the middle hole.

Three wheels of plastic with rubber surface were mounted on to aluminum angles and attached to the bottom plate with regular wooden screws. The wheels were mounted at a distance of 230 mm from the centre hole on the bottom plate like shown in Figures 3.2 and 3.6. The wheels and aluminum angles were found in the ECSE workshop, and were probably parts that were left over from earlier projects, but they worked fine for us.

A simplified model of the motor was made in IronCAD, and a bracket designed to hold it. The bracket was made out of 3 mm folded aluminum, see (1) in Figure 3.6 for a good view.

Middle stem:

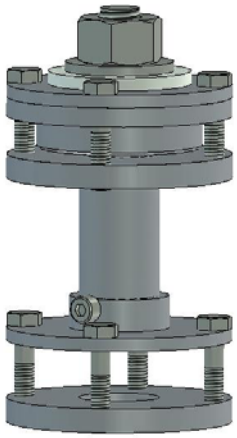

The middle stems function is to centre the rotating disc on the central hole in the base plate. The stem was built up of several parts as can be seen in Figure 3.3 to the left. All parts are made of aluminum except the slightly brighter washer on the top, which is made out of nylon to decrease the friction while rotating. The stem can be separated in to two major parts, one upper (rotating) and one lower (fixed). The upper one was bolted on to the big rotating disc, and the lower one was bolted on to the base plate.

Figure 3.3: *Middle stem.*

Lower part:

In the Figure 3.4 to the right, the three parts that creates the lower part of the middle stem can be viewed separately.

The top part to the right supports the bearing house of the upper part of the middle stem, described on the next page. At the top it was threaded with M12 thread, so it can be tightened on to the big disc and avoids wheel slippage. There is also a hole straight through all of these parts so signal cables that needs to be taken of the rotating part of the stand, can go through.

The middle part was tightened on the base plate with 4 bolts that are screwed in to the threaded holes in the bottom part.

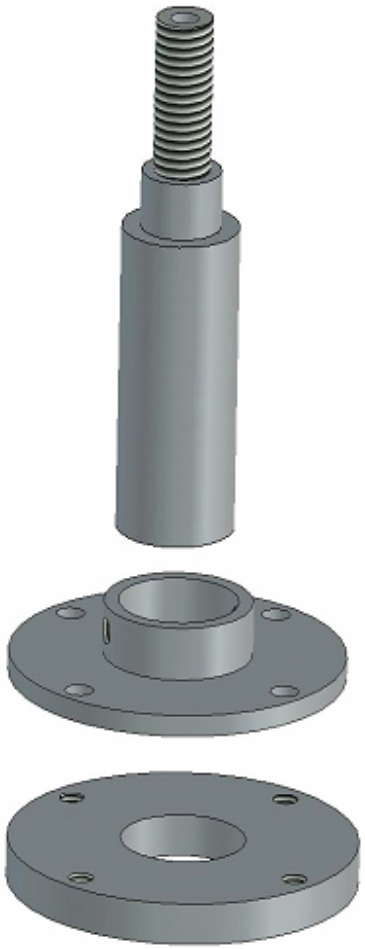

Figure 3.4: *Middle stem, lower part.*

Upper part:

The upper part of the mid stem (seen in Figure 3.5) consists of three custom made parts and one ball bearing.

The middle stem goes up through the two lower parts of this construction and stops on the ball bearing. The threaded part goes thru the top washer, and a nut can be tightened on top with a nylon washer between the nut and the aluminum washer. This nylon washer reduces the friction between the nut and the aluminum washer when the horizontal disc is turning.

All of these parts are then tightened together with four M6 bolts around the main disc (se Figure 3.8).

Figure 3.5: *Middle stem, upper part.*

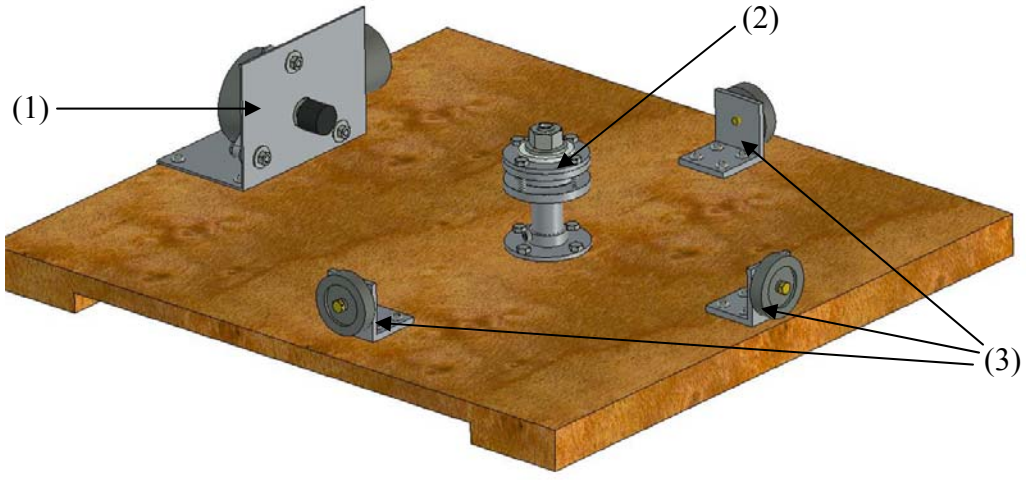

Figure 3.6: *Complete base,*
(1): Motor with bracket, (2): Mid stem, (3): Support wheels.

The disc that will hold the stand was made of 18 mm particle board. The centre of the disc was milled out, as can be seen in Figure 3.7, to make the upper part of the mid stem fit into the disc.

Figure 3.7: *Main rotating disc.*

To make a solid base for the stand two steel plates (1) in Figure 3.8 were constructed to hold the brackets (2) which in turn hold the legs. The reason why these plates were constructed is to decrease the force on the leg-brackets. When the device is folded together, these brackets work like joints. If a bolt that holds together the bracket with the leg is not proper released when folding, the force on the bracket will be quite big. If the brackets would be screwed directly into the particle board by wood-screws, there might be a risk that the wood- screws would crack out of the board. This is why the brackets are mounted on a bigger steel plate with bolts, and the plates in turn are mounted with bolts on the disc.

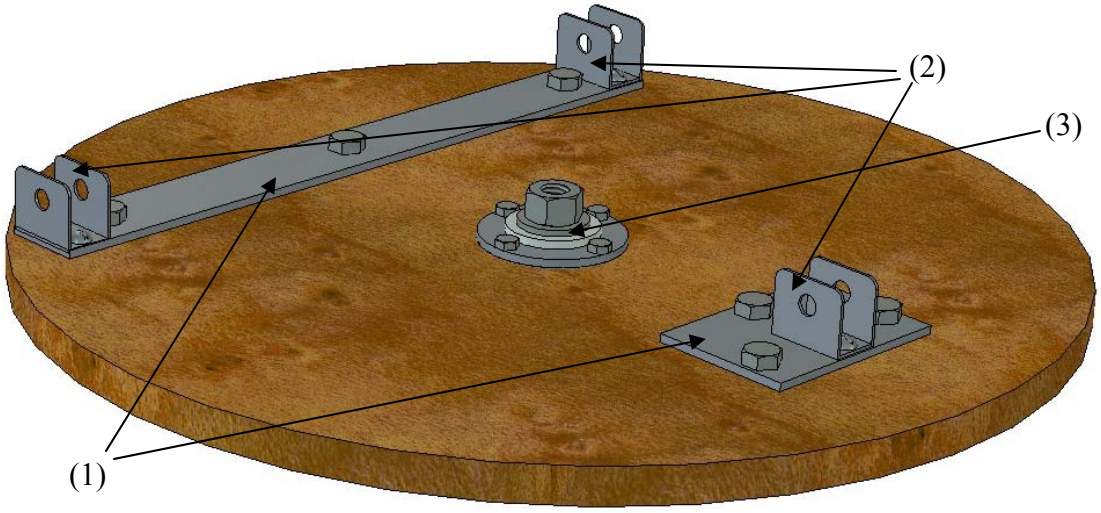

Figure 3.8: *Main disc,*
(1): Steel plates, (2): Leg brackets, (3): Upper part of centre stem.

3.2.2 Antenna stand

The antenna stand has to be very strong and solid but still need to be collapsible so higher portability can be achieved. With these considerations in mind we designed a 3 legged stand, as seen in Figure 3.9.

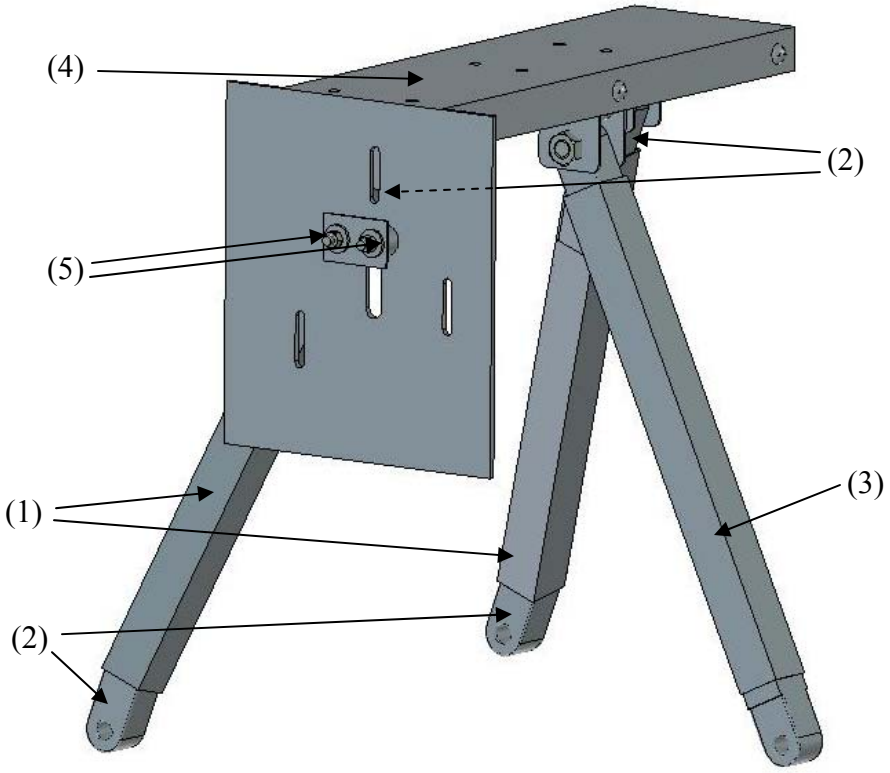

Figure 3.9: *Foldable antenna stand,*
(1): Legs mounted with 14° angle, (2): 14° leg holders, (3): Straight leg,
(4): Upper plate and motor bracket, (5): Belt tensioners.

With this design high stability and portability were achieved. Only the upper bolt holding the single legged side has to be dismounted prior to folding. To achieve maximum stability the two legs that are mounted on the same side (1), were mounted with an angle to increase sideway stability. To make this possible, and in the same time keep the collapsibility of the stand, the "leg holders" (2) had to be milled out in with corresponding angle the legs were set to have (14º in this case), se also Figure 3.10 for a better view of the leg-holders.

As the legs are not mounted on the same distance from the centre of the disc, the length of the legs needs to be of different length to keep the upper part of the device horizontal. The lengths of the legs were roughly calculated using basic geometry, but had to be slightly adjusted during assembly.

The final lengths of the legs are 299 mm for the two legs mounted on an angle (1), and 282 mm for the single legged side (3).

The same way of attaching the legs were used in the upper end as the lower end. To get a solid and lightweight base for the upper part, an aluminum profile was used. As the profile was hard to draw in IronCAD, a simplified model of the profile was made; it can

be viewed in Figure 3.11. The profile was chosen as a base of the top part due to its strength and light weight.

To make it possible to mount things on the profile, an aluminum sheet was folded to fit around it. This sheet also works as the upper motor bracket, see (4) in Figure 3.9.

The small ball bearings, (5) in Figure 3.9, work as belt tensioners for the belt transmission that drives the vertical movement. Without these tensioners the surface between the belt and the small drive pulley would be too small and the belt would slip. But with the tensioners in place, there were no slippage at all.

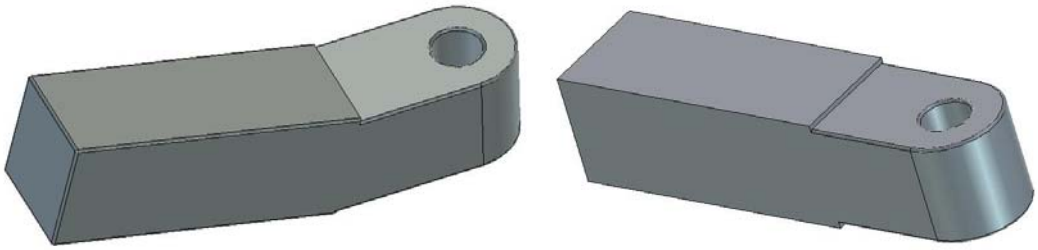

Figure 3.10: *Leg holders. Left: 14 degree angle. Right: Straight.*

.

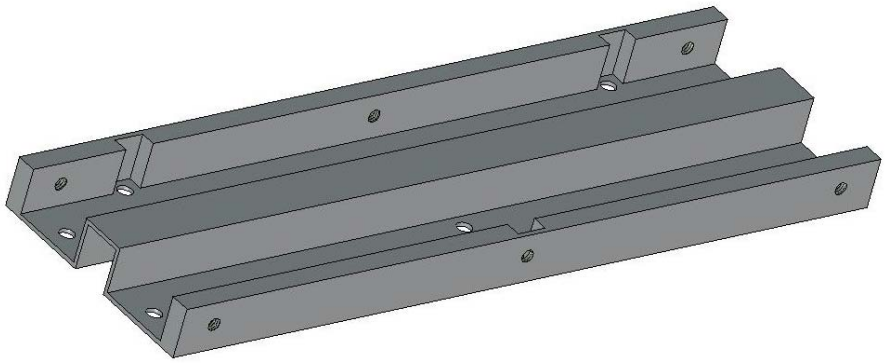

Figure 3.11: *Profile that makes the base of the upper part.*

3.2.3 Upper antenna driver

To make the antenna move in the vertical plane, the solution seen in Figure 3.12 was developed.

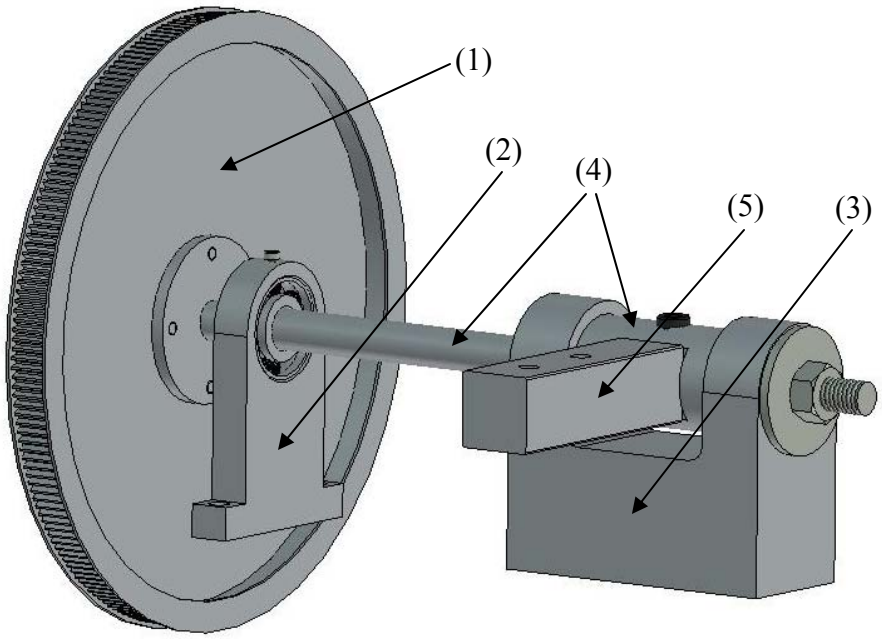

Figure 3.12: *Upper drive,*
(1): Big gear, (2): Small bearing house, (3): Big bearing house,
(4): Rotating shaft, (5): Antenna boom adapter.

To make it possible to still achieve collapsibility with the motor mounted, the motor was mounted on the right side of the antenna stand. A belt drive was used to make the antenna rotate around central bearing house.

The upper big gear, (1) in Figure 3.12, was found in the ECSE workshop along most of the parts in this project; it has a diameter of 180 mm. The smaller gear that is attached on the outgoing axis of the motors gearbox was very luckily also found among the workshops left-over parts and has a diameter of 13 mm (not showed in the Figure 3.12). This gives a gearing of 13.85.

The bearing houses (2) and (3) in Figure 3.12, were milled out of massive aluminum in the ECSE workshop by Anthony “Tony” Brosinsky. The holes in the bigger bearing house (to the right in Figure 3.13) were made to press-fit the ball bearings for best stability. The hole in the smaller bearing house was made slightly bigger to make it easier to take apart and assemble.

The rotating shaft, (4) in Figure 3.12 (also seen in Figure 3.14), was lathed and milled out of steel to hold for the forces that it will be exposed to. The hole to the left in Figure 3.14 is a conical hole used to tighten the big gear to the shaft. A corresponding hole is found at the outer washer holding the big gear. A cone shaped wedge was hammered through these holes to get rid of any slack.

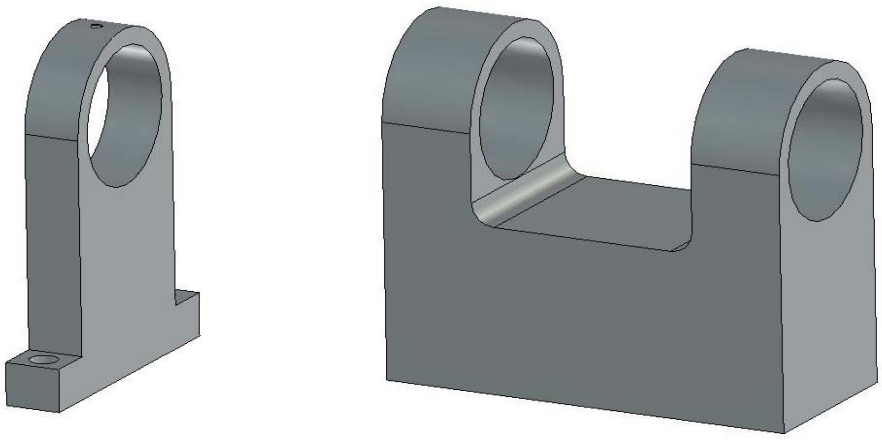

Figure 3.13: *Upper bearing houses.*

Figure 3.14: *Rotating shaft, without and with bearings.*

3.2.4 Antenna boom

To be able to calibrate the distance from the focal point of the reflecting disc antenna to the feed antennas, the boom that holds the feed antennas is needed to be adjustable, as well as the brackets that holds the feeds.

A square aluminum pipe, (1) in Figure 3.15, (same type that was used in the legs) was used as a base to the boom construction; it has a tight fit with the boom adapter, (5) in Figure 3.12, in one end and the other end joins with the out plastic part of the boom. A 90 º steel bracket, (2) in Figure 3.15, was used to connect the reflector disc to the antenna boom.

To avoid interference in the radiation pattern around the detecting feed antennas the outer parts of the boom were made of plastic. Plastic pipes were used to form the last part of the antenna boom that also is adjustable in length. The cross was made of plastic rods that are glued into holes that were drilled through the outer plastic pipe.

The part that joins the boom (with reflector and counterweight included) with the rotating shaft, what we call the boom adaptor, can be seen in Figure 3.16. It is made of steel with very high precision to avoid slack between the rotating shaft and the boom. The round shape of the end of the adapter was chosen because round shapes are easier to make with higher precision than square shapes.

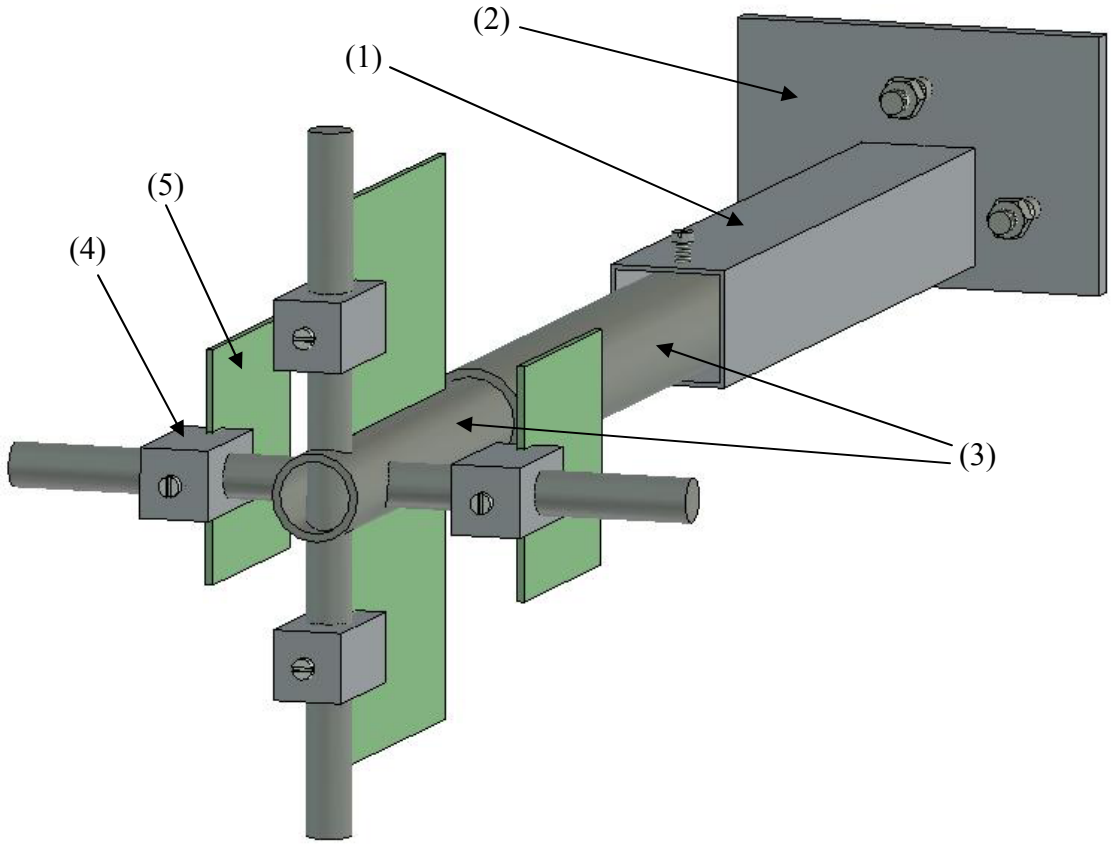

Figure 3.15: *Assembled antenna boom.*
(1): Square aluminum boom, (2): Steel reflector disc bracket,
(3): Plastic part of antenna boom, (4): Yagi bracket, (5): Yagi antenna.

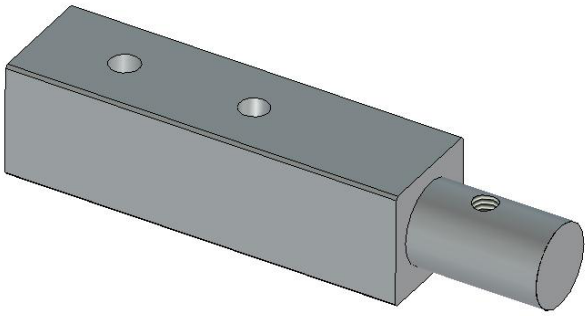

Figure 3.16: *Antenna boom adapter.*

3.2.5 Counter weight

To balance the weight of the reflector disc and the antenna boom, a counterweight was constructed. The reason of this was to decrease the tension on the drive-belt and the torque the vertical motor has to overcome to turn the antenna.

As the antenna has to be able to move 180° in the vertical plane, a special design was manufactured to fulfill that need. The design can be seen in Figure 3.17**.** With two separate arms holding the weights, the third leg, (3) in Figure 3.9, will pass between the two arms, and the 180° movement can be done.

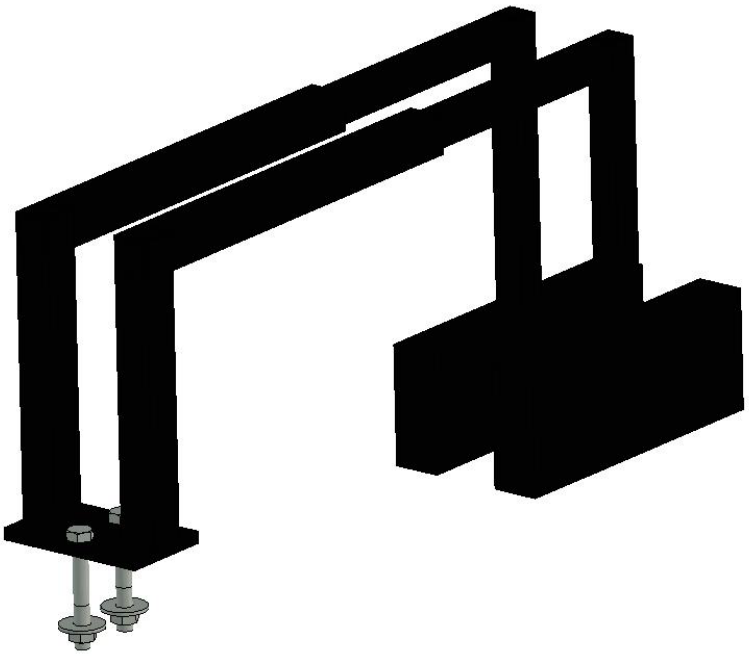

Figure 3.17: *Counterweight.*

4 Communication system

The purpose of the general system was to keep a stable communication between the UAV and the ground. The UAV is equipped with a transmitter that transmits the video signal with the carrier wave at 2.41 GHz. A receiver antenna with same frequency characteristics was placed on the ground. The signal was received and demodulated so that the final output signal was a clear analog video-signal.

4.1 Receiver antenna

In the introduction chapter the use of a reflector disc were discussed. Due to the transmitter's low radiated power a reflector antenna at the receiving end is a good option. The choice of antenna for the project was a reflector disc antenna from Hills Industries. This is a bi-directional antenna that can be used for both transmitting and receiving. See Figure 4.1 for a picture of the antenna.

Figure 4.1: *Reflector Grid Antenna from Hills Industries.*

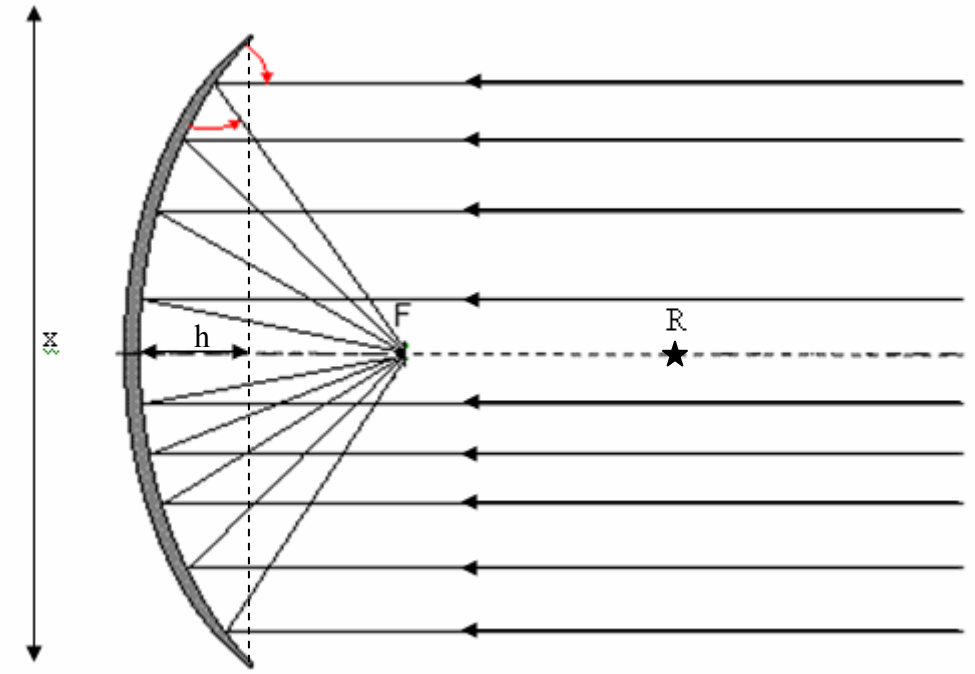

Figure 4.2: *Reflector beam.*

The reflector antenna gives a high gain due to the aggregation of the incoming signals in the focal point. See Figure 4.2.

To find the focal point of the Hills Grid reflector antenna formula 4.1 [1] was used. This is the formula to calculate the radius of a circle segment, and this reflector disc can be seen like that. What x, h and R correspond to in this case can be seen in Figure 4.2. The dimensions of the Hills Grid antenna were, x = 860 mm and h = 123 mm. With these dimensions, the Radius was calculated to 813 mm. As seen in Figure 4.2 the focal point is located half way between the reflector disc and the centre of the "circle" (R).

$$h(2R - h) = \left(\frac{x}{2}\right)^2 \qquad (4.1)$$

$$R = \frac{\left(\frac{x}{2}\right)^2}{2 \cdot h} + \frac{h}{2}$$

$$R = \frac{\left(\frac{860}{2}\right)^2}{2 \cdot 123} + \frac{123}{2} = 813\,\text{mm}$$

$$F = \frac{R}{2} \approx 406\,\text{mm}$$

This distance was verified by setting up the antenna in the anechoic chamber[8] and with the transmitter antenna placed 4 meter in front and at the same altitude, to get the wave in level between the two antennas. By sliding a small Yagi antenna along the antenna boom we observed where the strongest signal was received. It ended up at a distance of 400 mm from the disc. This differs slightly from the mathematically calculated focal point, but can be explained by minor measurement errors or a small skew in the reflector disc. This was finally the distance from the disc where the receiving Yagi-antennas were mounted.

4.1.1 Radiation Pattern

When the focal point was known the radiation pattern for the reflector disc can be measured. This was done in the anechoic chamber laboratory at the ECSE department (where we also measured where the focal point was located). The reflector antenna was mounted on a rotator that turned the antenna 360° degrees around its own axes. As the antenna rotates the received signal strength varies. At every degree the signal strength is measured and saved in a computer. The procedure was done twice to get both the horizontal and the vertical plane radiation patterns. The transmitting antenna had a gain of ~10 dB and the signal source level was 0 dBm. When all the data was received it was printed on a polar plot in MatLab[9], see Figure 4.3.

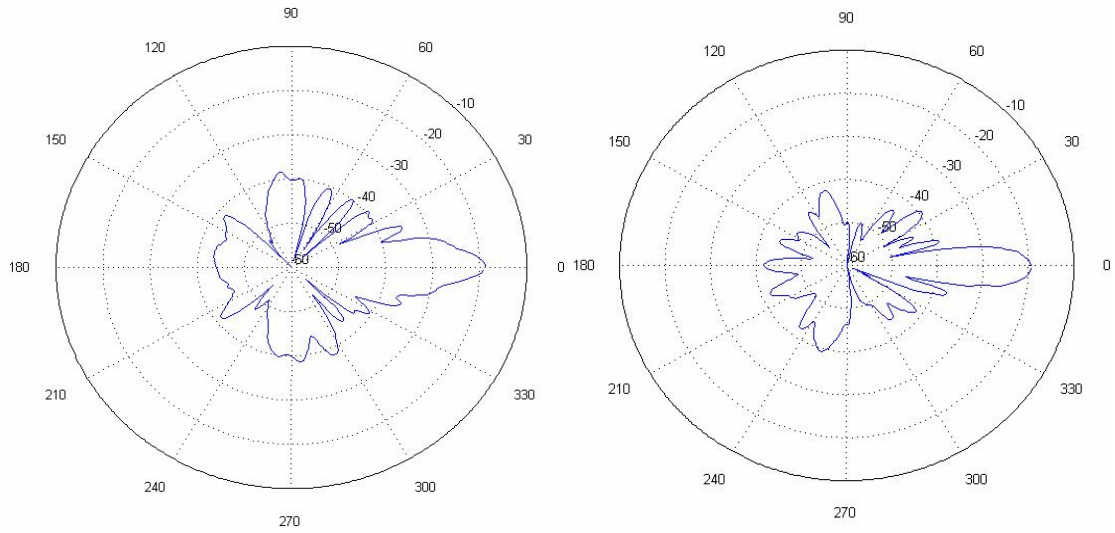

Figure 4.3: *Reflector disc received radiation in dBm. Left: H-plane, Right: E-plane.*

4.1.2 Gain and Directivity

The specified gain from Hills Industries is 23.5 dBi, which means that its gain is 23.5 dB compared relative to an isotropic antenna (0 dB gain). An isotropic antenna is an antenna that radiates the same power in all its direction (symmetrical). This can be done in theory, but is impossible to create in practice, because there will always be some directions that

[8] An electromagnetic shielded environment, ideal for antenna testing.
[9] Mathematical tool from Mathworks (http://www.mathworks.com/)

radiate more energy than others (unless a point source). In our case the gain of the antenna and the direction of the energy are directed towards/from the focal point. The radiation pattern shows the directivity of the reflector disc (Figure 4.3). The beamwidth of the antenna aperture is very narrow due to the high gain/directivity. The classification of beamwidth is where the signal strength has been attenuated 3 dB from both side of the main lobe (the focal point). Due to the different dimensions in the horizontal and vertical size and the fact that the feed antenna was mounted horizontally, the reflector disc has different beamwidths for the horizontal and vertical plane. The measured beamwidth for the reflector antenna was:

- Horizontal beam width was approx. 8° (4° on either side of centre lobe)
- Vertical beam width was approx. 10° (5° on either side of centre lobe)

To verify the specified gain (23.5dBi) we mounted the antenna in the anechoic chamber with its highest directivity in the horizontal plane towards the transmitting horn antenna. To prove this we used Friis formula expressed in dBm, known from [2][3]:

$$P_R\,(\mathrm{dBm}) = P_T\,(\mathrm{dBm}) + G_T\,(\mathrm{dB}) + G_R\,(\mathrm{dB}) - 20\log(r_{\mathrm{km}}) - 20\log(f_{\mathrm{MHz}}) - 32.44 \qquad (4.2)$$

P_R is the received power and P_T is the transmitted power, both in dBm. G_T is the gain of transmitted antenna and G_R is the gain of our receiving antenna, both in dB. The last parts are the free space loss for our specified frequency and distance, the constant 32.44 is to correct the use of non SI units like km and MHz, and get the result in dBm. With all these characteristics known we could measure and calculate the gain of the reflector disc.

The gain of the transmitting horn antenna, G_T was around 10 dB and the transmitting signal, P_T used was 0 dBm. The distance between the antennas was 4 meter and the frequency was 2410 MHz. The measured received signal P_R was -19.33 dBm. With Friis formula (4.2) the gain G_R of the reflector disc was 22.79 dB. Why this differs a little from the specified gain is mostly due to cable losses from the antenna to the spectrum analyzer that measures the signal.

4.2 Signal Propagation

The microwave signal transmitted from the UAV propagates differently depending on surrounding scenery. To get a stable point-to-point communication between the antennas there can not be any obstacles in the way. This was set to be the condition for where the application will be used, and the maximum distance (R) to the UAV will be 1 km. With these facts we can discard the problem with the curvation of the earth and assume an ideal LOS (Line Of Sight) link between the ground antenna and the UAV.

The antenna used on the UAV was a normal dipole with a transmitting power of 10 mW, which corresponds to 10dBm (see formula 4.3). As the dipole's gain varies, due to stronger gain in the horizontal plane and almost no radiation in the vertical plane, we decided after a discussion with Mr. S. Jenvey that the gain could be set to ~0 dB, as the direction of the UAV will vary along time.

$$P_{dBm} = 10 \cdot \log(\frac{P}{1\,mW}) \qquad (4.3)$$

$$P_{dBm} = 10 \cdot \log(\frac{10\,mW}{1\,mW}) = 10\,dBm$$

The gain of the receiving antenna was 22.79 dB with our Yagi feed in the focal point. When the power detector was coupled like in the datasheet, it has a sensitivity of -63 dBm (P_R = -63 dBm), read more about the power detectors in chapter 5.5. With these facts we can calculate the range of the LOS link, by solving R from formula 4.2.

$$20\log(R) = P_T + G_T + G_R - P_R - 20\log(f_{MHz}) - 32.44$$
$$\Rightarrow R = 610\,m$$

The result does unfortunately not fulfil the specifications of 1 km, but as we did not have an infinite amount of power detector chips, so we had to keep on working with these results.

5 Signal detecting unit

This might be the most important part of the project as the rest of the system relies on the fact that the right signal is detected.

During the development of the signal detecting system these facts where taken in consideration:

- *Detect the correct 2.41 GHz signal that is transmitted from the UAV*
- *Reduce the signal loss from the Yagi antennas*
- *Convert the RF signals to a DC Voltage for the microcontrollers analog input*
- *Where to place the feed antennas for best performance*

To implement this, Yagi-antennas were used to receive the 2.41 GHz signal. To decrease the risks of other signals interfering with the correct one, the antennas were constructed to be quite narrow in bandwidth. Narrow band pass filters were also used to suppress interfering signals.

To reduce loss and to match the antennas with 50 Ω feed cables the use of baluns was necessary. The last link in this chain was an RF power detector, which converts the RF signal into a DC voltage level. In chapter 2 Research, you can read about why these power detectors were chosen.

5.1 Antenna basics

Antennas can have many different shapes and work in different ways, but they have one thing in common, they all pick up electromagnetic waves.

Electromagnetic wave consists of one electric and one magnetic wave. The two waves are perpendicular to each other, as seen in Figure 5.1.

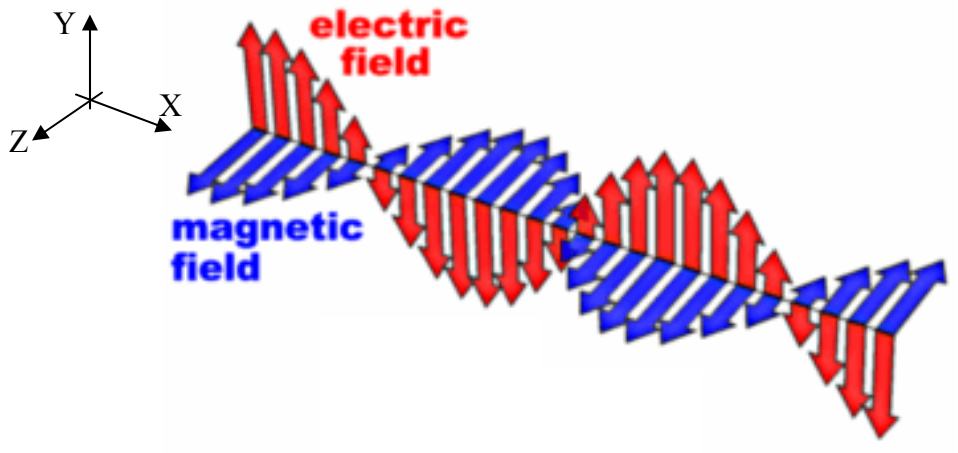

Figure 5.1: *Electromagnetic wave.*

In Figure 5.1, the arrows pointing in the y direction corresponds to the electric wave, and the arrows pointing in the z-direction corresponds to the magnetic field, the waves spread out in the direction of x.

There are antennas that use the electric wave plane to transmit and receive signals, as well as there are antennas that use the magnetic wave plane. Here follows a short description of a 75 Ω electric dipole.

The electric dipole is one of the simplest antennas, as stated by the name this is an antenna that works in the electric wave plane, often referred to as the E-plane. Figure 5.2 below describes the basics of such an antenna. As the current alternates in the dipole element, electromagnetic waves are spread out around it in the x-y plane, the electric waves (showed in the Figure 5.2) are aligned with the dipole, and the magnetic waves are perpendicular to the dipole and the electric waves.

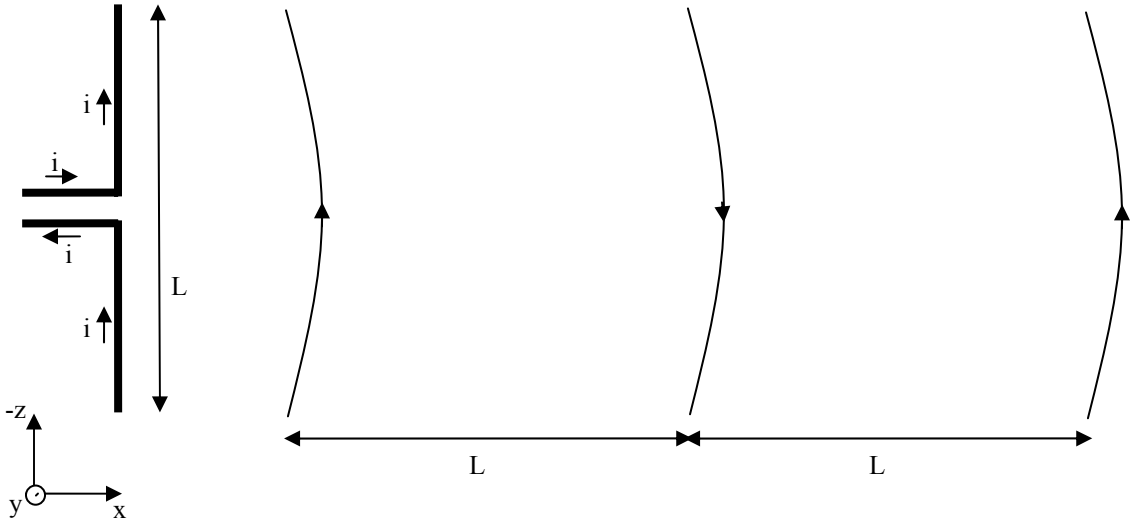

Figure 5.2: *Dipole electric wave propagation.*

Depending on the shape of the antenna, its ability of receiving or transmitting waves in different directions varies. That phenomenon is called radiation pattern. A dipole like above radiates waves with the same amount of power around the dipole (around the z-axis), but along the z-axis it is not radiating at all (in theory). Figure 5.3 shows three graphs taken from SuperNEC[10] simulation software (more about SuperNEC in section 5.2.1); they are showing the radiation pattern of an electric dipole.

[10] Antenna simulation software from Poynting Group (http://www.supernec.com/)

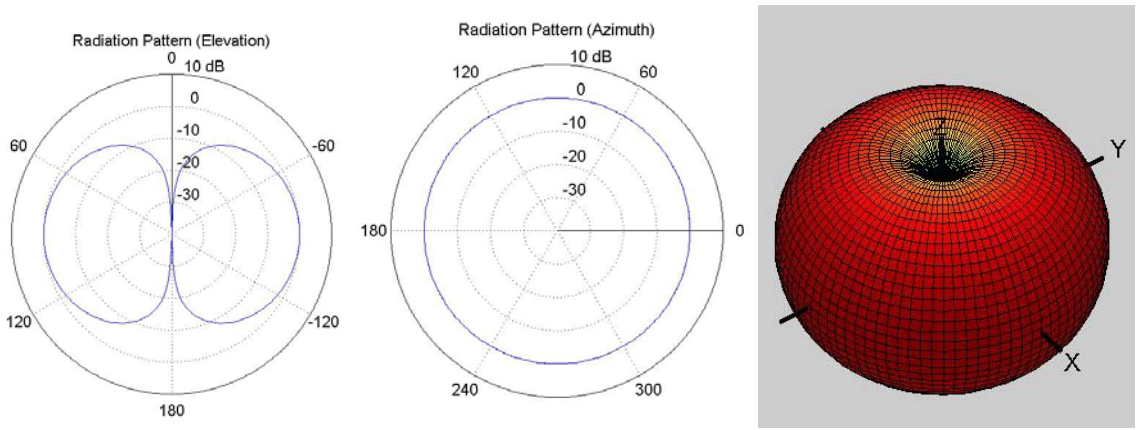

Figure 5.3: *Dipole radiation patterns.*

As can be seen in the Figure 5.3 the radiation pattern is omni directional in the x-y plane, more commonly known as the H-plane or Azimuth plane, and symmetric in the x-z, E-plane or Elevation plane. Azimuth and Elevation plane can sometimes be bad choice of calling the planes, because those are depending on how the antenna is mounted.

The length of a dipole element should be approximately half the wavelength of the transmitting or receiving frequency.

5.2 Feed sensor antennas

The feed antennas used in this project are of Yagi-Uda types. The Yagi-Uda antenna can be described as an enhanced dipole. One driven element (the dipole) and one or more passive element are aligned to form a Yagi antenna. By aligning the elements the radiation pattern can be changed, and a higher directivity can be achieved.

The length of the elements varies; the reflector should be slightly longer than the driven element, and the directors slightly shorter. The lengths of the elements are usually in this range [3]:

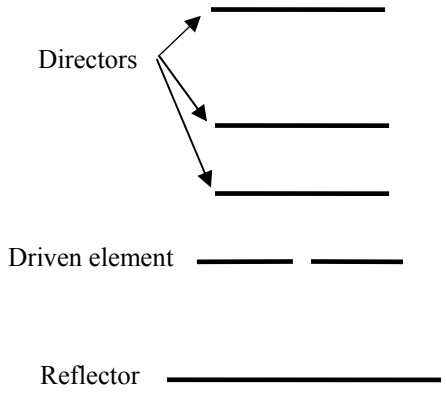

Figure 5.4: *Yagi model.*

- Reflector: 0.49λ
- Driven Element: 0.46λ
- Directors: 0.44λ

  Where λ is the wavelength.

This is only indications; it could and should be adjusted for better performance. The distance between the elements is the part where most of the characteristics of the antenna are settled. Typically the distances between the elements are 0.1λ to 0.25λ but as with the length of the elements this is only indications.

In this application, Yagi antennas will be used as receiving feed antennas, and therefore need to fulfil a beam width (the angle where the radiation pattern have decreased 3 dB from the maximum point) of about 110° in the H-plane and 80° in the E-plane. Why these proportions are chosen was primarily to suit the relative dimensions of

the reflector antenna. The Yagi antennas should only receive the reflected signal from the reflector disc and not other surrounding signals outside the disc. The feed antennas also need a front to back ratio of at least 10 dB to restrain signal sources from the wrong direction. After some testing, we realised that we needed a 3 or 4 element Yagi antenna to achieve a suitable radiation pattern.

5.2.1 Antenna simulations

When designing an antenna, simulation programs are very useful to simplify the development process. The most well known program and base of much other simulation software is the NEC[11]. A lot of different versions of NEC programs were tested during the development process e.g. 4nec2, Expert MiniNEC and SuperNEC. After several of tests of these programs, SuperNEC seemed to be the best for this application and was used to do the simulations for the final antenna.

SuperNEC is developed by Poynting Software (Pty) Ltd. In South Africa, and works like an add-on to Mathworks MatLab. It is not a Freeware program, but after contacting Poynting Software, we managed to get a limited student / academic version to use during development.

The environment in SuperNEC is very user-friendly and easy to work with. Figure 5.5 is a screen dump from the main window where the antennas is designed.

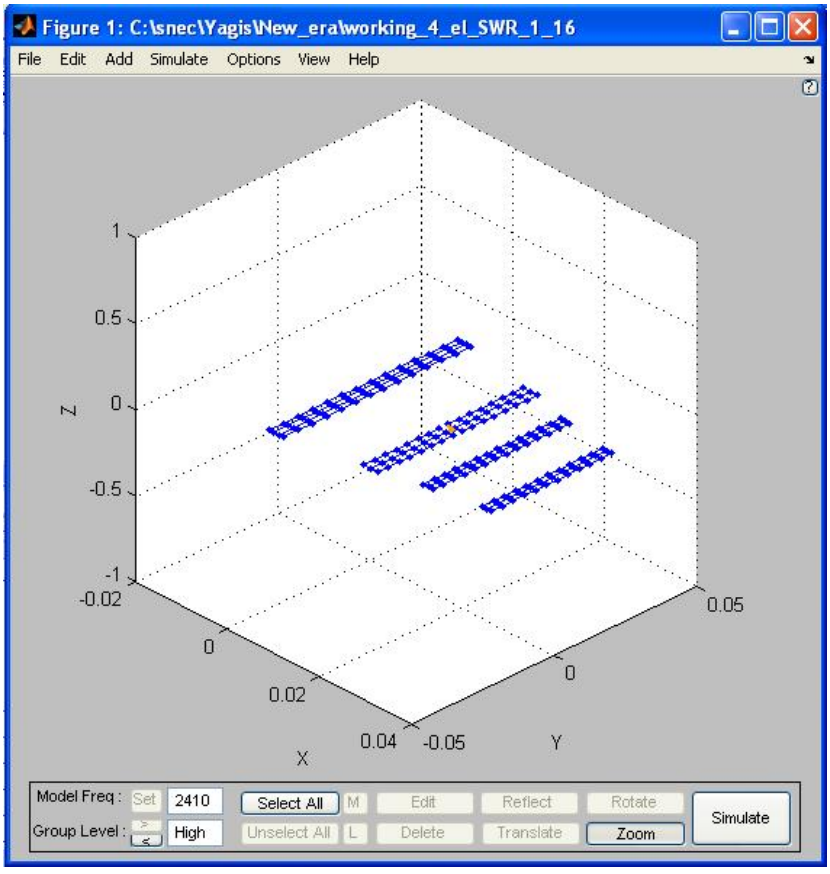

Figure 5.5: *SuperNEC, antenna simulation software.*

[11] Numerical Electromagnetic Code

One way, and maybe also the easiest, of constructing a Yagi antenna for over 1 GHz (where the wavelength is short) is to make them on PCB[12]s. This had to be taken into calculation during the simulations. That is why the antenna in Figure 5.5 looks a little bit odd. The width (not the length) of the element is not affecting the radiation pattern of the antenna very much, but it affects the electric characteristics of the antenna, which also can be simulated in SuperNEC.

After a lot of simulating, we finally settled with the results showed in Figure 5.6.

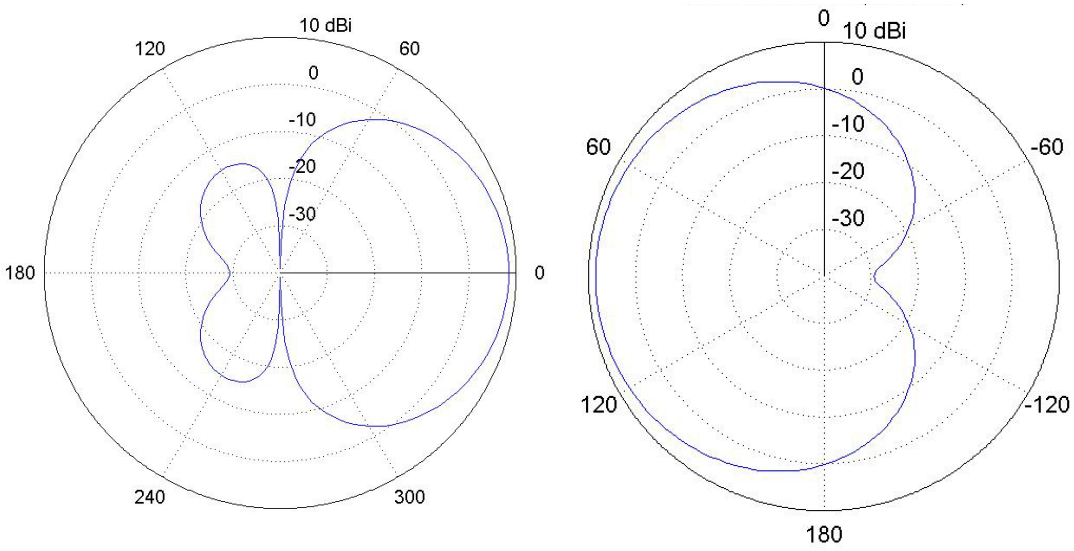

Figure 5.6: *Simulated Yagi radiation patterns (E-plane to the left).*

5.2.2 Transfer to FR4 PCB board

After finding a descent model of an antenna with a radiation pattern that fulfilled the specifications, the antenna was build by using copper tape on FR4 glass fibre boards, which is the same material that are very commonly used in regular circuit boards.

As an electromagnetic wavelength changes in different materials due to different dielectric constants, like FR4 board and air. The elements of the antenna had to be adjusted to correspond to the free space (which was used in SuperNEC simulations). After a lot of testing and cutting copper tape, the conclusion was that the wavelength on the surface of a 1.59 mm thick FR4 board is approximately 73 % of the free space wavelength. This means that the elements of the antenna should be 73 % of the length that were used in the simulation software.

When the right length of the Yagi elements was found and the simulated results corresponded in a good way to our copper taped Yagi antenna, four antennas were milled out in the PCB mill.

[12] Printed Circuit Board

5.3 Baluns

The balun[13] is used to balance the connection between a balanced port and an unbalanced port, e.g. between an antenna and a feeding cable. In our case the baluns main function is to spread the charges along the driven element symmetrically, to achieve a symmetric radiation pattern and increase the efficiency. It also help avoiding RF signals radiate from the cable, and keeps the SWR[14] at a stable level independent of cable length and objects close to the antenna.

Baluns can be constructed in many different ways. Two types of baluns that are relatively easy to realize at this frequency is the bazooka balun and the microstrip balun. These are also the two types that were tested and evaluated.

Figure 5.7 shows how the electric current moves in the end of a coaxial cable without a balun. As can be seen in the Figure 5.7, i_1 moves up and down the inner conductor and i_2 up and down the inside (due to the skin effect) of the sleeve. But in the point were i_2 should transfer on the dipole element, current is also leaking over to the outside of the sleeve. This causes differences of the current distribution in the dipole elements, which affects the radiation pattern in a bad way (becomes unsymmetrical).

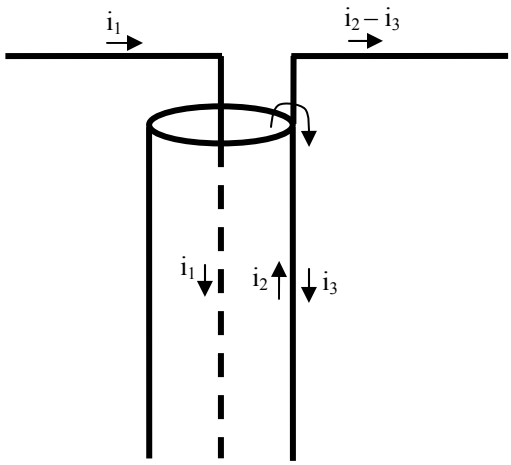

Figure 5.7: *Coaxial cable with dipole antenna.*

5.3.1 Bazooka balun

To avoid this to happen, a balun is used to stop i_3. A commonly used balun in frequencies of the VHF[15] region and above is the so called bazooka or sleeve balun.

This type of balun consists of an extra sleeve located on the outside of the coaxial cable as seen in Figure 5.8. The length of this sleeve should be a quarter of a wavelength long in the material of the outer isolator in the coaxial cable. This could be hard to know, but a good value to start at is ~75 % of the free space quarter wavelength. The lower part of the sleeve must be connected to the inner sleeve a quarter of a wavelength from the end of the cable. In the end of the cable and bazooka, there must be no connection. By

[13] Balun is an abbreviation for BALanced to UNbalanced
[14] SWR stands for Standing Wave Ratio and measures the loss of efficiency in i.e. antennas.
[15] Very High Frequency, 30 – 300MHz.

doing this, the potential in the outer and the inner sleeves will be the same over time. And hence the leak current i_3 will no longer exist, or at least be very small.

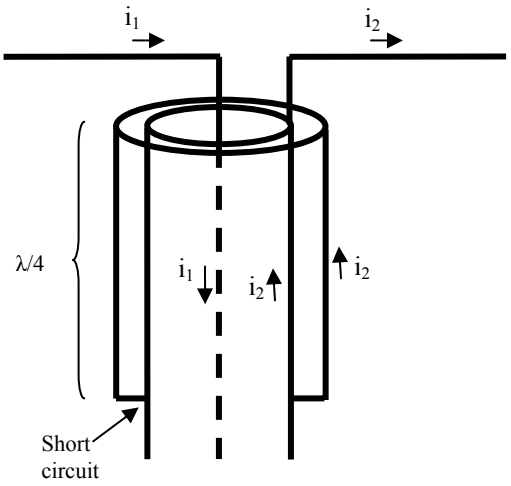

Figure 5.8: *Bazooka balun.*

5.3.2 Microstrip baluns

There are a lot of different layouts of microstrip baluns, some of them were tested during development with varying results. To be able to design a balun like this, 50 Ω characteristic transmission lines have to be used on the board to avoid reflections and losses. The most usual way to do a 50 Ω waveguide is to do a microstrip line on a board with an "infinite" ground plane (see Figure 5.9). But this was not possible in this case when the antenna would be located on the same board.

To do a 50 Ω stripline without a big ground plane is done by using the layout of Figure 5.9 but do the calculations with twice the thickness of the board it will be created on. This will correspond to the microstrip in Figure 5.10.

By using this type of microstrip, the 50 Ω transmission line problem was solved. The layout of the first microstrip balun tested can be seen in Figure 5.11.

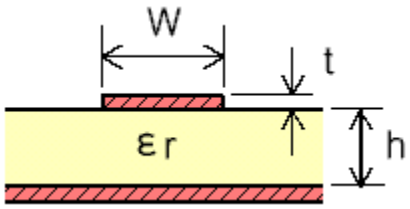

Figure 5.9: *Microstrip line with infinite groundplane.*

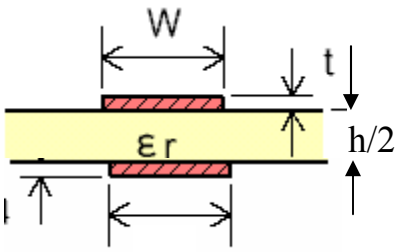

Figure 5.10: *Microstrip line, groundplane width equal to stripline.*

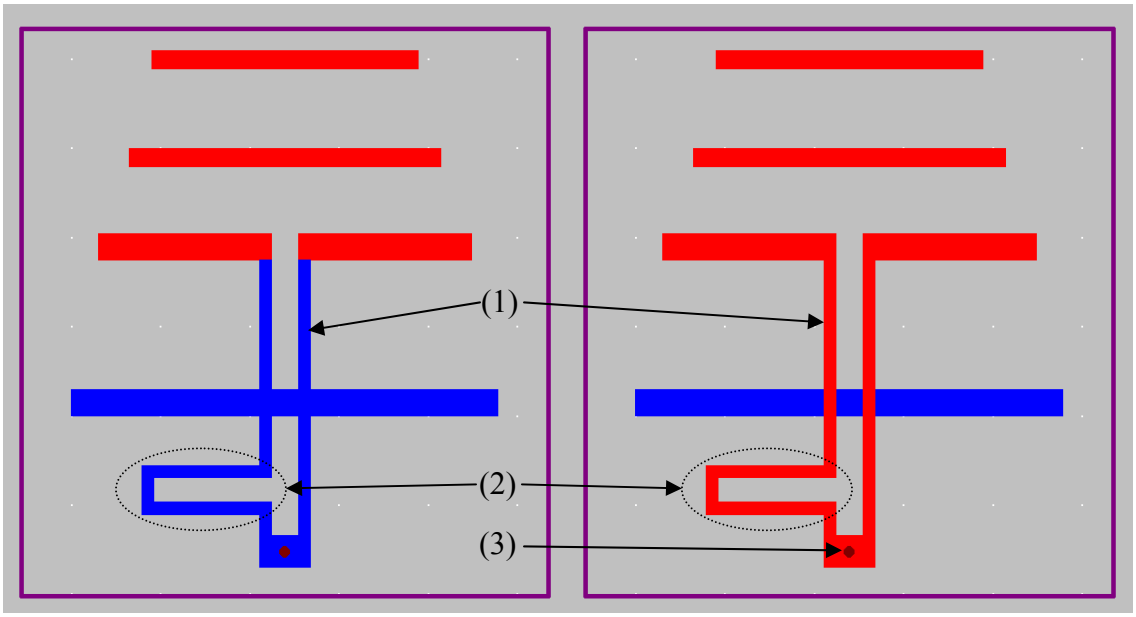

Figure 5.11: *Antenna with microstrip balun 1. Blue - Top Layer, Red - Bottom layer (1): Microstrip line, (2): Balun, (3): Feed point.*

The darker (blue) parts of this antenna/balun are the bottom layer of the PCB and the brighter (red) parts is the top layer. The idea of a balun like this is to only use the inner conductor of the coaxial cable to feed the driven element. The shield is connected to the bottom layer of the board, and works like a ground plane. The balun in this layout has a length of half a wavelength long which leads to that the signal in the left part of the dipole will be delayed half a wavelength. This layout worked quiet well with regards to keeping the SWR at a stable low level, but the radiation pattern was affected in a bad way, as well as the attenuation in the microstrip lines were too high. So this was not a good option.

A similar version of this type of balun, seen in Figure 5.12, was also tested, the main difference with the balun described above, is that the microstrip lines are shortened or actually taken away. This helps get rid of the losses caused by the microstrip lines. This layout worked better than the one above (but not very good) in matter of radiation pattern and losses, but the SWR was very sensitive to close lying objects.

Other layouts and types of microstrip baluns were also tested, but without good results.

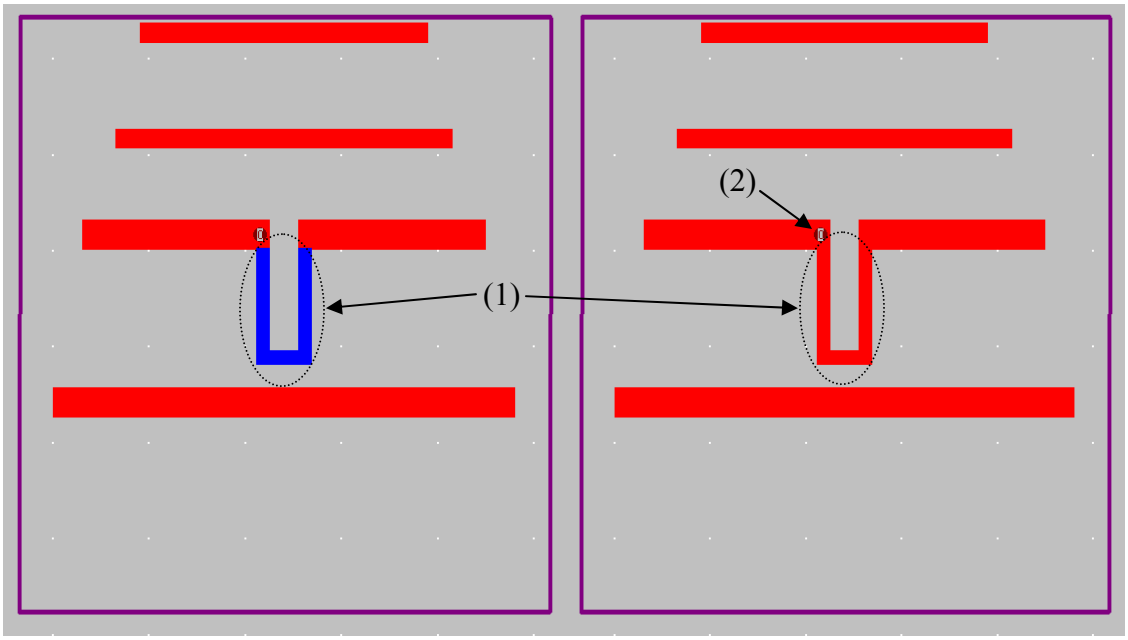

Figure 5.12: *Antenna Layout, balun 2. Blue - Top Layer, Red - Bottom layer. (1): Balun, (2): Feed point.*

5.3.3 Balun results

The balun that worked best of the ones above described was the bazooka or sleeve balun. With this balun, the SWR were kept on a stable level around 1.2, which was within the specifications, see Appendix 5 for Network Analyzer[16] plots. These measured SWR values are unfortunately not the true SWR of the antennas, because the coaxial cables connecting them have losses. The losses in the cable were measured with the Network Analyzer by connecting a piece of cable between port one and two on the analyzer, and then measure the losses on S12 (between port 1 and 2). With a cable length of ~250 mm, the damping was 0.8 dB at a frequency of 2410 MHz. The cable that connects the antennas to the power detectors are approximately three times that length, which means that there is a loss of 2.4 dB in each cable. When the SWR is measured with the Network Analyzer, the signals have to go "up and down" the cable, so the signal travels 1500 mm (6 * 250 mm). This means that the losses that have to be taken into calculation are 4.8 dB (6 * 0.8 dB), which corresponds to a loss of 2/3 of the signal power. (The cables used are not suitable for these frequencies, but were the only cables that were available to work with at the time).

To calculate the real SWR, formula 5.1 and 5.2 [3] were used.

$$\left|\rho_{\text{measured}}\right| = \frac{\text{SWR} - 1}{\text{SWR} + 1} \qquad (5.1)$$

$$\rho_{\text{real}}^2 \cdot (1 - \text{loss}) = \rho_{\text{measured}}^2 \qquad (5.2)$$

[16] A Network analyzer is an instrument that can be used to measure SWR and losses.

With a measured SWR of 1.2, the SWR of the antenna without the cable losses comes out like follows:

$$|\rho_{measured}| = \frac{SWR-1}{SWR+1} = \frac{1.2-1}{1.2+1} = \frac{0.2}{2.2} = 0.09$$

$$\rho^2_{measured} = 0.09^2 = 0.0081$$

$$loss = \frac{2}{3}$$

$$\rho^2_{real} = 3 \cdot 0.0081 = 0.024$$

$$\rho_{real} \approx 0.155$$

$$SWR_{antenna} = \frac{1+0.155}{1-0.155} = 1.37$$

With a SWR of 1.37, the specifications of the antenna were fulfilled. The radiation pattern of the antenna was also improved. One oddity in the E-plane occurred at around 225 degrees (see Figure 5.13); this might depend on the coaxial cable interfering with the radiation pattern or some asymmetry in the antenna. Unfortunately the front to back ratio is not the same (but it should be) in these Figures, this is due to the transmitting antenna was not exactly aligned with our antenna.

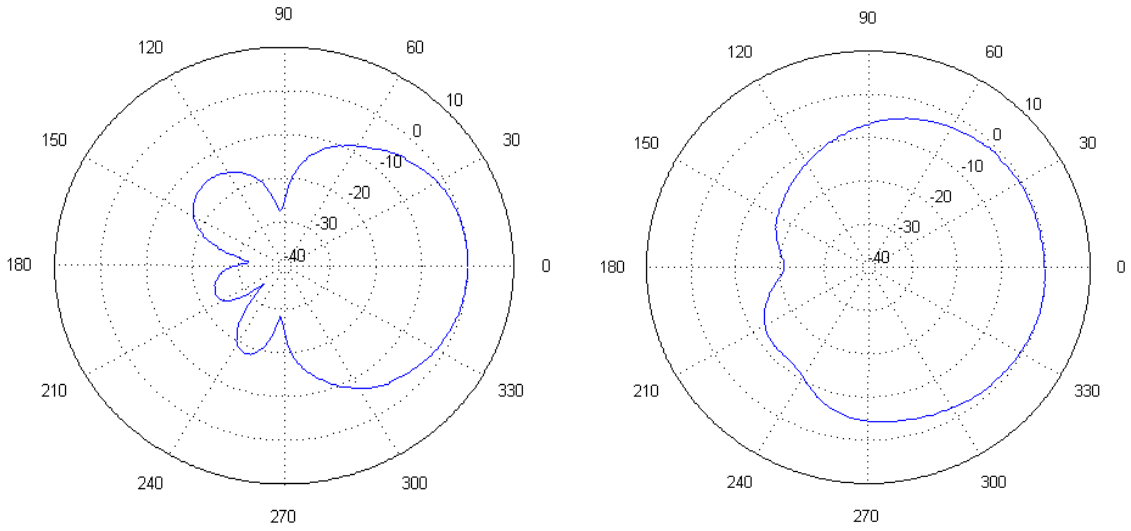

Figure 5.13: *Yagi radiation pattern, (E-plane to the Left).*

5.4 Power detector chip

The Linear Technology LT5534 is a high performance logarithmic RF power detector. It has a wide frequency range between 50 MHz and 3 GHz, and has a dynamic signal range of 60 dB. With the proposed coupling in the data sheet, the power detector will work in the range -3 dBm to -63 dBm, in other words 0.501 mW down to 0.501 nW. As the power detector has no known power limiter or functions that will block to strong signals, care has to be taken.

The RF input signal from an antenna is directly converted from a decibel scale to a linear DC output voltage. To achieve the dynamic range of 60 dB several detectors and limiters are joined together in a cascade; see Figure 5.15 for block diagram. Their outputs are summed together to produce an accurate log-linear DC level proportional to the input signal in dB. The output is buffered with a low output impedance driver and responds within 40 ns to a RF input signal change.

As mentioned the LT5534 has very high sensitivity, detecting signals as small as -63 dBm, but this lower level of signal can be adjusted either upward or downward, in other words the dynamic range can be moved. To get a higher range signals, an attenuator is simply inserted in front of the RF input. For lowering the dynamic range and to get better sensitivity, a narrow band L-C matching network can be used. Depending on what application the chip is used for, the sensitivity of the detector can be tuned between -75 dBm to -62 dBm.

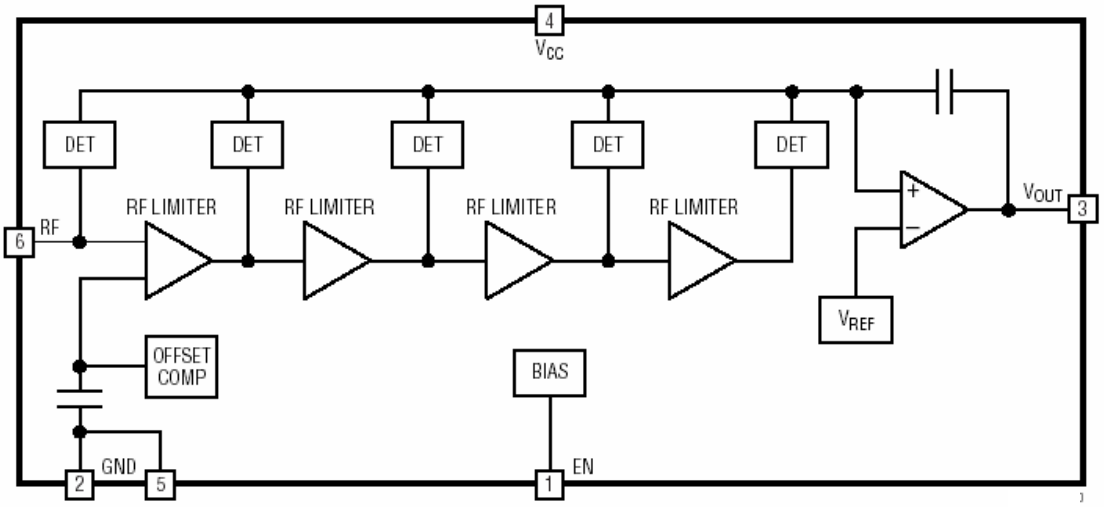

Figure 5.15: *Block diagram of the LT5534 power detector chip.*

5.5 Filter

A filter is a device that selectively filters signals depending on the performance of the filter, making some ranges of frequencies pass through and to attenuate others. There are a lot of different filters, (i.e. low-pass, high-pass, band-pass and band-stop), all with different characteristics. Filters can easily be built with both active and passive components, like inductors, conductors, resistors and operational amplifiers.

There are also numerous amounts of pre-made filters, (i.e. cavity filters, crystal filters and ceramic filters.). What filter type to choose depends on the application.

5.5.1 Ceramic filters

The ceramic components are made of high stability piezoelectric ceramics that function as a mechanical resonator. The frequency is primary adjusted by the size and thickness of the ceramic element.

The filter type that was used in this project was a ceramic single chip surface mounted three-section band-pass filter from MuRata®. The filter has a centre frequency of 2450 MHz and a bandwidth of 100 MHz. See Figure 5.16 below for a picture.

Figure 5.16: *MuRata 2.45GHz BP filter.*

Why we choose this particular filter depend on:

- The difficulty to realize an own filter at the frequency 2.4 GHz.
- The small size, which makes the component easier to integrate with the other small components.

The filter provides a good attenuation around 20 dB at 280 MHz offset from the centre frequency. The size of the filter is 2.0*2.5*0.9 mm^3, the transfer function can be seen in Figure 5.17.

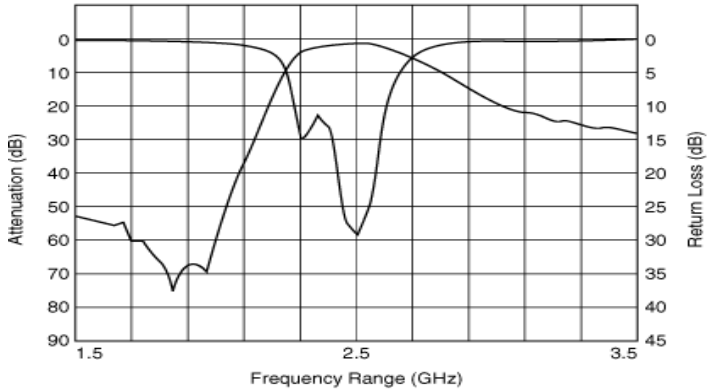

Figure 5.17: *Murata BP filter frequency response.*
For full specification, see appendix A5.

5.6 Power detector boards

The usage of the LT5534 chip has been of crucial importance for the realization of the signal detection. But as the LT5534 has a frequency range from 50 MHz to 3 GHz, filtering is also of big significance. Finally it is very important to manufacture the two circuit boards (PCB) with high accuracy. At least to get two detector pairs as similar as possible, so that the detector pair for each plane will have the same characteristics. Therefore two power detectors were included on one double sided circuit board, both to make it easier to mount on the final application and to get less pieces to work with. The purpose of the 50 Ω track was to improve the matching individually with the coaxial cable (50 Ω) and the power detector's input.

The development of the power detecting circuit boards has been made in TraxMaker® which is a part of Microcode Circuit Maker®. See Figure 5.18 below for final layout.

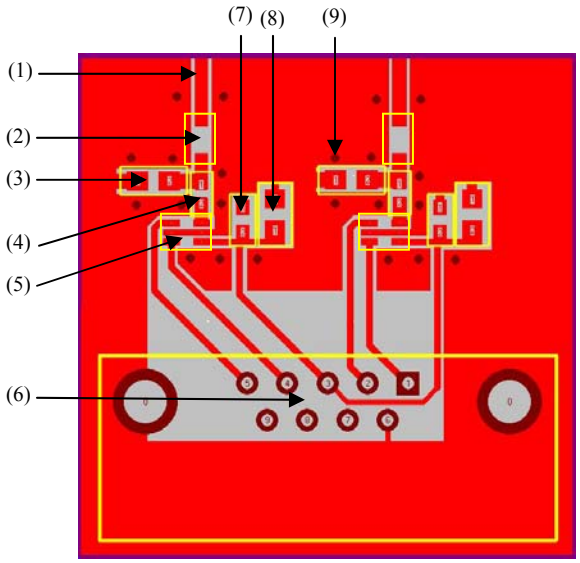

Figure 5.18: *Power detector layout,*
(1): 50Ω Transmission line, (2): MuRata BP filter, (3): 47Ω Resistor,
(4): 1nF Capacitor, (5): LT5534 Power Detector, (6): 9-pin connector,
(7): 100pF Capacitor, (8): 100nF Capacitor, (9): Via hole.

The design and layout of the board is of big importance to suppress interference, especially around the RF signal tracks, (1) in Figure 5.18. It is also important to get a good match between the signal cable and the board and power detector. This was done by making a grounded coplanar waveguide (GCPW)[17] [4] (see Figure 5.19) with 50 Ω characteristics for 2.41GHz. See formula 5.3 for used formulas.

[17] Read more about GCPW at http://www.jlab.org/accel/eecad/pdf/050rfdesign.pdf

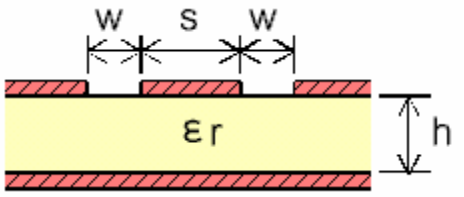

Figure 5.19: *Coplanar Waveguide with Ground Plane.*

$$Z_o = \frac{120 \cdot \pi}{2 \cdot \sqrt{\varepsilon_{eff}}} \cdot \frac{1}{\frac{k}{k'} + \frac{k1}{k1'}} \qquad (5.3)$$

where

$$k = \frac{s}{s + 2 \cdot w} \quad ; \quad k' = \sqrt{1 - k^2} \quad ; \quad k1' = \sqrt{1 - k1^2}$$

$$\varepsilon_{eff} = \frac{1 + \varepsilon_r \cdot \frac{k'}{k} \cdot \frac{k1}{k1'}}{1 + \frac{k'}{k} \cdot \frac{k1}{k1'}} \quad ; \quad k1 = \frac{\tanh(\frac{\pi \cdot s}{4 \cdot h})}{\tanh(\frac{\pi \cdot (s + 2 \cdot w)}{4 \cdot h})}$$

Z_0 was set to 50 Ω and the width of the track was set to 1 mm. With these values we can solve the spacing around the track to get the right dimension for a good match. The FR-4 board has the following specifications:

Table 5.1: *FR4 board specifications.*

Thickness(h)	**ε_r**	**Cu Thickness**
1.59 mm	4.2 (at 2.4 GHz)	36 µm

MatLab were used to solve w (spacing), with an impedance of 50 Ω and a track width (s) of 1mm, the spacing ends up at 0.17 mm on each side of the track. Due to the restrictions of the machine these exact measurement can not be implemented. The thinnest spacing the machine can mill out is 0.2 mm, and with this dimension we re-calculated the Z_0 in MatLab. The final input impedance of the power detector board is then 51.9 Ω instead of 50 Ω, with s = 1mm and w = 0.2 mm, which still is good enough. As a complement to these calculations, a coplanar waveguide calculator from I-Laboratory [5] was used to confirm the results.

The via-holes are used to electrically connect the ground plane to the surrounding conductors on the board's top layer. The main function for doing this was to assure that the potential stays the same all over the PCB and by this make the board less sensitive for interfering signals and noise.

Two boards were milled out in the PCB-mill, and the components carefully soldered in place, se Figure 5.20 for final result.

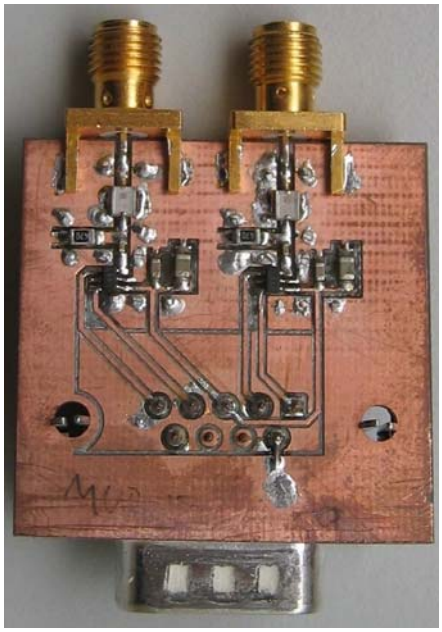

Figure 5.20: *Final power detector board.*

The following graph shows the characteristics from the two power detector boards, the measuring was done with a signal generator where two measurements were done (frequency response and logarithmic power response).

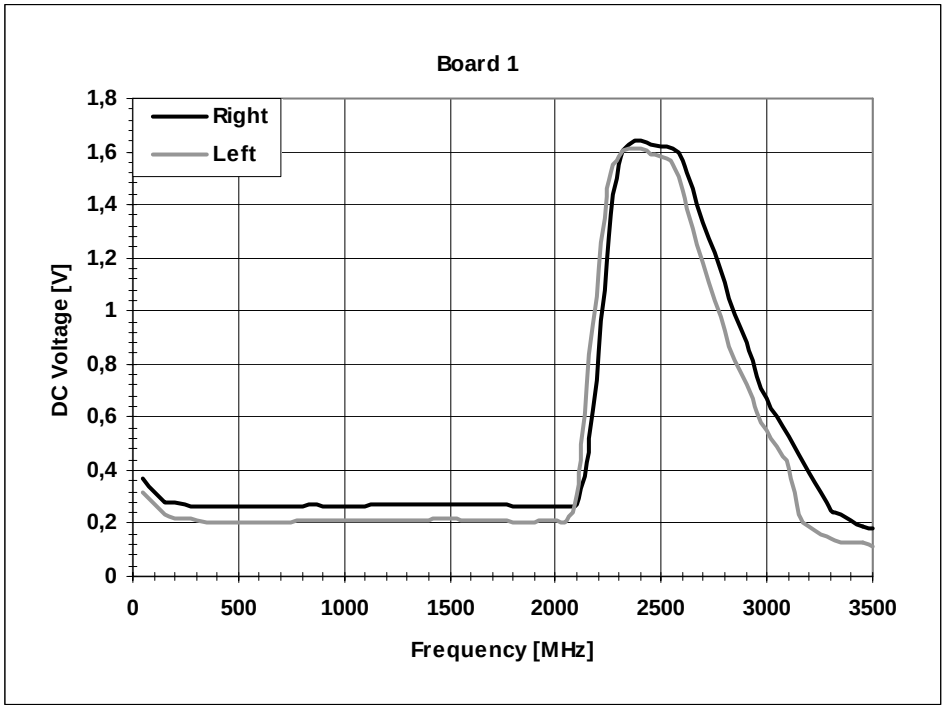

Figure 5.21: *Board 1 Output Voltage vs. Frequency (-20 dBm input signal).*

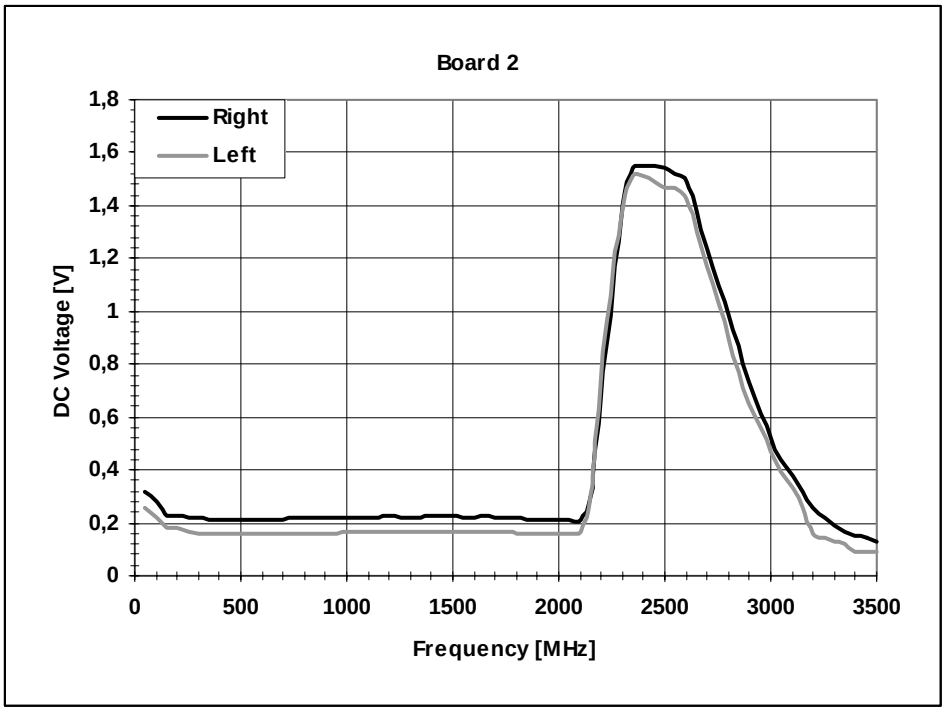

Figure 5.22: *Board 2 Output Voltage vs. Frequency (-20 dBm input signal).*

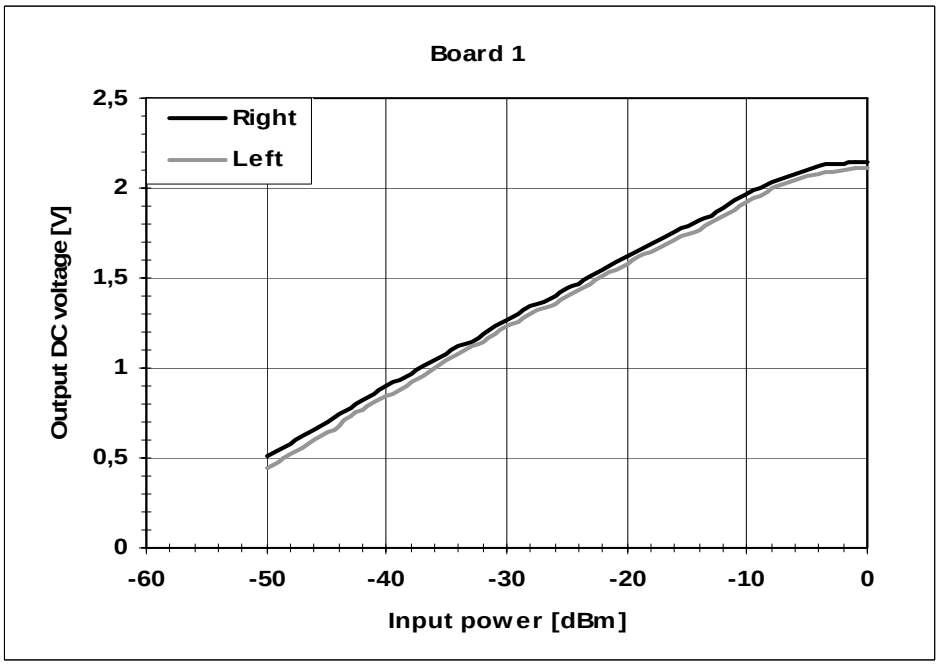

Figure 5.23: *Board 1 Output Voltage vs. RF Input Power (2.4 GHz input).*

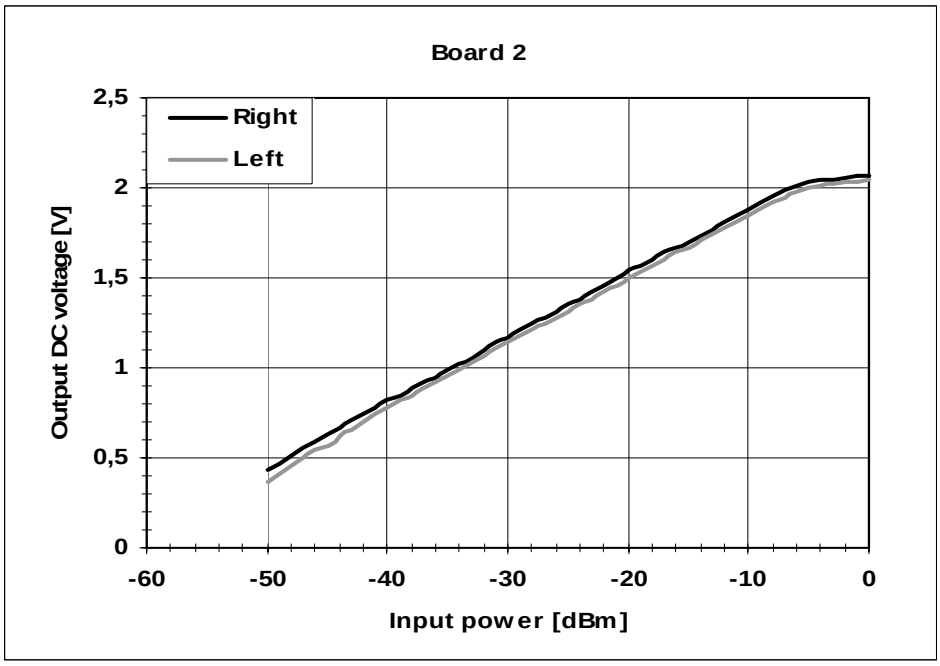

Figure 5.24: *Board 2 Output Voltage vs. RF Input Power (2.4 GHz input).*

There are still some small differences between the boards and the two detectors on each board, as seen on the Figures above. But the differences are small enough to be compensated in the software after the analog to digital conversion.

5.6.1 Shielding

One dilemma with these power detector boards were that they receive signals without any antenna connected. The measured signal strength received from the boards itself was around 1V, which correspond to -34 dBm. This was when a 10 dBm signal was transmitted in the anechoic chamber with a transmitter antenna gain of 10 dB. This problem could not be left out because it can produce an incorrect output to the microcontroller. To solve this problem the power detectors were placed on the other, non reflecting side of the reflector disc. They were also shielded from other signals like WLAN[18] and other interfering equipment. Two small grounded aluminium boxes were constructed to hold the power detector boards. This electromagnetically shields the boards, and the only signal received is from the Yagi feed antennas. The boxes were made in the workshop and we had three connectors out from the boxes. Two inputs for the receiving signals plus one output that connects to the microcontroller via a 9-pin connector. See Figure 5.25 for the result.

[18] Wireless Local Area Network

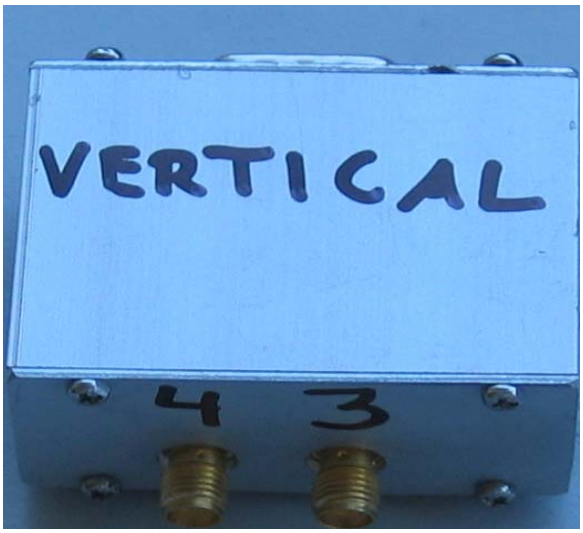

Figure 5.25: *Shield box for power detector board.*

5.7 Where to place the feed antennas

This problem can be solved in many ways, but there are two factors that could not be avoided. If the feed antennas are placed to close to the focal point, the system might start to self oscillate, due to the restrictions of the DC motors (the resolution). If the antennas are placed to far apart, the UAV can fly too far out of the reflector antennas mainbeam and the received signal might be too weak. Another problem with too much spacing between the antennas is that it can detect the side lobes of the reflector disc, which would make the tracking device point in the wrong direction. In Figure 4.3 and 4.4 the radiation pattern of the reflector disc shows how many degrees from the focal point the side lobes are located. With the radiation pattern as a reference we choose to place two horizontal feed antennas slightly outside the reflector antennas horizontal beam width, more exactly with an angle of 4.3° (or 30 mm) from the focal point. According to the radiation pattern plots the signal level has attenuated 3.5 dB at this distance.

For the vertical feed antennas there was a physical limitation, due to the dimensions of the centre Yagi antenna in the focal point, see Figure 5.26. The centre antenna has a width of 50 mm, which makes it impossible to place the vertical feed antennas any closer than 50 mm from the focal point without interfering with the radiation patterns. The vertical feed antennas were placed with an angle of 7.1° out from the focal point with an attenuation of 5 dB. With these positions the side lobes were no obstacle in the vertical plane, but the signal level is attenuated a bit more than in the horizontal plane. See Figure 5.26 for the final assemble of the Yagi antennas.

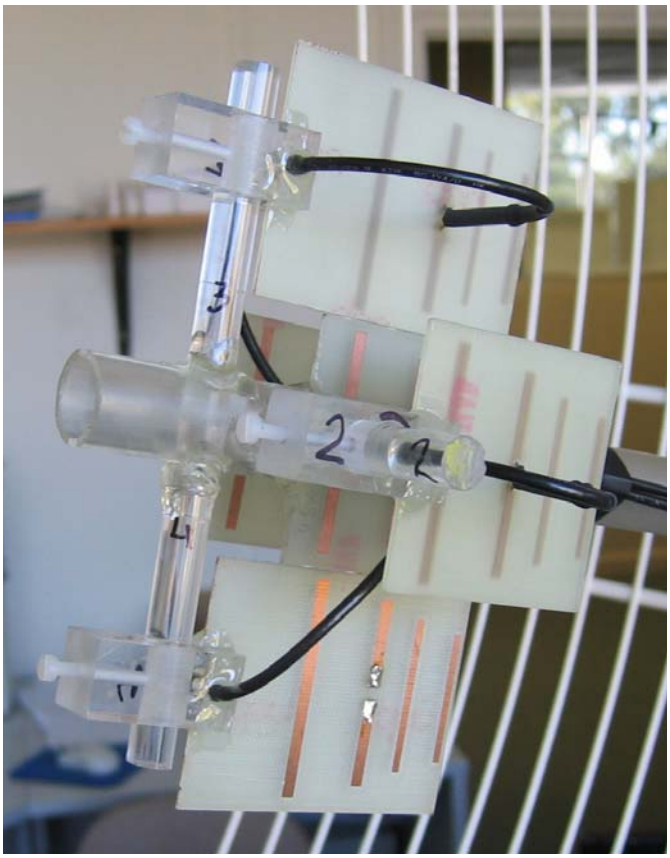

Figure 5.26: *Final Yagi assemble.*

With an attenuation of 5 dB the gain at the vertical feed antennas decreases to 17.79 dB. With this new gain, a new maximum distance can be calculated with Friis formula (4.2).

$$20\log(R) = P_T + G_T + G_R - P_R - 20\log(f_{MHz}) - 32.44$$
$$\Rightarrow R = 343\,\text{m}$$

This is the received signal strength when the antenna is pointing straight towards the UAV. When the transmitter starts to move, for example to the right, the mainbeam moves in the opposite direction, and the left Yagi antenna, seen from behind, will detect a stronger signal. So even if the detectors can not detect the signals when the system is in balanced, they will detect a stronger signal from one of the feed antennas when the UAV flies out of the "mainbeam". Because of this, the maximum tracking distance will not decrease as much as in the calculations above.

As can be seen in Figure 5.27 the aperture size of the reflector disc gets slightly smaller when the beams comes in with an angle (UAV on its way out of the main lobe).

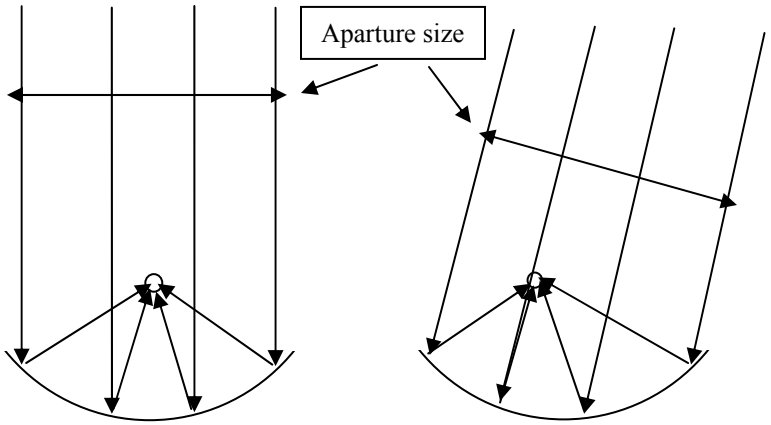

Figure 5.27: *Reflector reflections.*

6 Actuator system

The actuator system in this project consists of two DC motors that are controlled by two commercial RC speed controllers.

6.1 DC Motors and Gearing

The motors that are being used are two old windscreen wiper motors that already was the property of the ECSE department. The motors might not be ideal for their purpose in this project, but as there were no budget to buy a couple of new motors they had to do. We did not have access to any information regarding these motors and gearboxes, so the motors and gearboxes were taken apart, so further examination could be done.

6.1.1 Gearing

The maximum speed out from the gearbox was measured to 32 rpm, by calculating the ratio of the gearbox the initial speed of the motor could be determined. As seen in Figure 6.1 there is a wormgear axle that drives the two bigger gears. They drive a third even bigger wheel for the final gear (not showed in the picture). To calculate the gearing we counted the teeth on the wheels, and the pitch of the gearing on the worm gear.

The gearing from the worm gear to the first wheel was determined by the following calculations:

$$\frac{C_{gear}}{W_{pitch}} = \frac{31.05 \cdot \pi}{3} \approx 32 \qquad (6.1)$$

Where C_{gear} is the circumference of the cog wheel and W_{pitch} is the pitch of the worm gear (and the cog wheel). The gearing between the next two cogwheels is just determined by measuring the diameter of the wheels. The big wheel has a diameter of 48 mm and the small 15.7 mm, which means the gearing, is 48:15.7 which is approximately 3:1. This leaves us with a total gearing of 96:1 (32*3:1), which means that the final driver rotates 96 times slower than the motor.

With a gearing of 96:1 the maximum speed of the motor at 12 Volt is ~3100 rpm (~32 rpm * 96). With these facts we also calculated the overall gearing, from the DC motor to the actual driven wheel for each plane. For the horizontal movement there is a rubber wheel with a diameter of 35 mm that drives the big horizontal disc directly at a distance of 240 mm from its centre. This gives an additional gearing of 13.7:1, see formula 6.2.

$$\frac{\text{Diameter}_{\text{Horizontal disc}}}{\text{Diameter}_{\text{driver}}} = \frac{240 \cdot 2}{35} = 13.7 \qquad (6.2)$$

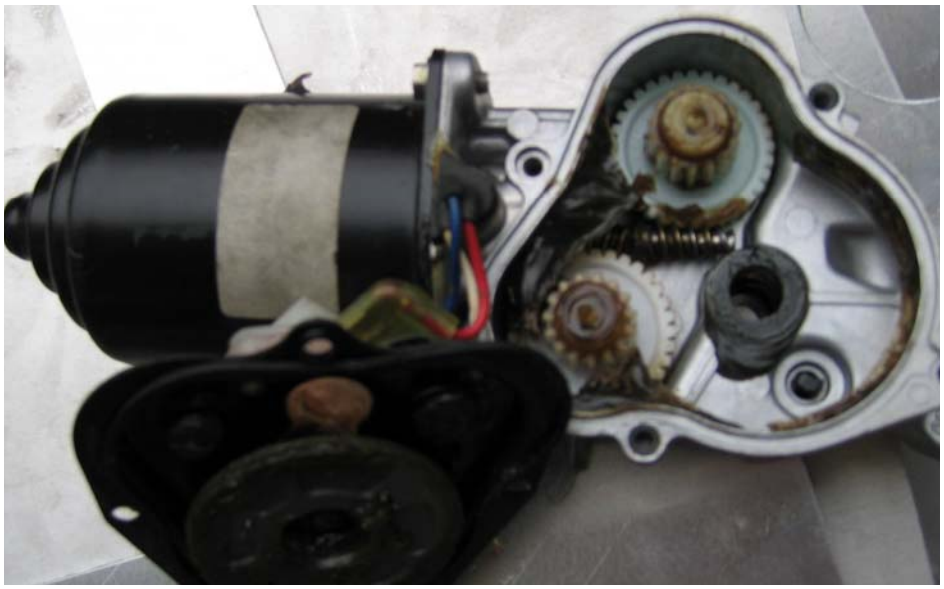

Figure 6.1: *DC Motor with gearbox.*

For the vertical plane the same formula is used (6.3) to determine its additional gearing. Here the drive wheel has a diameter of 13 mm and it drives a bigger wheel with the diameter of 180 mm. The actual transference between the two wheels is by belt-drive and the extra gearing for the vertical plane is 13.85:1, see formula 6.3.

$$\frac{\text{Diameter}_{\text{Vertical disc}}}{\text{Diameter}_{\text{driver}}} = \frac{180}{13} = 13.85 \qquad (6.3)$$

The total gearing from the DC motor to the actual drive for each of the plane ends up with:

- Horizontal: $96 \cdot 13.7 = 1315 : 1$
- Vertical: $96 \cdot 13.85 = 1329 : 1$

6.1.2 Motor torque

The toque needed to steer the antenna stand can roughly be calculated with formula 6.4 and 6.5 (formulas taken from Physics Handbook [6]). This might not correspond to the real torque needed, but gives an idea what would be needed.

$$\tau = I \cdot \alpha \qquad (6.4)$$
$$\tau = F \cdot r \qquad (6.5)$$

Where I = Rotation Inertia, α = Angular acceleration, F = Force and r = radius.

To find the moment of inertia, the following equation is used:

$$I = m \cdot r_1^2 \qquad (6.6)$$

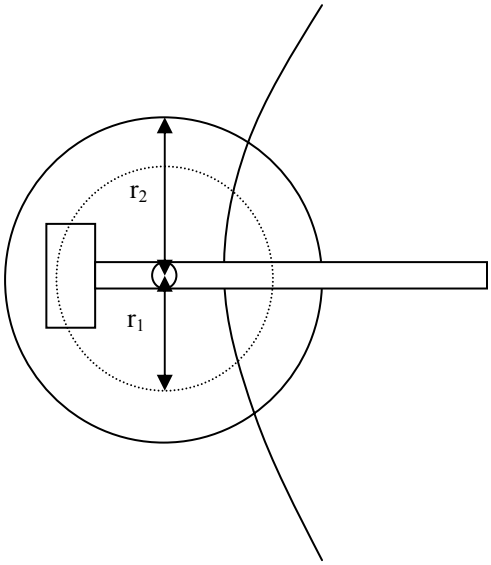

Figure 6.2: *Simplified top view of tracking device.*

Where r_1 is the mean distance from the centre to the rotating weight. This distance is hard to measure because the quite complicated construction. A rough approximate distance of 200 mm was used. With this distance and a mass of 14 kg, formula 6.6 can be used to calculate the moment of inertia:

$$I = 14 \cdot 0.2^2 = 0.560 \,\mathrm{kg} \cdot \mathrm{m}^2$$

To calculate the torque, the angular acceleration also needs to be known. This is calculated with the following formulas:

$$\alpha = \frac{\omega}{t} \ \mathrm{rad/s}^2 \qquad (6.7)$$

Where ω is the maximum angular speed derived from maximum speed the tracking device can turn.

$$\omega = \frac{\theta}{t_\theta} = \frac{2\pi}{25.5} = 0.247 \ \mathrm{rad/s}$$

t is the time it takes to accelerate from standing still to maximum speed, which is set to 1 second. This gives an angular acceleration of:

$$\alpha = \frac{0.247}{1} = 0.247 \ \mathrm{rad/s}^2$$

Now the torque can be calculated, using formula 6.4.

$$\tau = 0.560 \cdot 0.247 = 0.138 \ \mathrm{Nm}$$

The force that needs to be applied at distance r_2 is determined by rearranging formula 6.5 slightly:

$$F = \frac{\tau}{r_2} = \frac{0.138}{0.23} = 0.601 \text{ N}$$

To this force, frictions and forces caused by wind also have to be added, but after we tested the windscreen motors we realized that they were more than powerful enough. Hence no time was spent measuring the torque of the motors.

6.2 Speed controllers

Because of the microprocessor's low power output it is impossible to supply the DC motors with power without an additional power supply. Therefore a speed controller or a DC motor drive (H-bridge) that drives the motors is needed. Commercial RC speed controllers are easy to use together with microprocessors like the PIC16F877 and it uses a technique called Pulse Width Modulation; PWM (read more about PWM in chapter 7.2.2). By changing the pulse width of the PWM signal, the average output power can be lowered due to shorter pulse width or raised with a wider pulse width (or the opposite depending on the design of the speed controller).

The standard that is being used is the Radio Control (RC) community standard. The speed controller used in this project was a Marine ESC-50, which is a speed controller designed for model boats (see Figure 6.3).

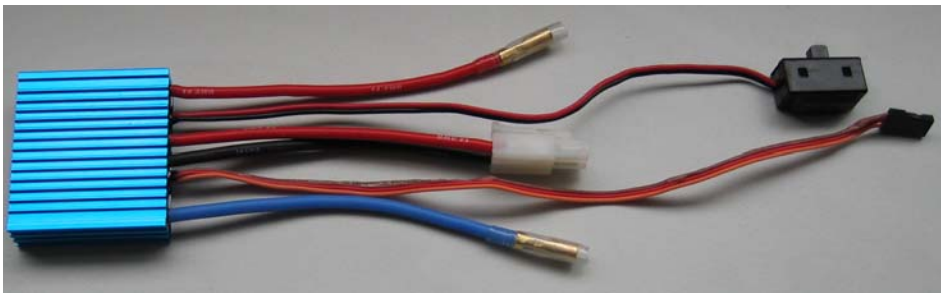

Figure 6.3: *Marine ESC-50.*

The RC standard uses a 50 Hz signal with pulse width varying between 1 and 2 ms. A neutral control pulse is defined as the signal that the speed controller first needs when it starts, the pulse width for neutral is 1.5 ms. If an incorrect signal is present at the start up of the application, the speed controller will not respond.

Table 6.1: *Pulse Width specifications.*

Pulse Width	Direction
1.5 ms	Neutral / Stop
1.0 – 1.5 ms	Clockwise (+)
1.5 – 2.0 ms	Counter-clockwise (-)

The Marine ESC-50 is capable of supplying up to 50A of continuous motor current in one direction. In the opposite direction it can only supply up to 20A of constant motor current. This is one of the problems with a model boat speed controller, because it makes the tracking device move faster in one direction. In our requirements for how fast the reflector disc should follow the slower direction is used as reference. The speed controllers is easily switched on and off with a power switch, which function is to stop the power supply to the DC motor.

7 Controlling unit

The control unit is based on the PIC16F877 microcontroller from Microchip. The development board used was the PIC-P40B-20MHz prototype board from OLIMEX[19]. That board comes with a power supply circuit, crystal oscillator circuit, serial communication RS232[20] port and ICSP/ICD[21] port.

A bootloader[22] was burned to the PIC16F877, so easy re-programming over the serial communication port could be done. The software development environment used was Microchip's MPLAB (version 7.01) with HiTechs PICC compiler. The reason why these tools were used was mostly due to previous experiences.

7.1 Microchip PIC16F877

The PIC16F877 microprocessor is a standalone device optimized for control applications. It is a powerful controller with many features and is relatively cheap. For our application this microprocessor is more then powerful enough.

The PIC16F877 has 8K Flash program memory, 10-bit A/D converters, 33 I/O pins and many other features in a 40-pin DIP package [7]. See Figure 7.1 for full pin layout.

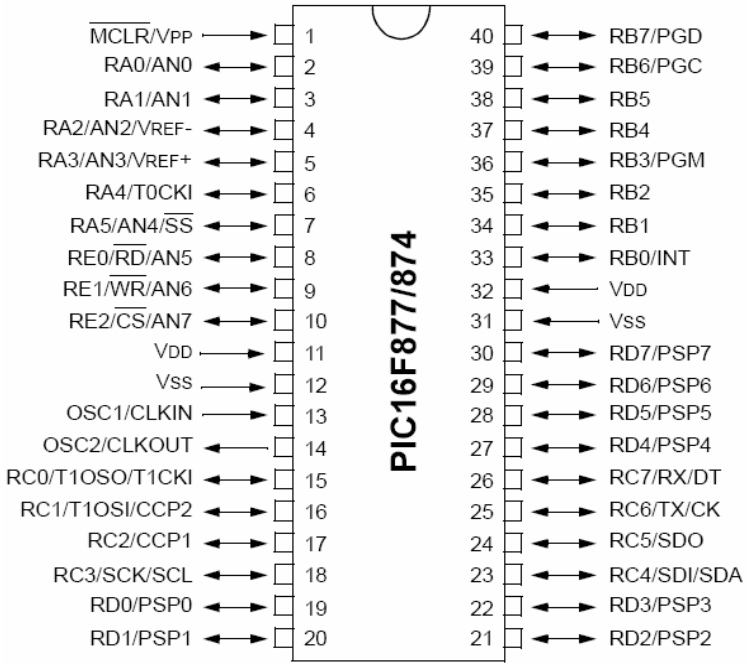

Figure 7.1: *Microchip PIC16F877 pin layout.*

[19] Olimex (http://www.olimex.com/dev/index.html)
[20] Serial data communication standard
[21] A port that makes it possible to perform in circuit debugging
[22] A program that is running in the lower memory area, that makes it possible to re-program the processor using the serial port.

The ports that are used on the microprocessor are mainly port A and port E, the other ports are also used but they are not as important for the performance as port A and port E. See Table 7.1 for used pins. All the ports are bi-directional input/output ports and depending on how the register for each port is initialized, the declaration for each pin can be set as either input or output.

Port A is used to convert the DC level from the signal detection system to a digital value. The resolution of the A/D can be set up to 10-bits, but only 8-bits are used in this application. This is due to the flickering output signal from power detectors, so the two Least Significant Bits (LSB) after the A/D conversion will be discarded. The resolution is still good enough for the program to detect differences between the voltage levels from the power detectors.

Formula for the resolution:

$$\text{Resolution} = \frac{V_{ref}}{256} \tag{7.1}$$

$$\text{Resolution} = \frac{5\,\text{V}}{256} = 19.53\ \text{mV/bit}$$

Due to the fact that the maximum voltage from the power detectors is 2.4 V, the A/D range is unnecessary high. This can be improved simply by connecting two 100 kΩ serial coupled resistors over the supply voltage from the microprocessor to ground and connecting pin RA3 between the two resistors. By doing this, the reference voltage decreases to half (2.5V) and the resolution of the A/D increases. The new resolution is 9.76 mV/bit instead of 19.53 mV/bit, as seen in formula below.

$$\text{New Resolution} = \frac{2.5\,\text{V}}{256} = 9.76\ \text{mV/bit}$$

Port E:s main function was to send the correct PWM signals to the speed controllers depending on the DC voltage on Port A:s analog inputs. The pin RE1 is the output control signal for the azimuth plane and pin RE2 generates the control signal for the elevation plane. How this PWM signal was implemented to work at 50 Hz is explained in section 7.2. The third pin on Port E, RE0, is used as an input to determine on which side of the 0° reference the antenna (and also the UAV) is located (more about this in section 7.2.5).

Table 7.1: *Used pin details.*

Used pin details		
PORT	**PIN**	**Function**
PORT A	RA0	Analog input power detector 1
	RA1	Analog input power detector 2
	RA2	Analog input power detector 3
	RA3	Voltage reference
	RA5	Analog input power detector 4
PORT B	RB0	Manual horizontal steering +
	RB1	Manual horizontal steering -
	RB2	Manual vertical steering +
	RB3	Manual vertical steering -
PORT C	RC6	Receive data serial
	RC7	Transmit data serial
PORT D	RD0	Manual/Automatic control switch
	RD1	Manual/Automatic diode
	RD2	Vertical in balance diode
	RD3	Horizontal in balance diode
	RD4	Enable/Disable vertical power detector
	RD5	Enable/Disable horizontal power detector
PORT E	RE0	Vertical position sensor
	RE1	PWM out Horizontal
	RE2	PWM out Vertical

7.2 Software

The software in this application is written in C and compiled with Hi Techs PICC Light Compiler. The compiler is free to use but limits the memory usage to 2 kB, still it works fine because the written program in this application is relatively small. Earlier experiences with HT PICC were also a reason of using this compiler.

The software's main task is to read analog values from the power detectors, compare these and set the pulse length of the PWM so that the motors will steer the antenna towards the target and hence decrease the differences between the power detectors. When the difference in DC voltage between a pair of power detectors is within a specified limit, the pulse length of the specific PWM signal is set to 1.5 ms. This means that the motors will stand still. A diode is set to light when the target is in balance to inform the user about this. Serial communication is also available if the DC levels on the analog inputs of the processor should be monitored. To decrease the load of the processor, the DC values are only transmitted after every 30 analog read. An improvement of this system is to add a display that shows the DC levels and other useful information, but time was not given to do this.

7.2.1 Program flow charts

The program consists of one main loop, that repeatedly checks if it is time to read new analog values, if there is a new character in the USART[23] buffert or if the system is set to manual mode, see Figure 7.2 for flow chart.

Three interrupts also needs to be taken care of. Two of the interrupts are generated from the internal timers, timer1 and timer2. These timers generate the PWM signal to the speed controllers (more about this in section 7.2.2). The interrupt handlers for these interrupts controls if the PWM pins (RE1 and RE2) should be set high or low. The last interrupt is generated if a new character is found in the USART read buffert, the interrupt routine sets a variable bit high, so the character can be read later. Why the character is not read immediately in the interrupt routine is to make the interrupt routine as short and fast as possible.

When a new analog value is read from the power detector outputs, there are also some compares and calculations to be done, before the correct PWM signal can be set, see Figure 7.3 for a flowchart over this procedure. Observe that if the analog input is too high, the power detectors are turned off, and the control diodes on the main unit starts to flash. This is made of security reasons to save the power detectors for a too strong RF signal, which could destroy them. The only way to restart the power detectors is to remove the too strong RF signal and reset the main unit.

As the system can move 180 degrees in the vertical plane, the horizontal Yagi-antennas will "change place", left becomes right and vice versa. An optical sensor indicates on what side of the "0" degree mark the antenna is located. The software also has to compensate for the small differences in signal strength from the power detectors (as seen in Figures 5.21 to 5.24). After this is done, the analog input values are compared and the PWM is set to make the tracking device move towards the UAV. The DC-levels are transmitted over the serial interface every 30 analog read.

[23] Universal Synchronous/Asynchronous Receiver/Transmitter

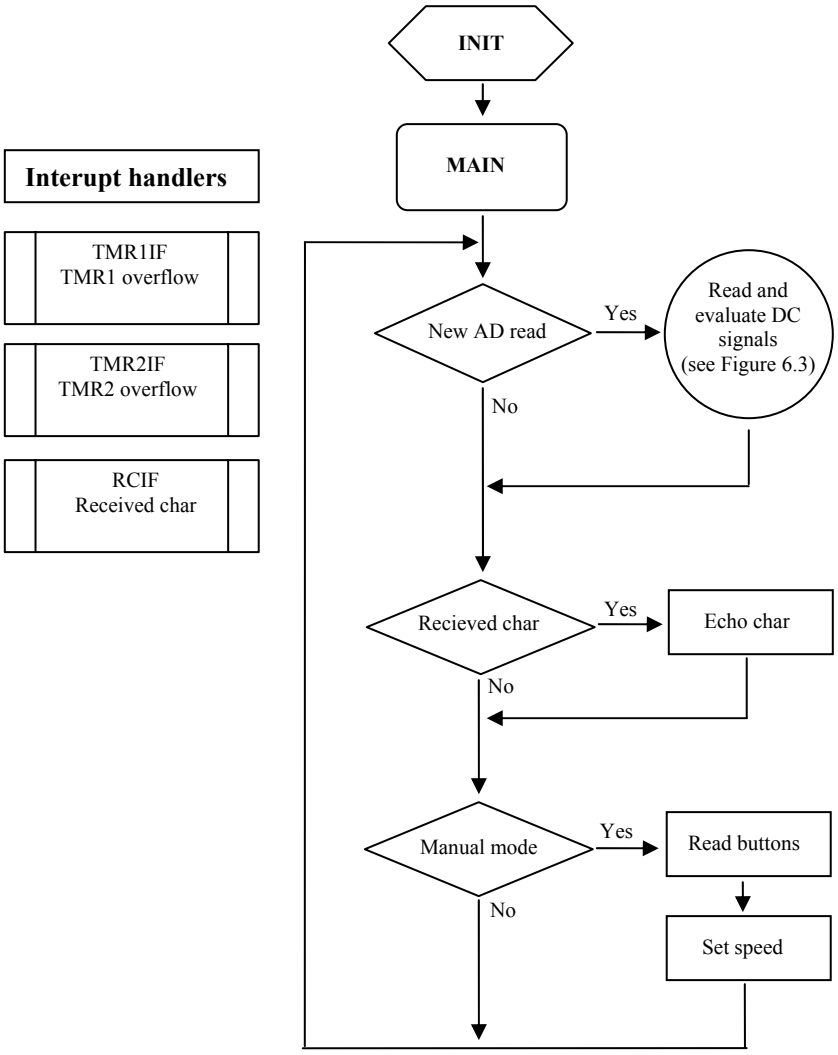

Figure 7.2: *Program flow chart.*

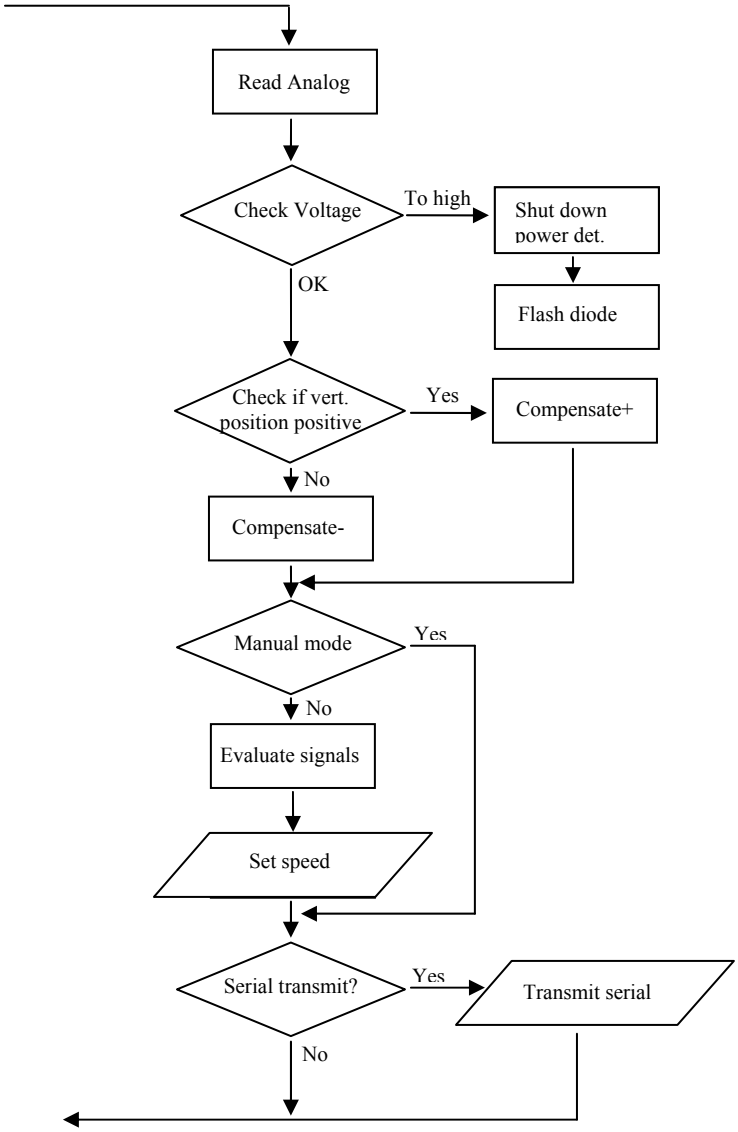

Figure 7.3: *Analog read and compare flow chart.*

7.2.2 PWM

Pulse Width Modulation, is a technique that can be used to control the amount of power to a load without loosing any significant power in the driver. A DC level is pulsed with a set frequency, by varying the pulse length; the average power can be controlled.

In our application a secondary power supply is needed due to the high currents running through the DC motor. This power supply (the speed controller) needed a PWM signal of 50 Hz with the pulse length varying between 1 and 2 ms (read more about the speed controller in chapter 6.2).

The Microchip PIC16F877 has an internal "pre-made" PWM module, but it has limitations, it can not [7] produce as low frequent signals as 50 Hz. So an own PWM routine had do be developed. This was used with the help of the processors internal timers (timer1 and timer2).

Timer1 was set to generate an internal interrupt every 10 ms (100 Hz), and with a control bit the two outputs, pin RE1 and RE2 can each generate a signal at 50 Hz. Timer2 was used to control the pulse width of the two outputs, so that the duty cycle could vary with time. The same control bit as in Timer1 is used to manage which output that is changing.

Timer1 can be operated in two different modes, as a timer and a counter, both with 16 bits resolution. To set the correct mode the "clock select bit" TMR1CS (T1CON<1>) is either set or cleared. In this application timer1 is used as a timer and therefore the T1CON bit is cleared. The timer is enabled by setting the on/off bit TMR1ON (T1CON <0>). The functional use of timer1, as mentioned before, is to generate an interrupt every 10 ms, so two independent PWM signals can be generated.

Timer1 starts to count from a specified value ($0 - 2^{16}$) and when overflow occurs (at 2^{16}), an interrupt is generated [7]. To know what this start value is supposed to be to generate a 100 Hz signal, the oscillator frequency needs to be known. In our application a 20 MHz (F_{osc}) crystal was used.

$$T_{1int} = 4 \cdot \frac{1}{F_{osc}} \cdot T_{1pre} \cdot \text{Number\_of\_inst.\_cycles} \qquad (7.2)$$

Where T_{1int} is the required time between interrupts and T_{1pre} is the prescaler[24] value. By re-arranging formula (7.2), the number of instruction cycles can be decided. The formula then looks like this:

$$\text{Number\_of\_inst.\_cycles} = \frac{T_{1int}}{T_{pre}} \cdot \frac{F_{OSC}}{4}$$

In our case:

$$\text{Number\_of\_inst.\_cycles} = \frac{10 \cdot 10^{-3}}{1} \cdot \frac{20 \cdot 10^{6}}{4} = 50000$$

This means that timer1 needs to increase 50000 times before an overflow and an interrupt occurs. This value is subtracted from 2^{16} and written to the TMR1RESET_HIGH and TMR1RESET_LOW registers.

[24] Prescaler, decreases the speed of the counter by a fixed multiplier (1, 4 or 16)

Timer 2 is an 8-bit timer, with both a prescaler and a postscaler[25] [7], and it is in this application used to set the correct pulse width for the PWM. Due to the specification of the speed controllers, which need a pulse width between 1-2 ms, the postscaler and prescaler is set depending on how fast the timer should increase.

To get the correct interrupt interval with a 20 MHz crystal the prescalers control bits T2CKPS1 and T2CKPS0 (T2CON<1:0>) is set high to get a prescaler of 1:16. The postscaler is set to 1:3 by setting the control bits 3-6 in the T2CON register to 0010. With these settings Timer2 only increases every 48 (16*3) instruction cycle. Timer 2 generates an interrupt when it has increased to the same value as the 8-bit register PR2 (see Figure 7.4 for timer2 block diagram). The formula for Timer2 interrupt generation looks like this:

$$T_{2int} = \frac{4}{F_{osc}} \cdot PR2 \cdot T_{2pre} \cdot T_{2post} \qquad (7.3)$$

With formula 6.3 the interrupt interval could be calculated:

$$T_{2int} = 200 \cdot 10^{-9} \cdot [0 \rightarrow 255] \cdot 16 \cdot 3 = [0 \rightarrow 2.448] \cdot 10^{-3}\ \text{s}$$

The time it takes for Timer2 to generate an interrupt, varies depending on the PR2 register. The PR2 register is updated after every A/D conversion and comparison of the 4 feed antennas. As the speed controllers need an initialized pulse width of 1.5 ms to work the PR2 is set to 155, which corresponds to a pulse width of 1.5ms.

During runtime PR2 is set to 155 plus/minus the difference of the DC levels from the power detectors, every other time from the horizontal and vertical planes. As mentioned before a control bit is used to keep track of which PWM output that should change.

The procedure goes like this, for every interrupt Timer1 generates, PR2 register is set (depending on last analog read), the corresponding output pin (RE1 or RE2) is set high and Timer2 is started by setting the TMR2ON high. Timer2´s output register TMR2 is then incremented until it matches the PR2 and generates an interrupt. When this occurs the TMR2 resets and puts the defined output pin (RE1 or RE2) low (and new analog values are read). This is repeatedly done every 10 ms (100 Hz). See also Figure 7.5 for a timing diagram of the PWM.

[25] Postscaler, a multiplier that sets how many times the counter has to reach a specific value before an interrupt is generated (1, 4 or 16 times)

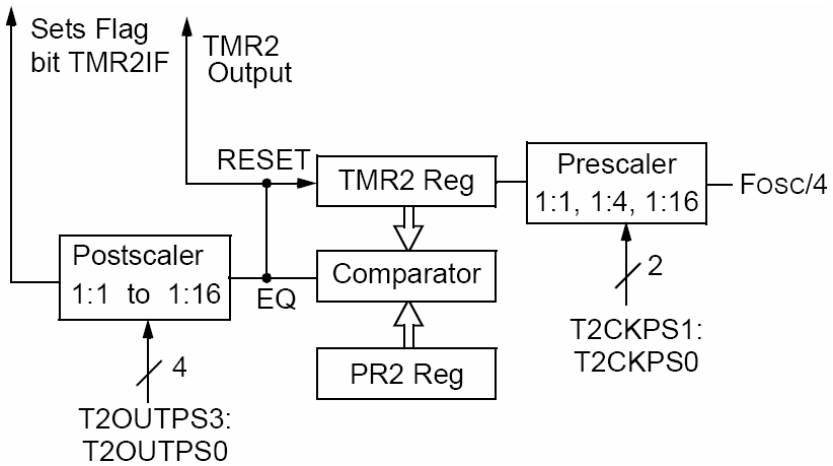

Figure 7.4: *Timer2 Block Diagram.*

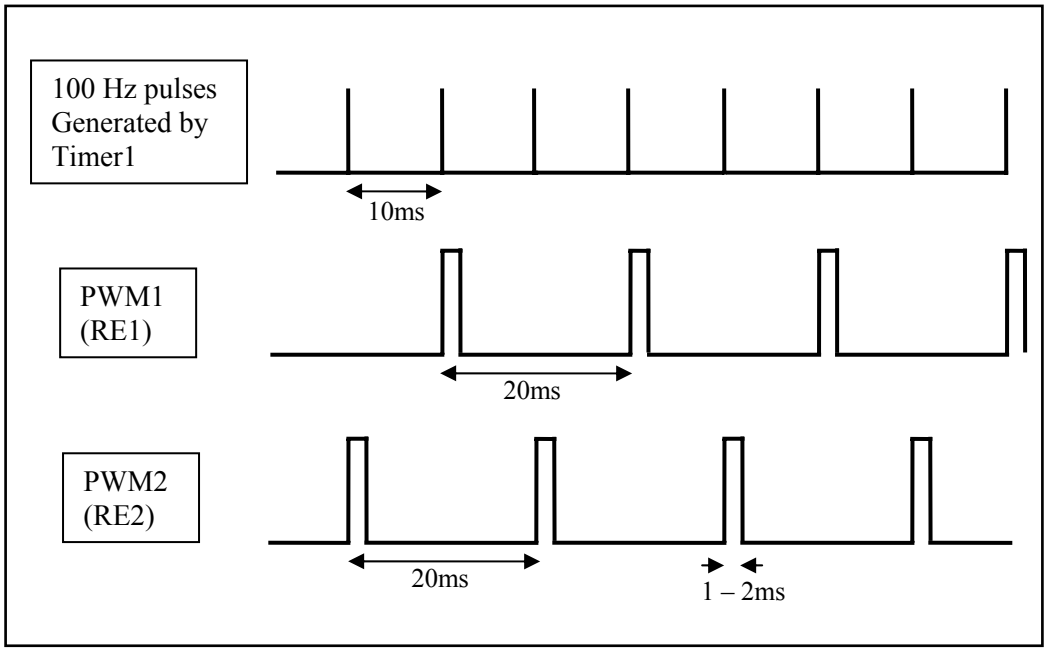

Figure 7.5: *PWM timing diagram.*

7.2.3 AD-routine

The PIC16F877 have a 10-bit analog to digital converter with 8 pins that can be configured as both digital inputs/outputs, analog references or analog inputs. In this project four of these inputs were used as analog inputs and one as an analog reference. The analog reference is set to a voltage level which is supposed to be the maximum voltage that the analog inputs can reach. From formula (7.1), a reference voltage of 2.5 V was used because the maximum voltage the power detectors can climb up to is ~2.4 V. By using the lower reference voltage, higher resolution can be achieved as the A/D conversion only converts between 0 to 2.5 Volt instead of 0 to 5 Volt.

As explained earlier in this report, the A/D routine in this project was only run in 8-bit mode, because 10-bit mode was superfluous in this application.

The Analog to Digital conversion is repeated after every time Timer2 have generated an interrupt. As four power detectors were used, four analog to digital conversions have to be performed. These values is later compared, subtracted and written to the PR2 register to set the pulse width.

7.2.4 Compensation

Due to the differences between the four power detectors some kind of compensation was needed. In Figures 5.23 and 5.24 we show that the errors for the two pairs of detectors are constant independent of the input signal strength. To get the exact difference, the stand was placed in the anechoic chamber to make sure that no surrounding signals were interfering. With no input signal at all the power detector chips gave an output as followed, seen from behind the antenna stand:

- The upper antenna's detector chip ~11 mV
- The lower antenna's detector chip ~17 mV
- The right antenna's detector chip ~13 mV
- The left antenna's detector chip ~10 mV

With these values the compensations for the vertical and horizontal chips were 6 mV respectively 3 mV. The compensations were done in the software where the weakest detector output was increased to match its pair detector.

7.2.5 Vertical Location Sensor

To get the system to steer correctly, one thing needed consideration. Due to how the horizontal feed antennas are placed on the antenna boom, the microprocessor compares the two DC levels from the power detector boards to steer in the correct direction. This means that if the left Yagi, seen from behind, has the strongest signal level the motor should steer the antenna to the right to obtain balance again between the two vertical Yagi antennas. Once the reflector disc goes past the vertical 0° degrees reference the horizontal feed antennas change place, the right Yagi becomes the left one and vice versa. This was solved by using an optical sensor that is either high or low depending on the location of the vertical movement. See Figure 7.6.

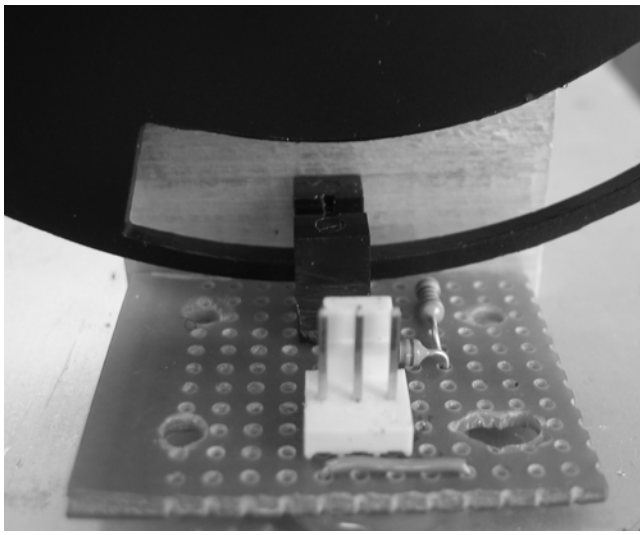

Figure 7.6: *Optical Sensor.*

The black disc has a 95° open space and it begins exactly when the vertical position of the reflector disc is at the 0° reference mark. The rest of the black disc is solid which makes the optical sensor change state depending on location. This state is continuously checked by the microprocessor to know where the antenna is in the vertical plane. When the optical sensor change state the microcontroller makes the necessary changes for the comparisons between the two horizontal Yagi antennas.

This always makes the antenna stand move in the correct direction of motion.

7.3 Safety control

Due to the mechanical restrictions in the vertical plane an emergency break was needed. This was chosen to be left out as a task for the microprocessor and instead two mechanical switches was mounted on the antenna stand. The purpose of these switches was to break the power to the DC motors when the reflector antenna reaches a position further away than -95° and +95° from the relative 0° (where the antenna is pointed straight up). This was required because otherwise the DC motor could drive the reflector disc against the stand and cause damage to the equipment. This safety control is a protection in case the microprocessor will end up in a dead-lock (or some other unforeseen error in the program) and give the wrong control signal to speed controllers.

The switches are located where it should be impossible for the antenna to be, due to the UAV can not fly under the horizon (-90° or 90°). (This might not be 100 % true as the UAV can fly in a valley with the tracking device stranding on a hill. In a special case like this the tracking device has to be leaned to keep track of the UAV.) If the antenna would end up in either of these positions the switches will break the power and the only way to steer out of the position is to manually control the tracking device. Before this can be done the controlling unit has to be switched to manual mode and a safety reset switch that overrides the emergency switches needs to be pushed in. This button was placed away from the manual control unit, so a “dead mans grip” has to be used to steer the antenna back on track. Figure 7.7 below shows the schematic of this safety protection.

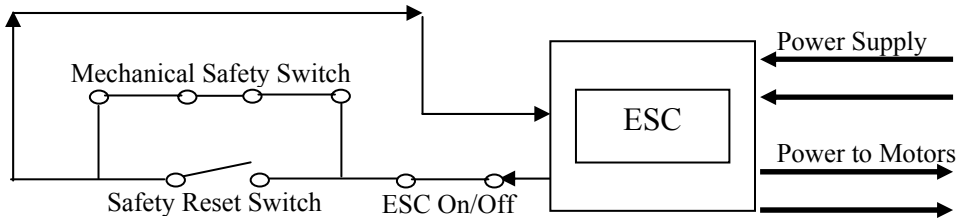

Figure 7.7: *Safety control schematic.*

As seen in the schematic the speed controller is switched off if the loop is opened, which will break the power to the DC motor. The speed controller's on/off button should always be on and depending on the additional switches status the loop is either opened or closed. To supply to the DC motors constantly with power the loop needs to be closed. The mechanical switches do not conduct when they are activated and the safety reset switch function is reversed. This makes it possible to put the power back on if the situation occurs and to steer it manually.

8 Testing

Two tests were made with the final product, first in the anechoic chamber and later out on the field. The tests in the anechoic chamber were done mostly to finish the final compensation, where we only could do the test in the azimuth plane. The control of the different planes works more or less exactly the same, due to the similar gearing with the same DC motors. With this in mind we adapted the control of elevation plane in same way as for the azimuth plane. One thing we could not simulate in the anechoic chamber was the maximum speed that the UAV has at closer distances. This was later tested in the field where the UAV, see Figure 6.1, was mounted with a transmitter antenna and video camera.

8.1 Anechoic Chamber

The purpose of the tests in the anechoic chamber was to resemble a real flight test, which is hard to implement due to the ideal conditions in the anechoic chamber. The antenna stand was placed on a rotating disc, with a horn antenna used as a transmitter. While the disc turned the antenna out of balance, the horizontal actuator system compensated the difference by turning the antenna in the opposite direction. This was done for the horizontal plane. In the vertical plane the transmitter antenna was moved by hand, but with the same result as for the horizontal plane.

To resemble the distance between the UAV and the antenna two attenuators was used to lower the power from the transmitted horn antenna. To calculate the theoretical received power at 1 km Friis formula (4.2) was used.

$$P_R\,(\mathrm{dBm}) = P_T\,(\mathrm{dBm}) + G_T\,(\mathrm{dB}) + G_R\,(\mathrm{dB}) - 20\log(R_{km}) - 20\log(f_{MHz}) - 32.44$$

$$P_R\,(\mathrm{dBm}) = 10 + 0 + 23 - 20\log(1) - 20\log(2410) - 32.44$$

$$P_R\,(\mathrm{dBm}) = \text{-}67\ \mathrm{dBm}$$

Knowing the intended received power at 1 km we calculated the transmitted power that should resemble the same environment in the anechoic chamber using the same formula (4.2) from Friis. The distance between the transmitting and the receiving antenna in the anechoic chamber was four meter, and the approximate gain of the transmitting antenna was ~10 dBi.

$$P_T\,(\mathrm{dBm}) = P_R\,(\mathrm{dBm}) - G_T\,(\mathrm{dB}) - G_R\,(\mathrm{dB}) + 20\log(R_{km}) + 20\log(f_{MHz}) + 32.44$$

$$P_T\,(\mathrm{dBm}) = \text{-}67 - 10 - 23 + 20\log(0.004) + 20\log(2410) + 32.44$$

$$P_T\,(\mathrm{dBm}) = \text{-}48\ \mathrm{dBm}$$

As seen in the calculations above, a sensitivity of -67 dBm is needed to detect the signals at this distance. The specification of our power detectors were -63 dBm and should not work here, but our tests proved that they did. This proves that the power detectors can detect signals lower that -63 dBm (but the logarithmic response of the chips is very bad with this weak signal).

8.2 Field test

The final test was to actually see if the tracking system could track a flying UAV. A flight test was arranged on a close rugby field the 12 of July, with Terry Cornell, Stewart Jenvey and the pilot Ray Cooper. The UAV used during the flight test was the plane in Figure 8.1, an extremely lightweight electrical driven plane.

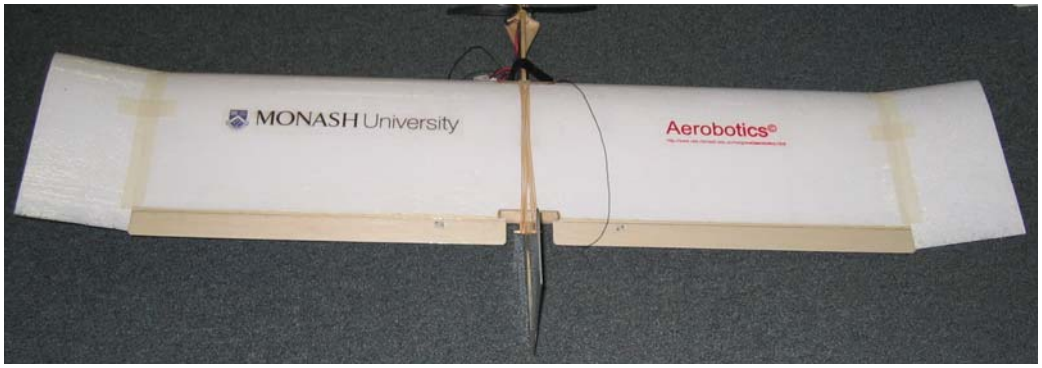

Figure 8.1: *UAV used during flight test.*

A 10mW video transmitter was placed on the small lightweight UAV. The tracking system was aimed towards the plane before lift-off.

The results of the test came out really good; the tracking system was able to track the UAV just as planed. The tracking antenna followed the UAV in a satisfying way at longer distances (approximately up to 600 meter) and a good video signal was received.
The only problem was when the UAV flew at closer distances (<~80 meter) and did sharp turns in the azimuth plane with a high elevation angle, the UAV was then lost. This was predicted due to the speed of the DC motors is to slow and the problem was already taken into consideration.

9 Results, Conclusion and Considerations

In this chapter the result of the different parts will be discussed. Both positive and negative critics will be taken in aspect. We do this to give some helpful hints and considerations about the future development of the project.

9.1 The reflector antenna

The reflector disc antenna is a good choice for this project. First of all it has a high gain and directivity that is well suited for the one-to-one communication with UAV. The second thing is of course the sensor antennas placed around the focal point, which makes the whole idea with comparing the different signals in the different planes work and make it balance at the right position correctly. One problem with the used antenna is the weight, but if the same aperture size and gain would be kept, the reflector antenna would have to be made of another more lightweight material, that probably would increase the price significantly.

9.2 The mechanical design

The mechanic solution works fine as it is, but there are of course improvements that can be done.

One drawback of the design is the weight, with a total weight of 23 kilo it is not very easy to handle. But still, it can not be too light weight either, as strong stability is of big importance. Some easy improvements that could be done, is to use a more light weight bottom plate and main rotating disc. This could easily be realized by removing "unused" material of these parts. But the best solution would be to have these parts made by aluminium as well, as the particle board also is very sensitive to water, and a bad choice for outdoor usage.

9.3 Signal detecting unit

This unit works in a satisfying way, but due to losses the sensitivity decreases. This is because there are losses in several spots in the chain (from antenna to power detector chip). First of all the cables used are not suitable for the 2.41 GHz frequency, the measured loss from the cable between the antenna and the power detector board is ~2.4 dB. Another loss that can not be avoided is the ~2 dB attenuation from the band-pass filter, plus small losses in the 50 Ω track on the power detector board makes the total loss around 5 dB. These losses are critically due to the sensitivity of the power detecting system decreases from -63 dBm to -58 dBm.

The sensitivity of the power detector chip is another part that can be improved. This is done by changing the passive component on the input of the power detector chip. Due to the fact that we only had 4 power detector chips to work with, we did not want to risk the working layout proposed by Linear Technology with an own, maybe better or worse layout. With this in mind we choose Linear Technology's -63 dBm schematic.

9.4 Actuator system

The biggest problem with this system is the problem to keep track of the UAV at short distances due to the high gearing of the DC motors. The motors together with the speed controllers used in this project were far from ideal for their purpose, as the speed range of the motors not were big enough. This results in a jerky run when the UAV is far away, and in shorter distances it might not keep up with it.

The shortest distance away from the tracking device the UAV can fly in a perpendicular direction at 20 m/s is around 80 meter away horizontal. This is calculated from the maximum speed the motors can turn the device, which also seemed to be about the right distance in the real test flights.

Another thing that can be improved is the speed controllers. The antenna-stand now moves faster in one direction. This is because the power for the different direction is not the same. The backward direction has less power than the forward direction; this is probably a good idea for model boats, but not the ideal solution for tracking devices.

9.5 Software

The software works fine, but there is room for improvements. A lot of optimization could probably be done to save memory, but as the program currently compiles under 2 kB, no big effort was made to decrease the memory usage.

The control algorithm could probably also be improved.

Another thing that would improve the function of the tracking device would be an automatic compensation algorithm to compensate for the error in the logarithmic response in the power detectors at very weak signal reception (below -55 dBm).

9.6 Overall consideration

This was a very appealing project that gave us opportunity to use a lot of theory from different courses we have taken through the years at LTU. It also gave us an opportunity to learn 3D-CAD which was a totally new experience for both of us, and also work with other software like SuperNEC and Traxmaker.

We really hope that the tracking device will come in handy for the UAV-group at Monash University, and that they keep on developing the system.

10 Bibliography

[1] Råde, Lennart. Westergren, Bertil. (2001). *Mathematics Handbook for Science and Engineering BETA. 4:th edition*. Lund: Stundentlitteratur. ISBN 91-44-00839-2

[2] Jenvey, Stewart. *Antennas and Propagation Formulae, course material, LTU course code SME122 (2004).*

[3] Jenvey, Stewart. (2002). *Antennas and Propagation, course material, LTU course code SME122 (2004).*

[4] Hertley, Rick. *RF/Microwave PC Board Design and Layout*.
URL: http://www.jlab.org/accel/eecad/pdf/050rfdesign.pdf

[5] I-Laboratory. *Coplanar Waveguide with Ground Calculator*
URL: http://www1.sphere.ne.jp/i-lab/ilab/tool/cpw_g_e.htm

[6] Nordling, Carl. Österman, Jonny. (1980, 1999). *Physics Handbook for Science and Engineering. 6:th edition*. Lund: Stundentlitteratur. ISBN 91-44-00823-6

[7] *Microchip PIC16F877 Data Sheet*
URL: http://ww1.microchip.com/downloads/en/DeviceDoc/30292c.pdf

[8] Leslie, Martin. *Example Programs.*
URL: http://cermics.enpc.fr/~ts/C/EXAMPLES/

Appendix

A.1 Mechanical drawings

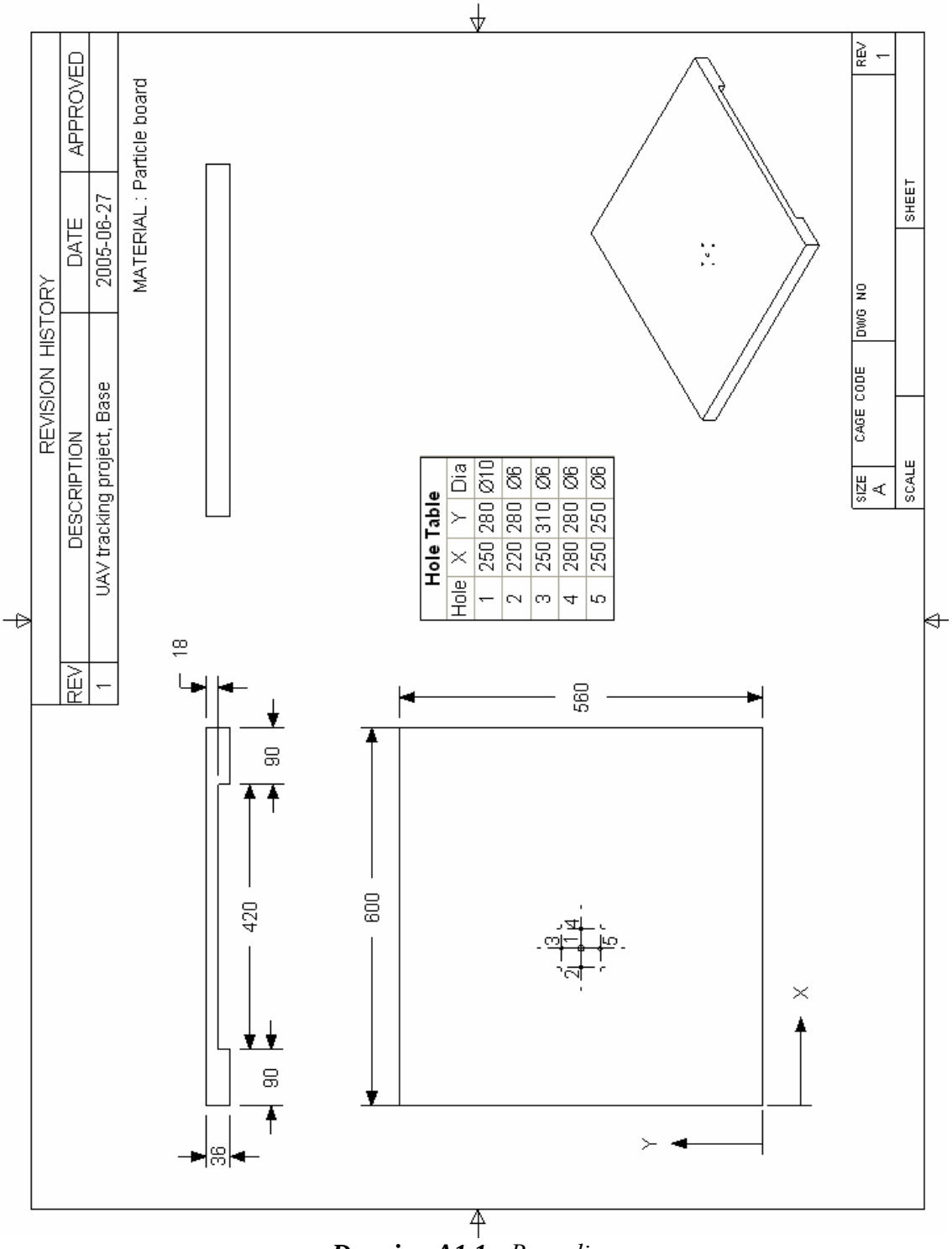

Drawing A1.1 : *Base disc.*

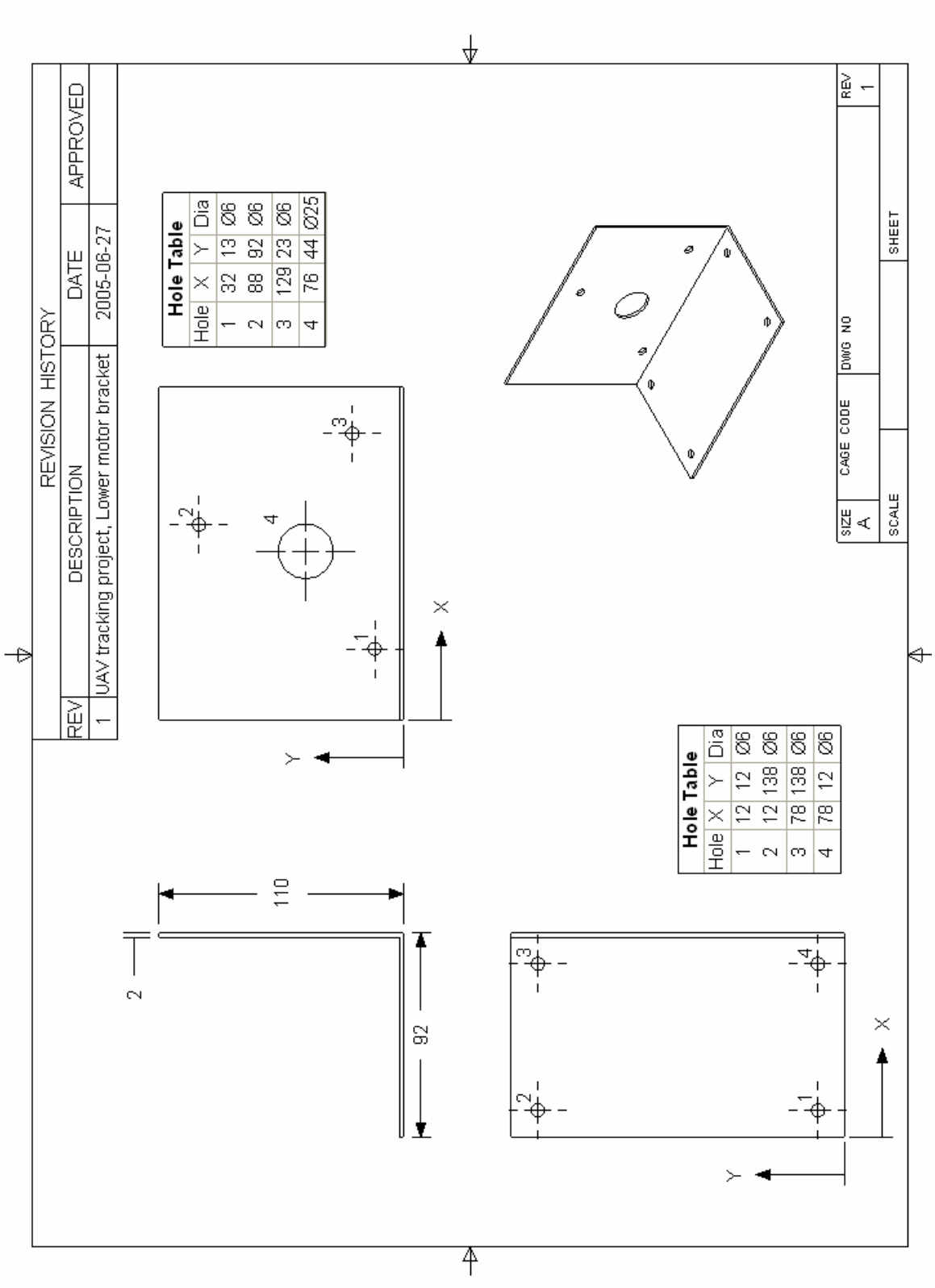

Drawing A1.2 : *Lower motor bracket.*

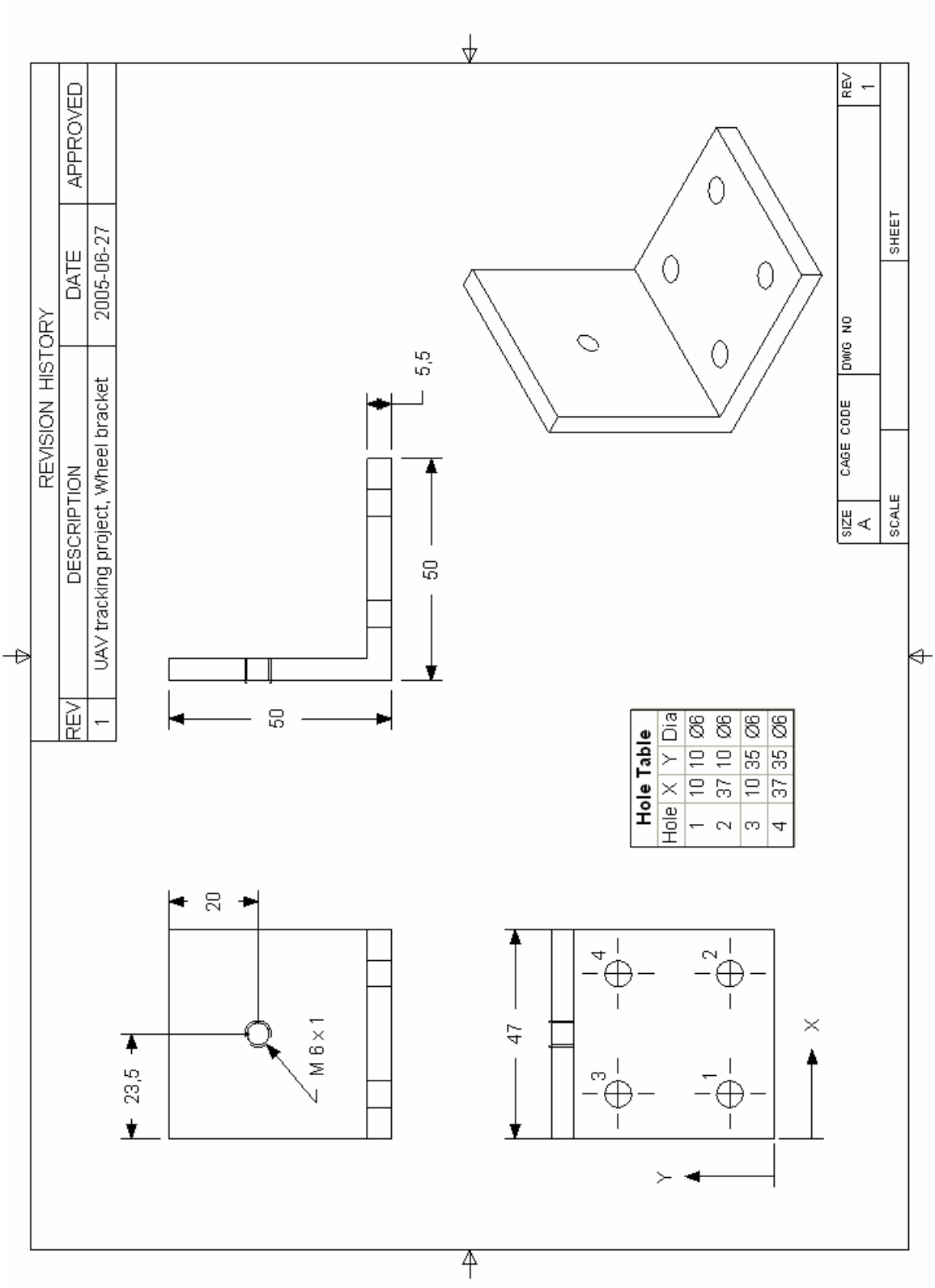

Drawing A1.3 : *Support wheel bracket.*

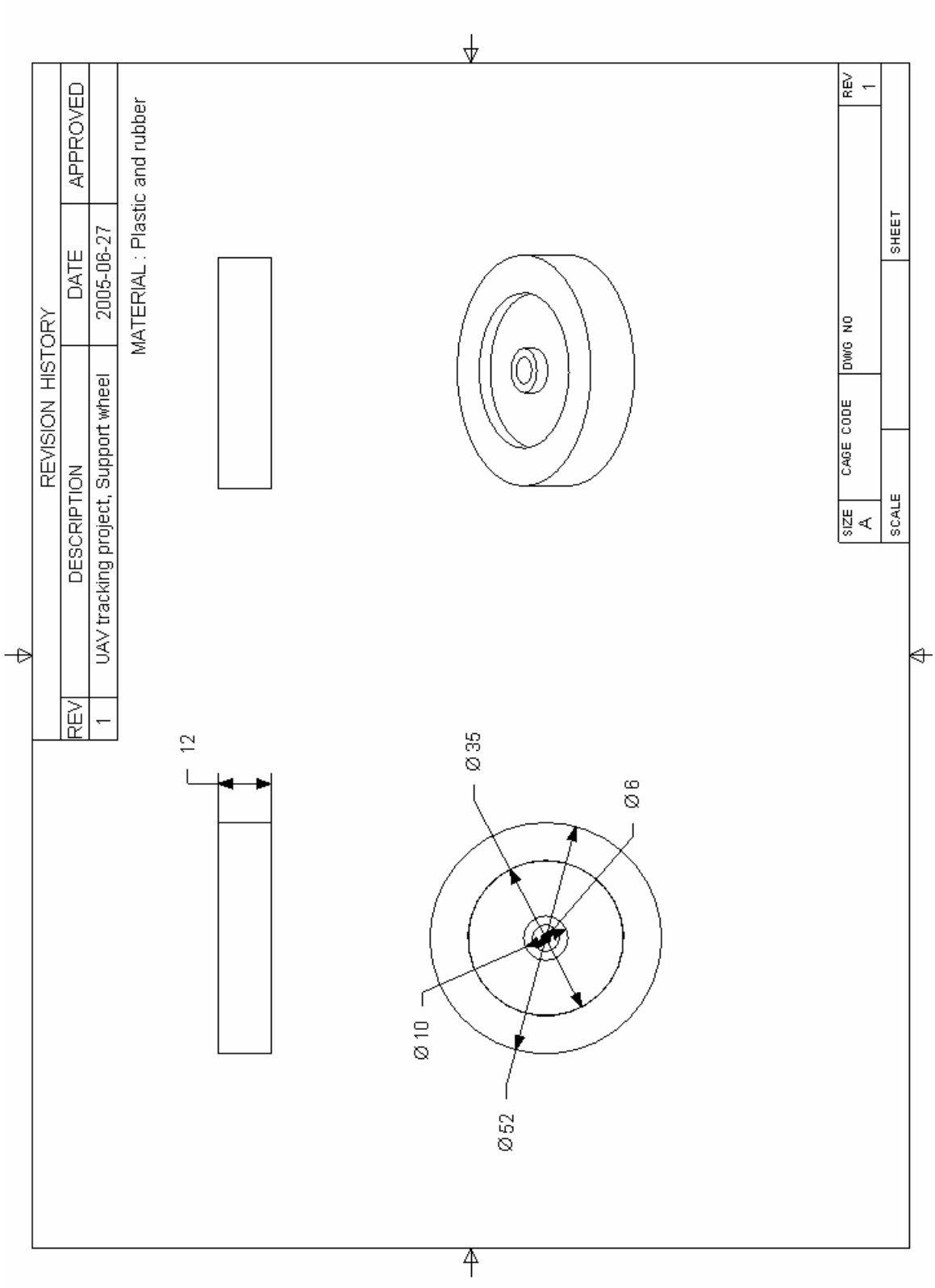

Drawing A1.4 : *Support wheel.*

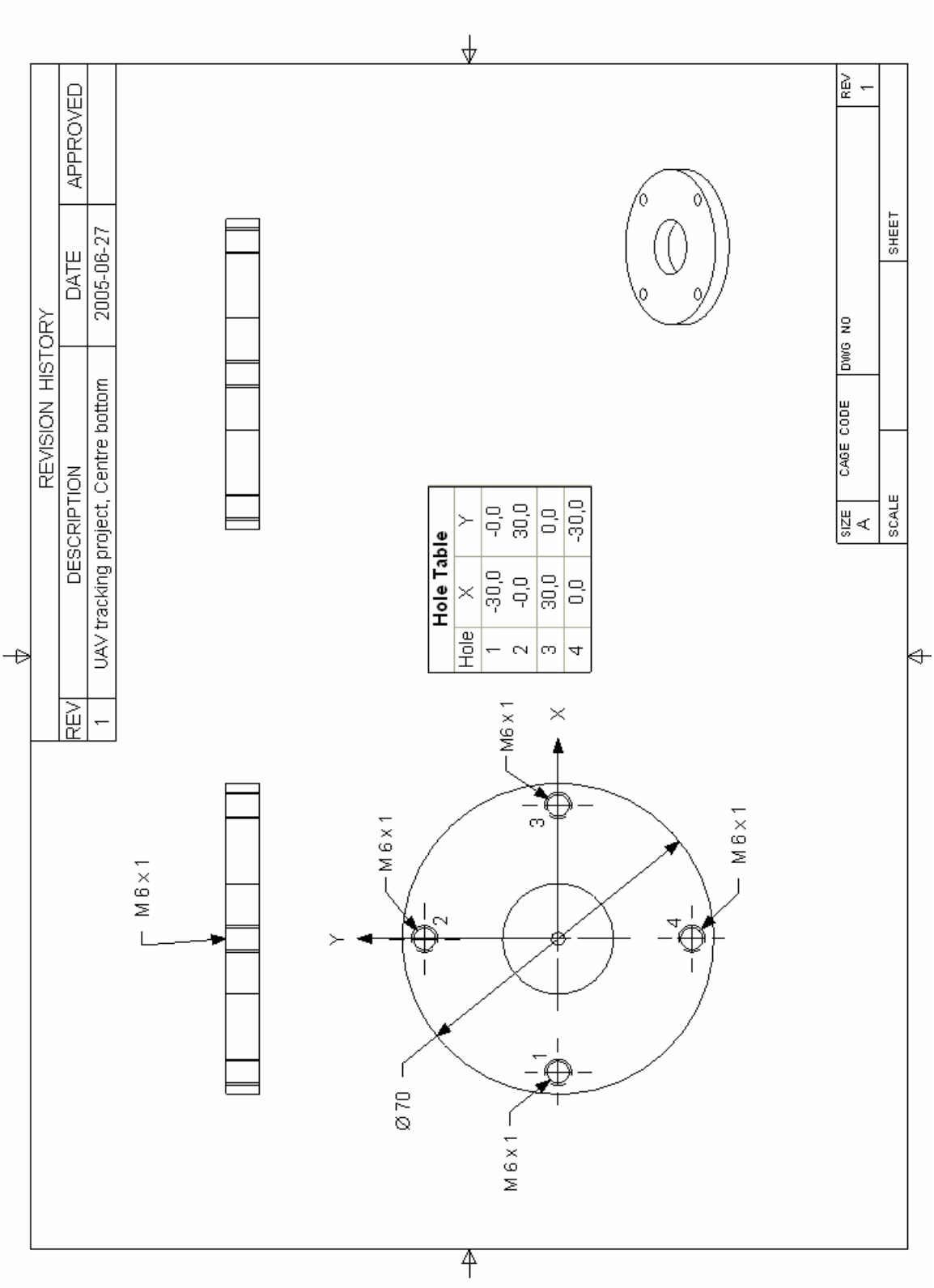

Drawing A1.5 : *Centre bottom.*

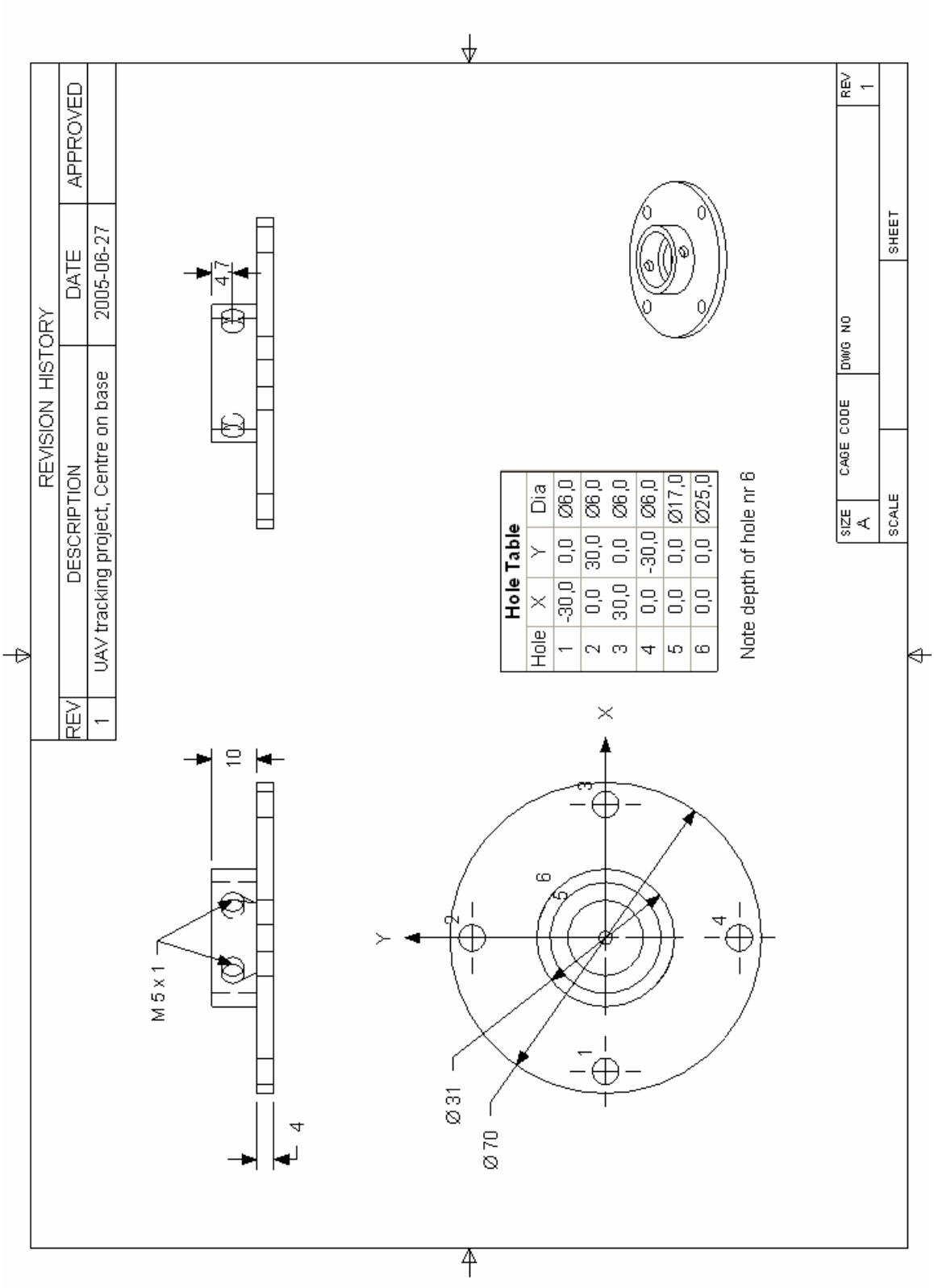

Drawing A1.6 : *Centre top on base.*

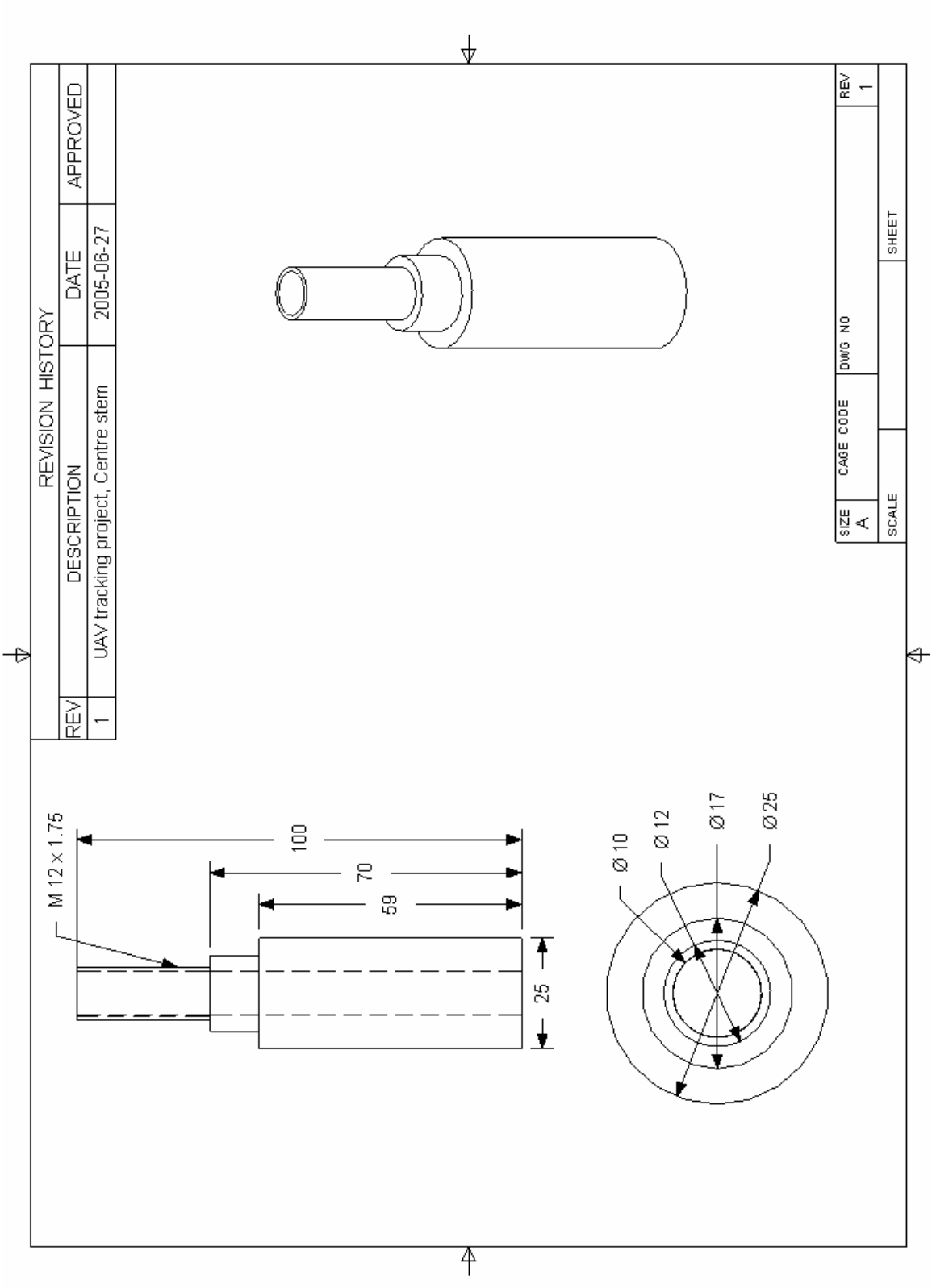

Drawing A1.7 : *Central stem.*

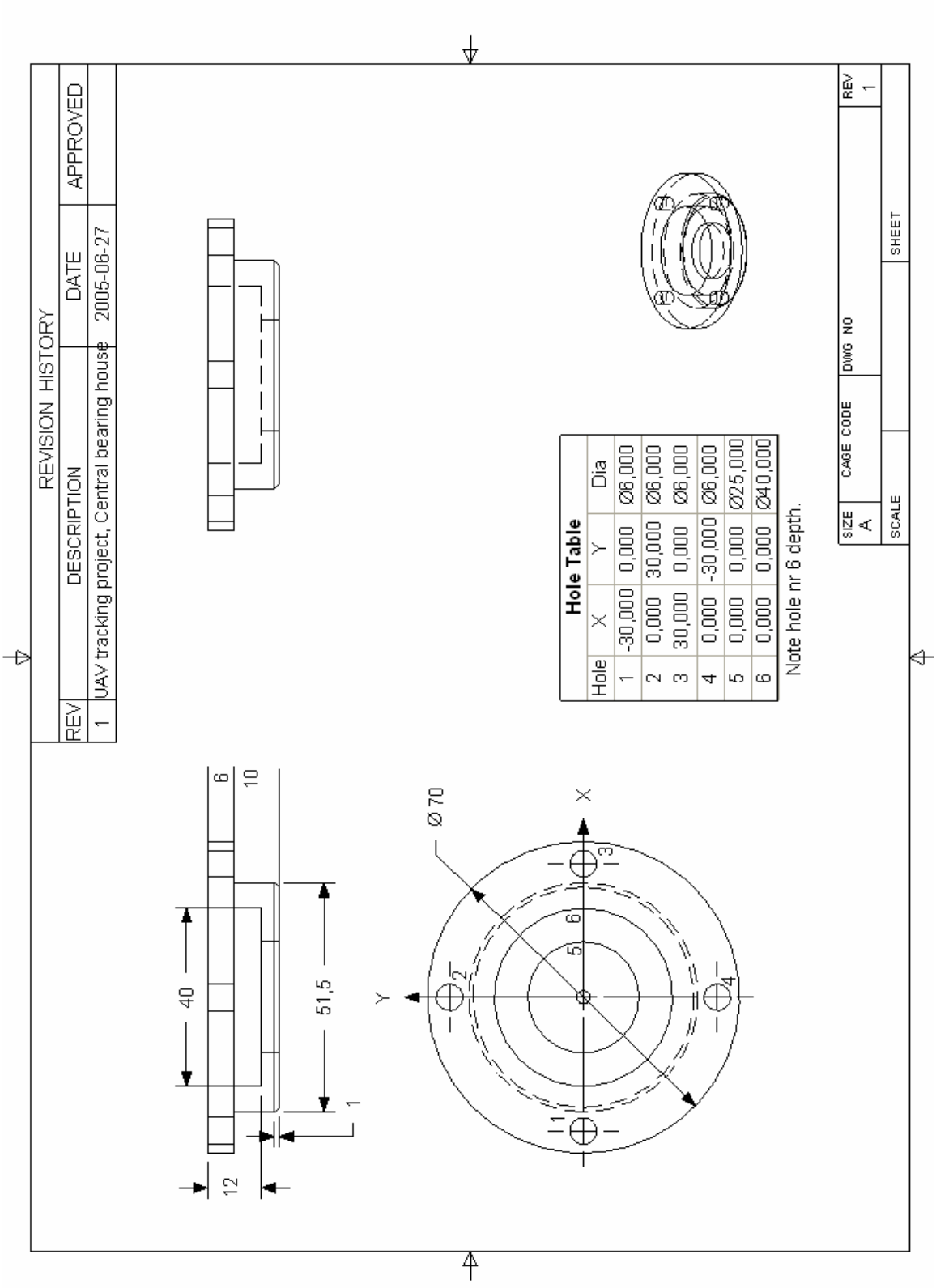

Drawing A1.8 : *Central bearing house.*

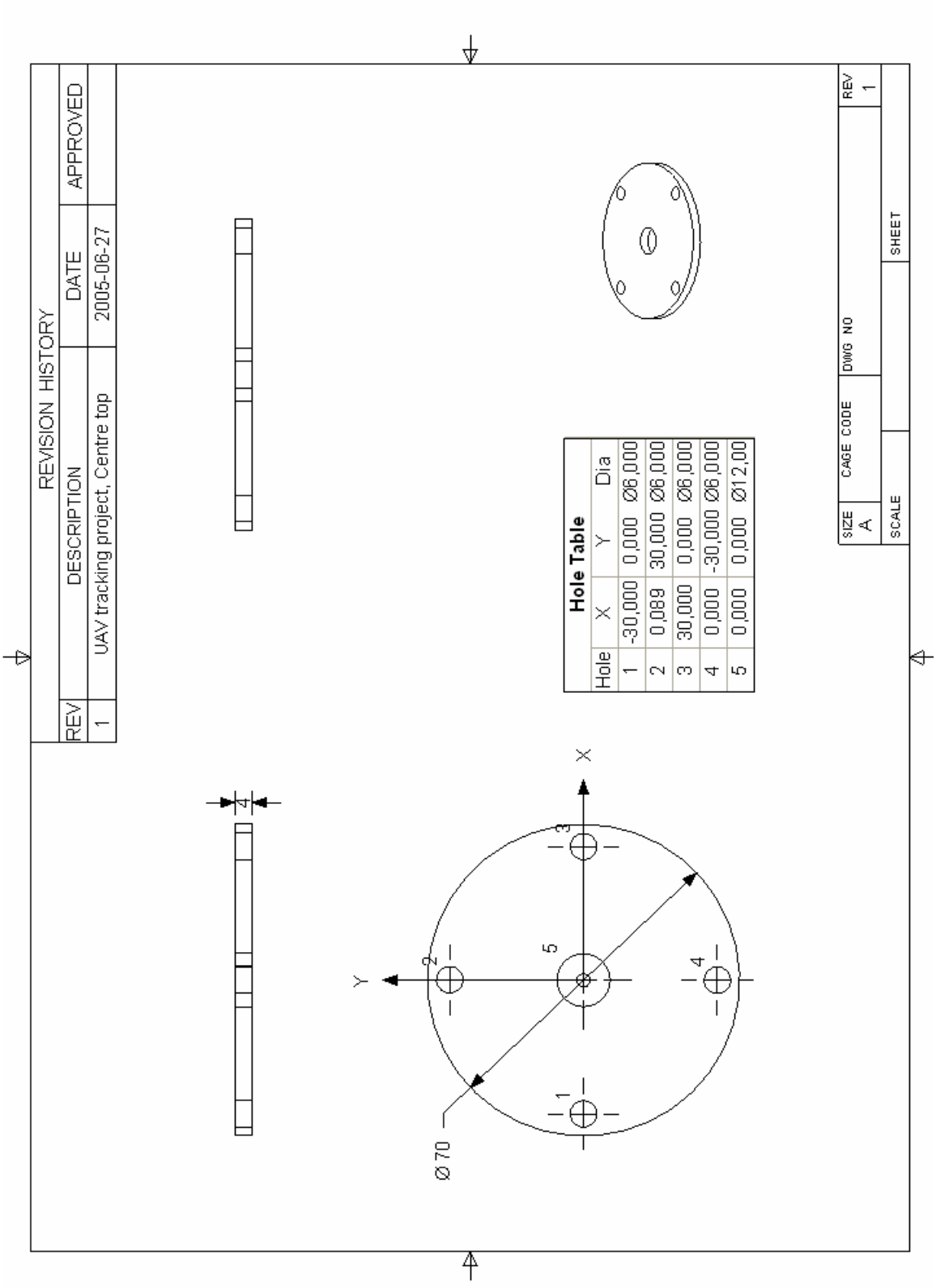

Drawing A1.9 : *Central top.*

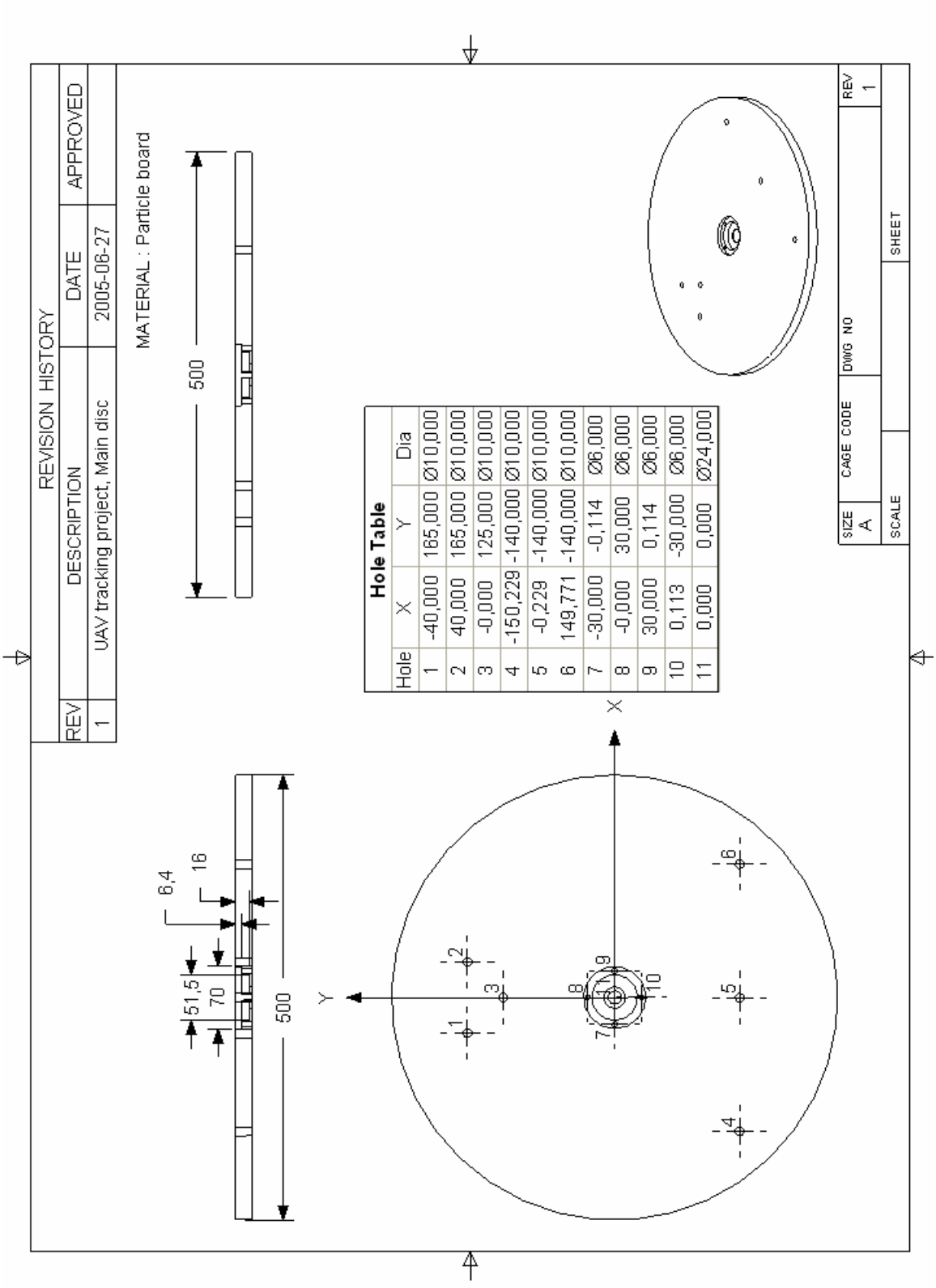

Drawing A1.10 : *Main disc.*

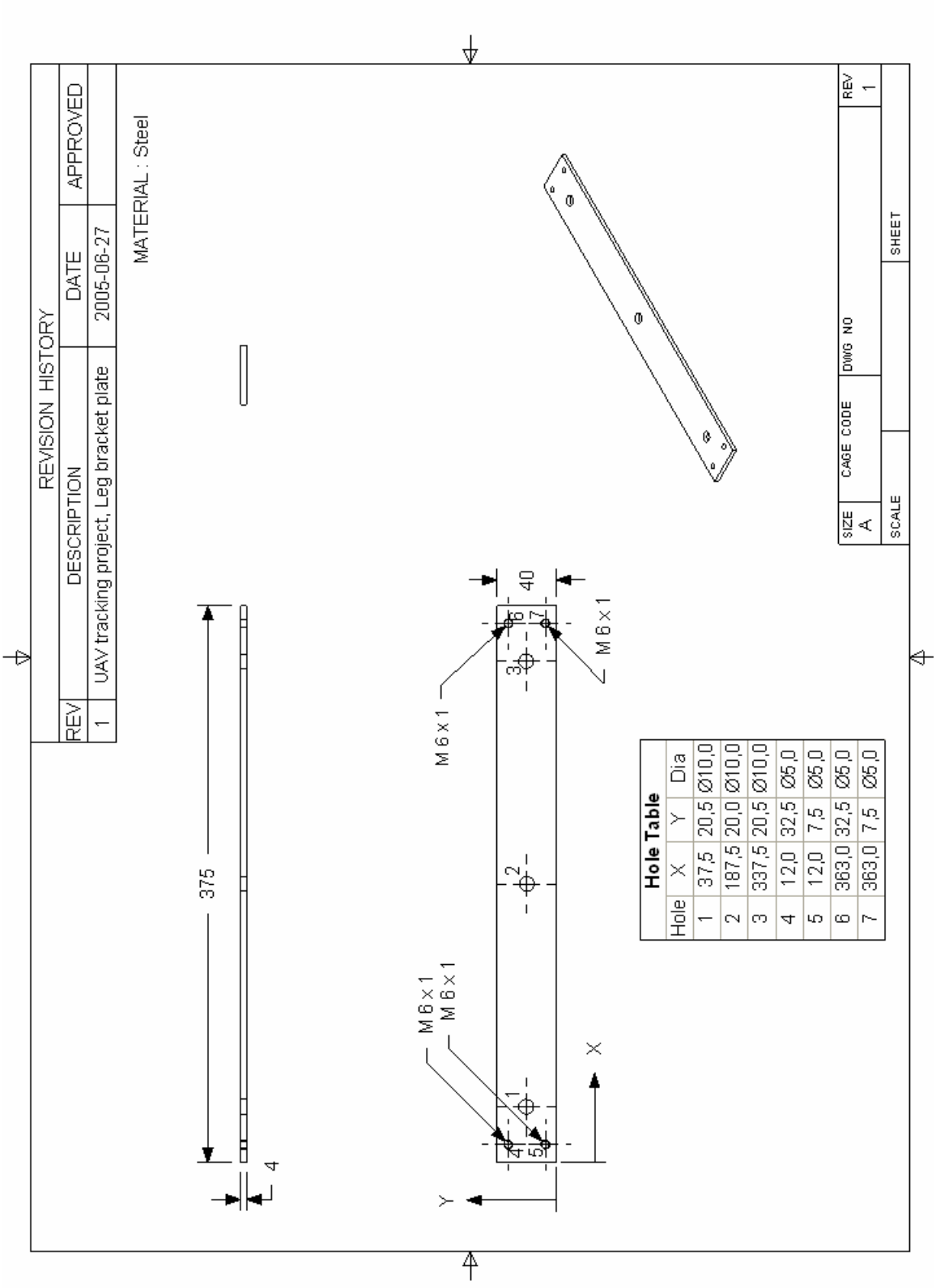

Drawing A1.11 : *Big leg bracket plate.*

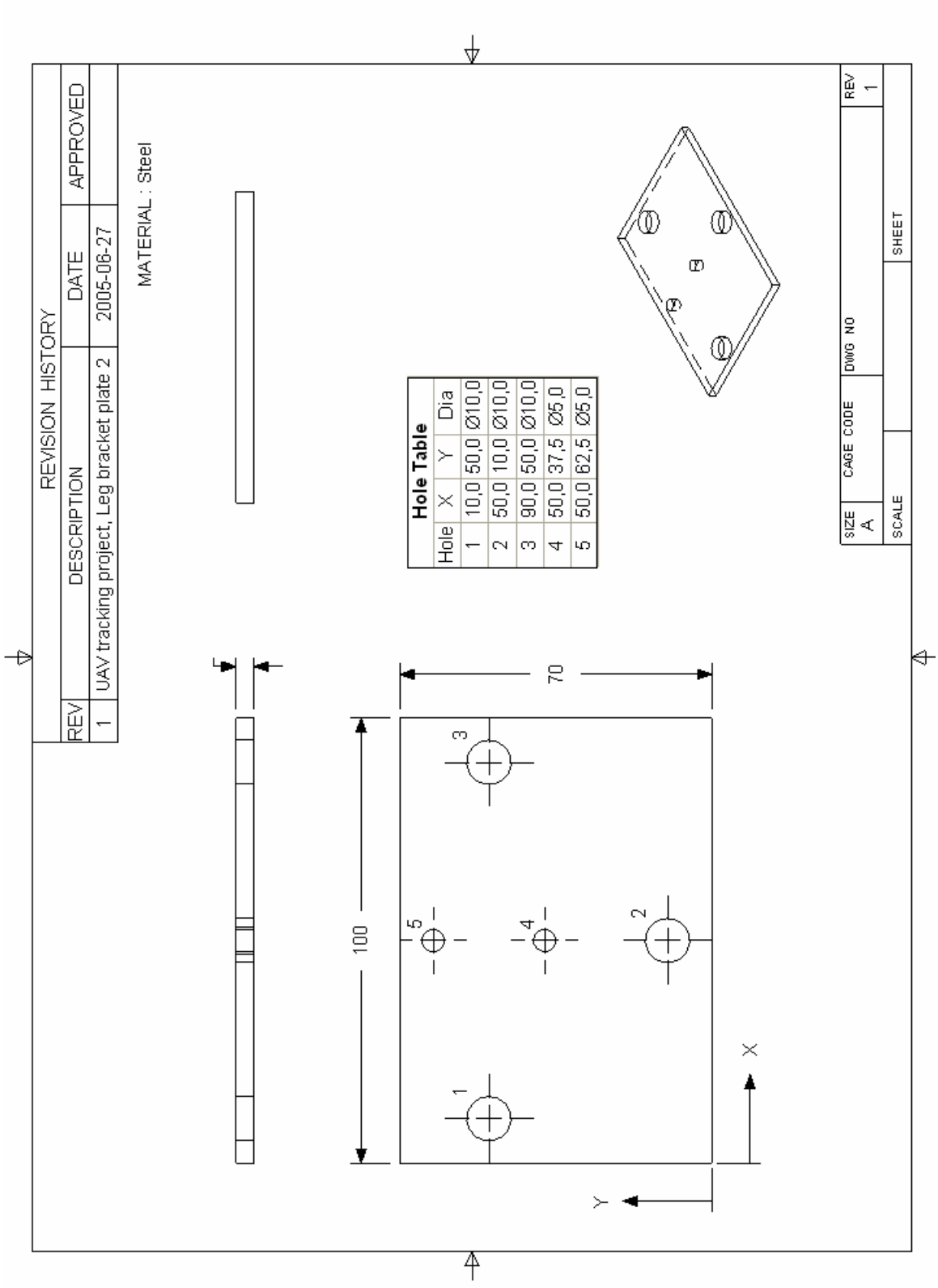

Drawing A1.12 : *Small leg bracket plate.*

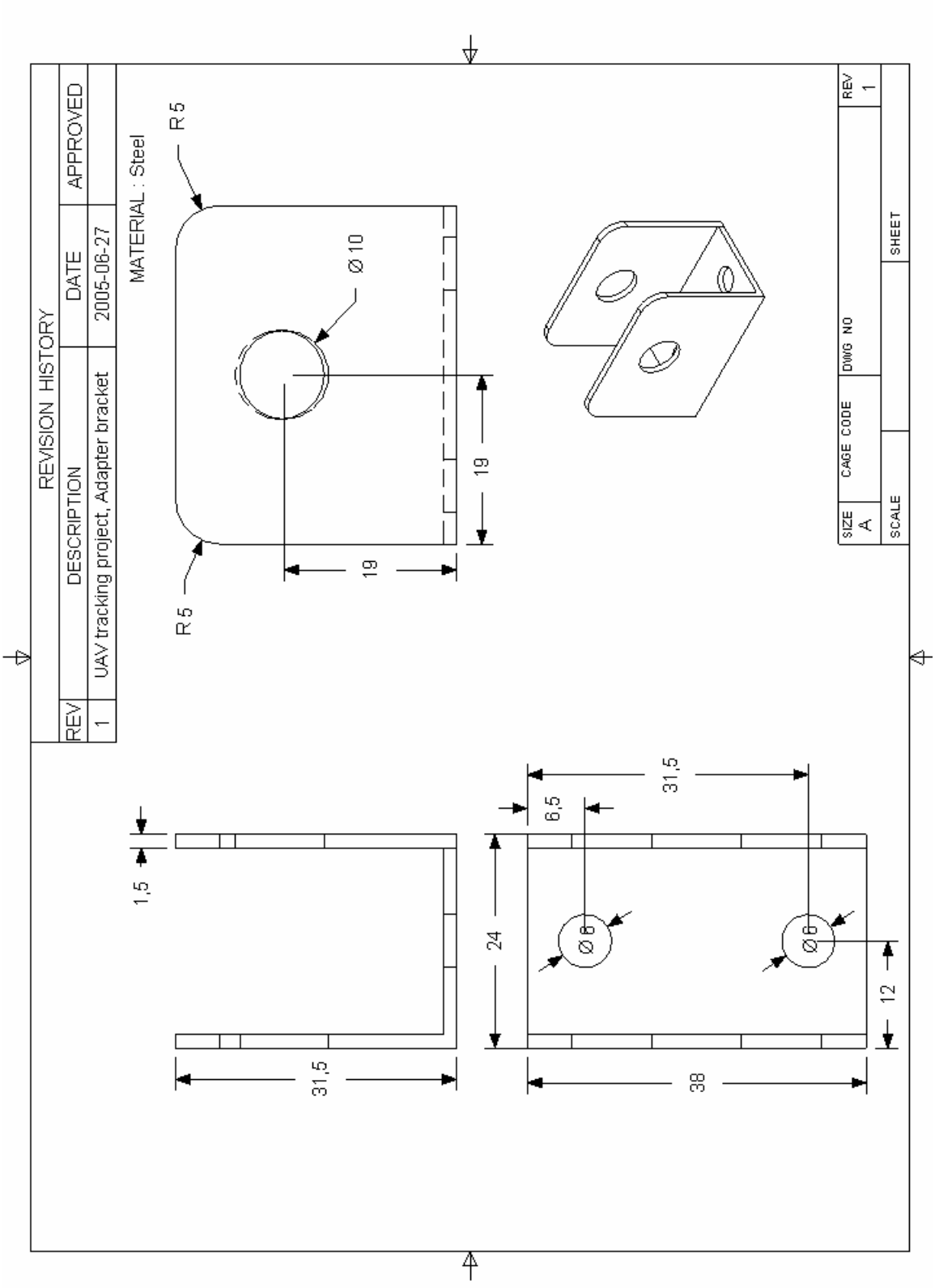

Drawing A1.13 : *Leg adapter bracket.*

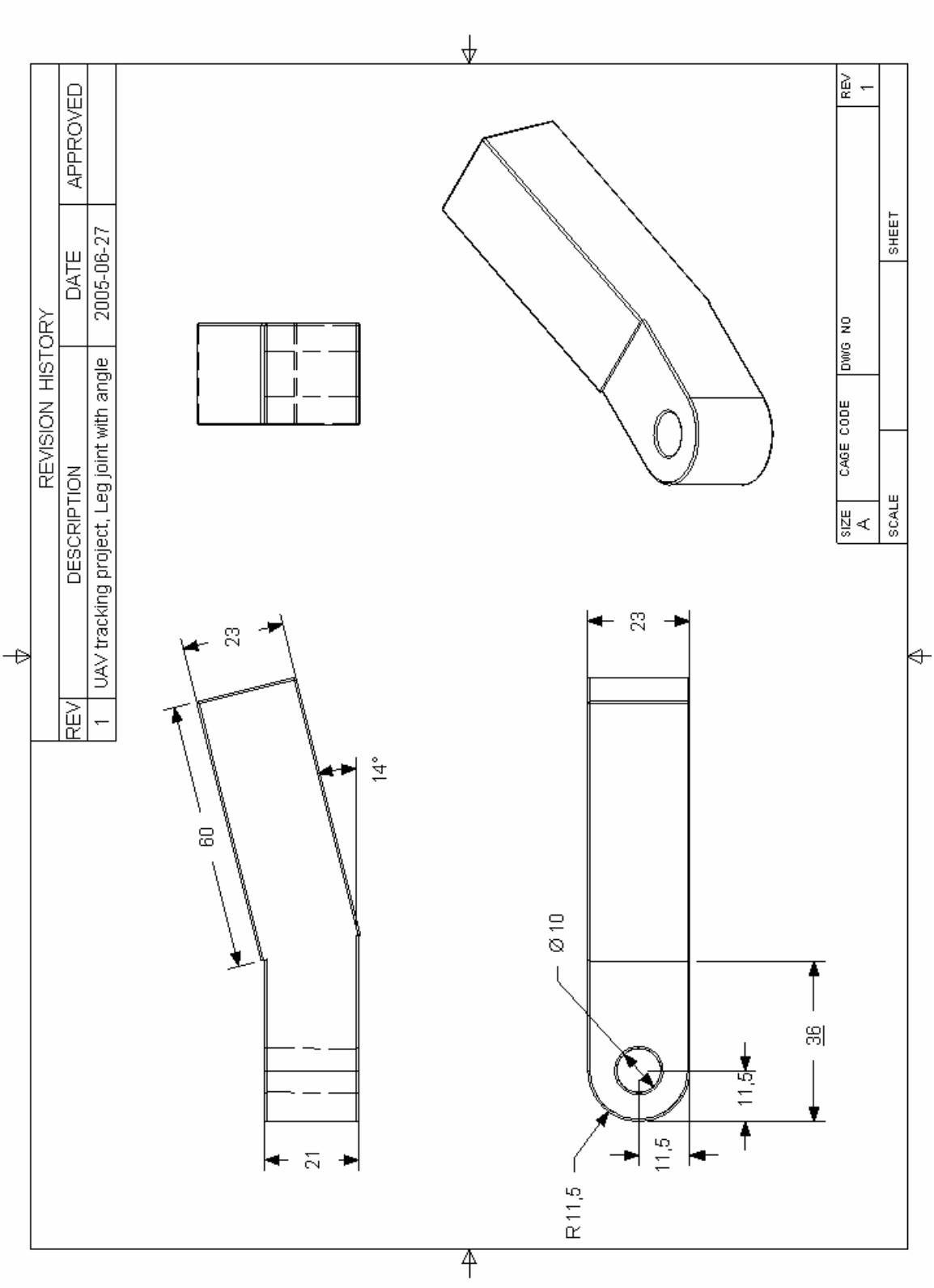

Drawing A1.14 : *Leg joint with angle.*

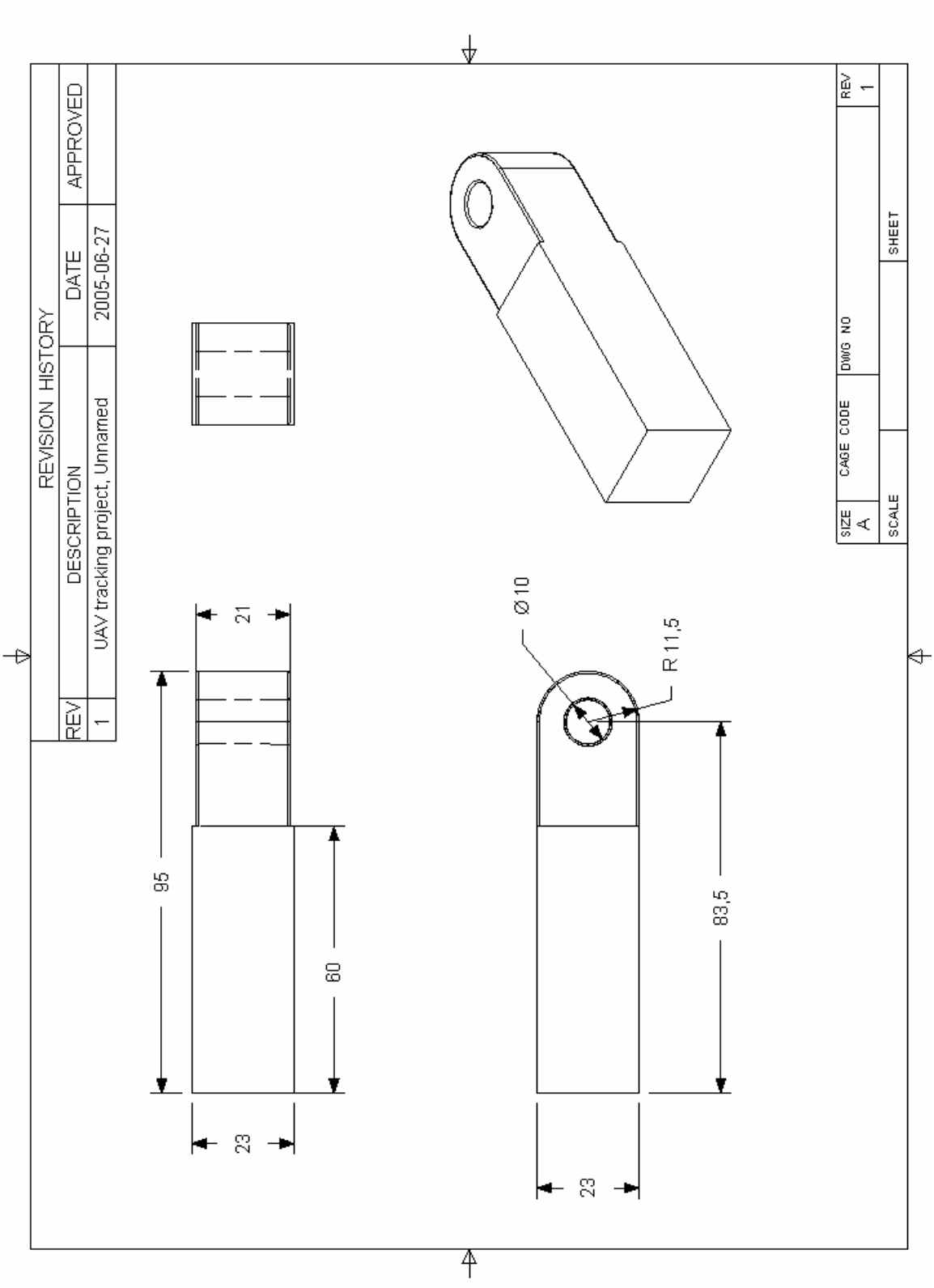

Drawing A1.15 : *Leg joint, straight.*

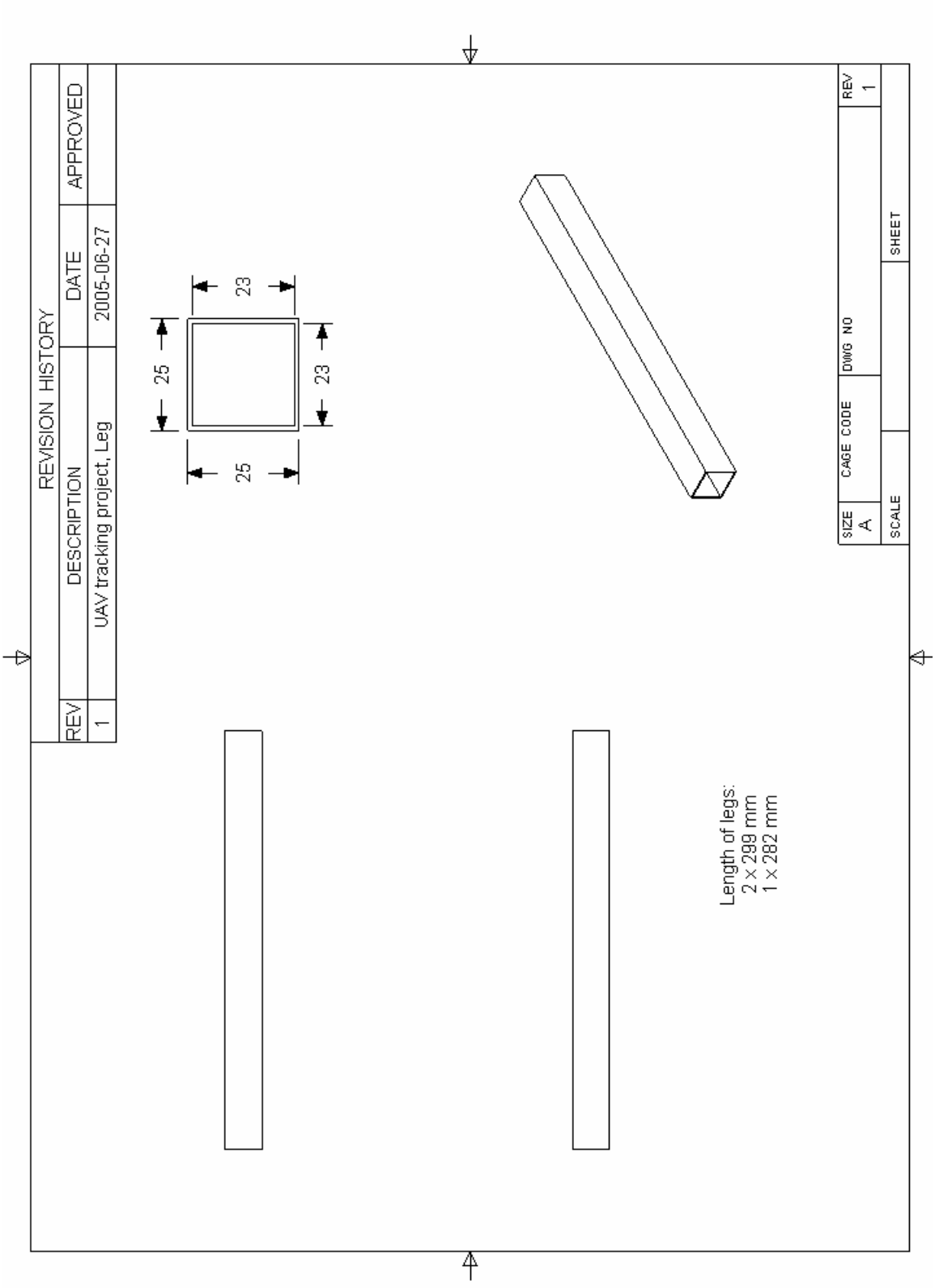

Drawing A1.16 : *Legs.*

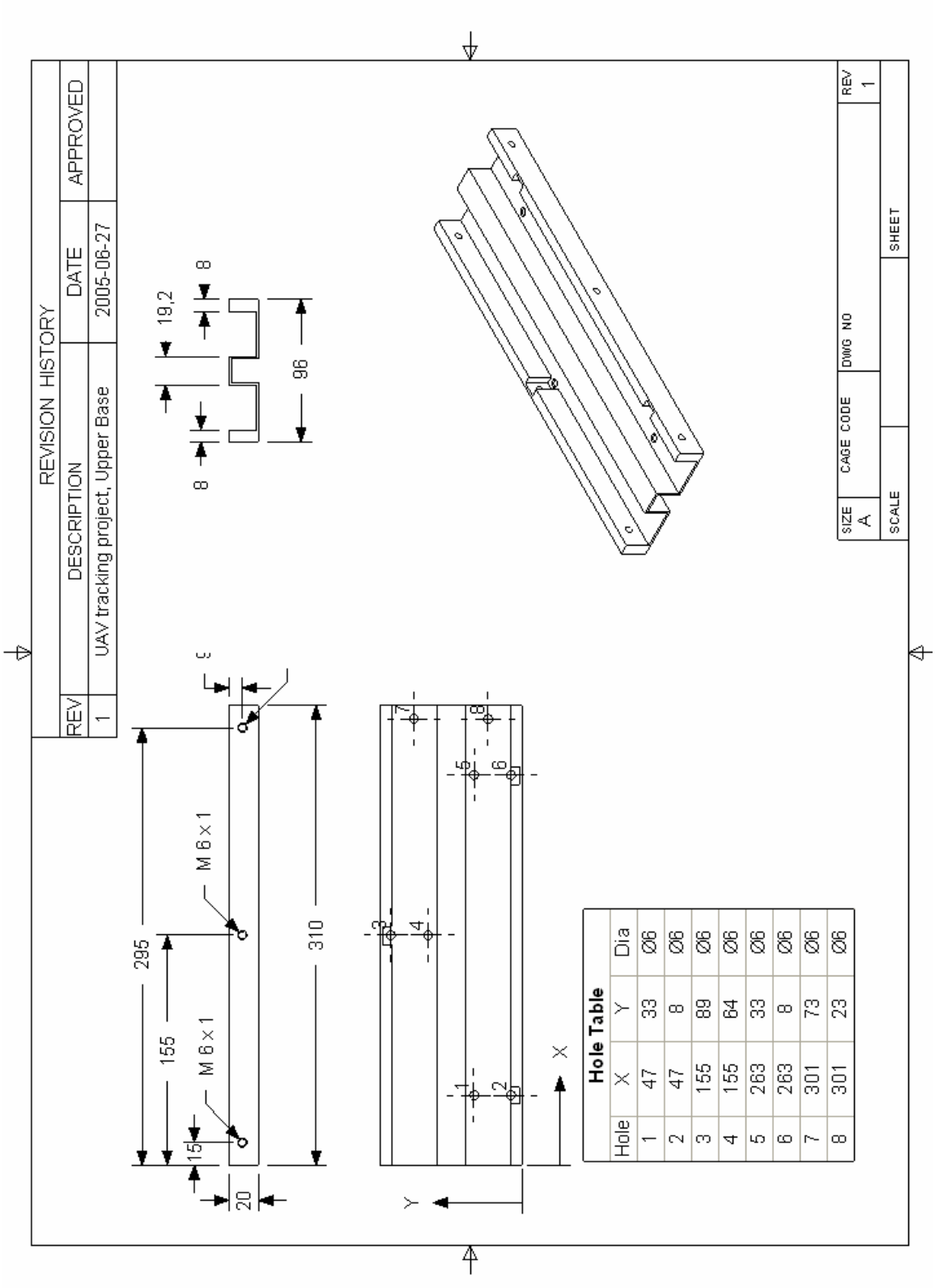

Drawing A1.17 : *Upper base.*

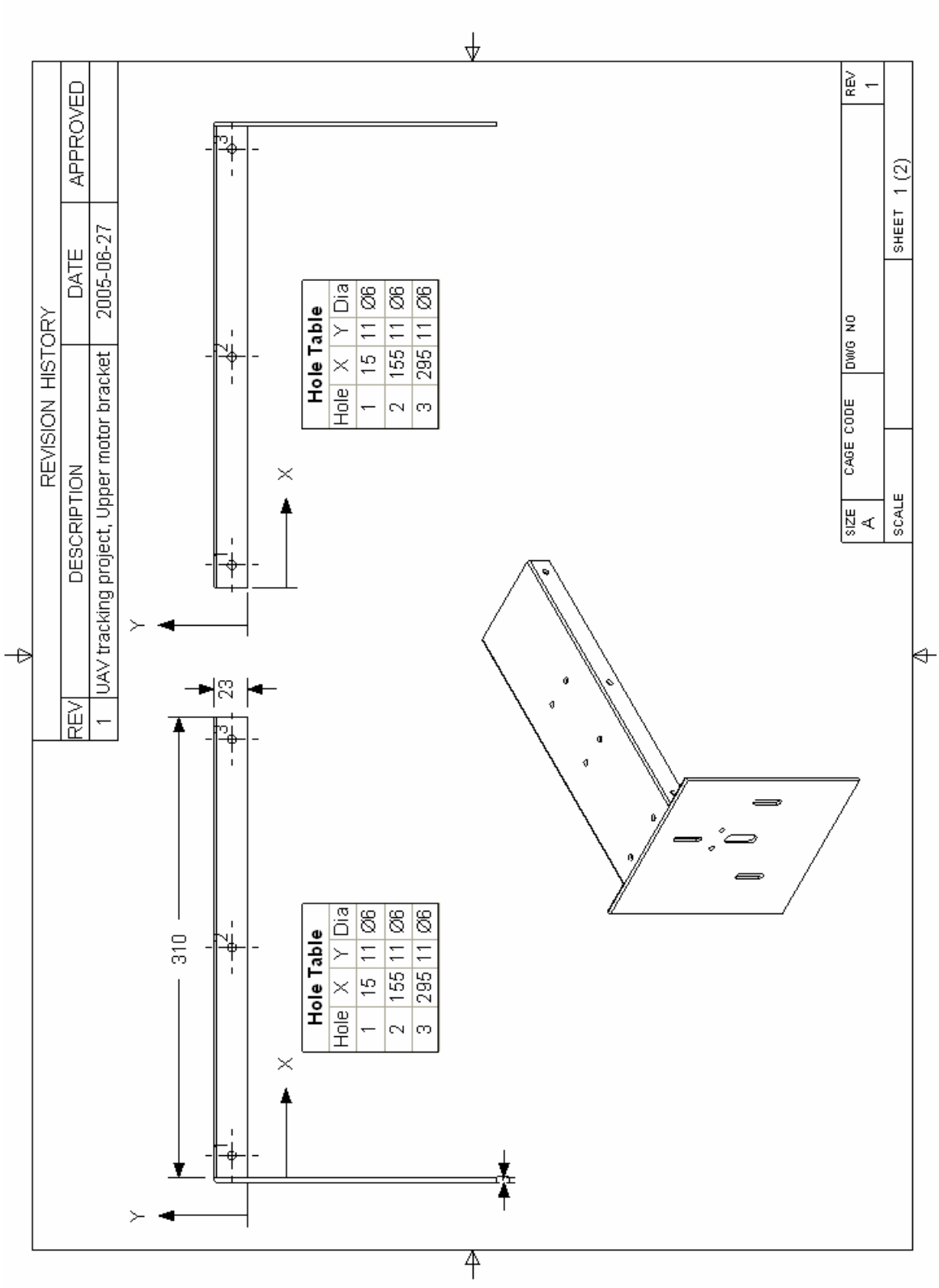

Drawing A1.18 : *Upper motor bracket (view 1).*

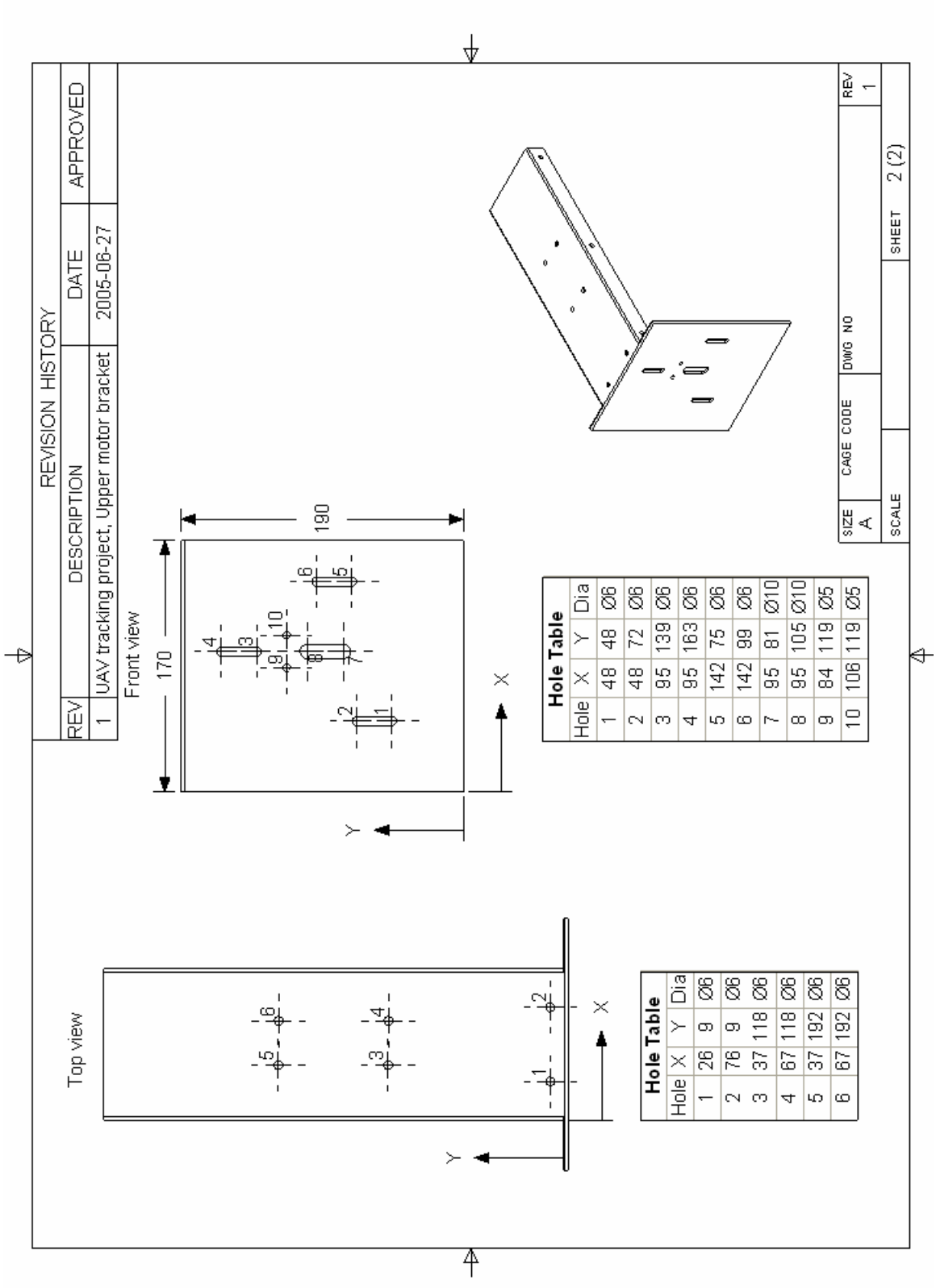

Drawing A1.19 : *Upper motor bracket (view 2).*

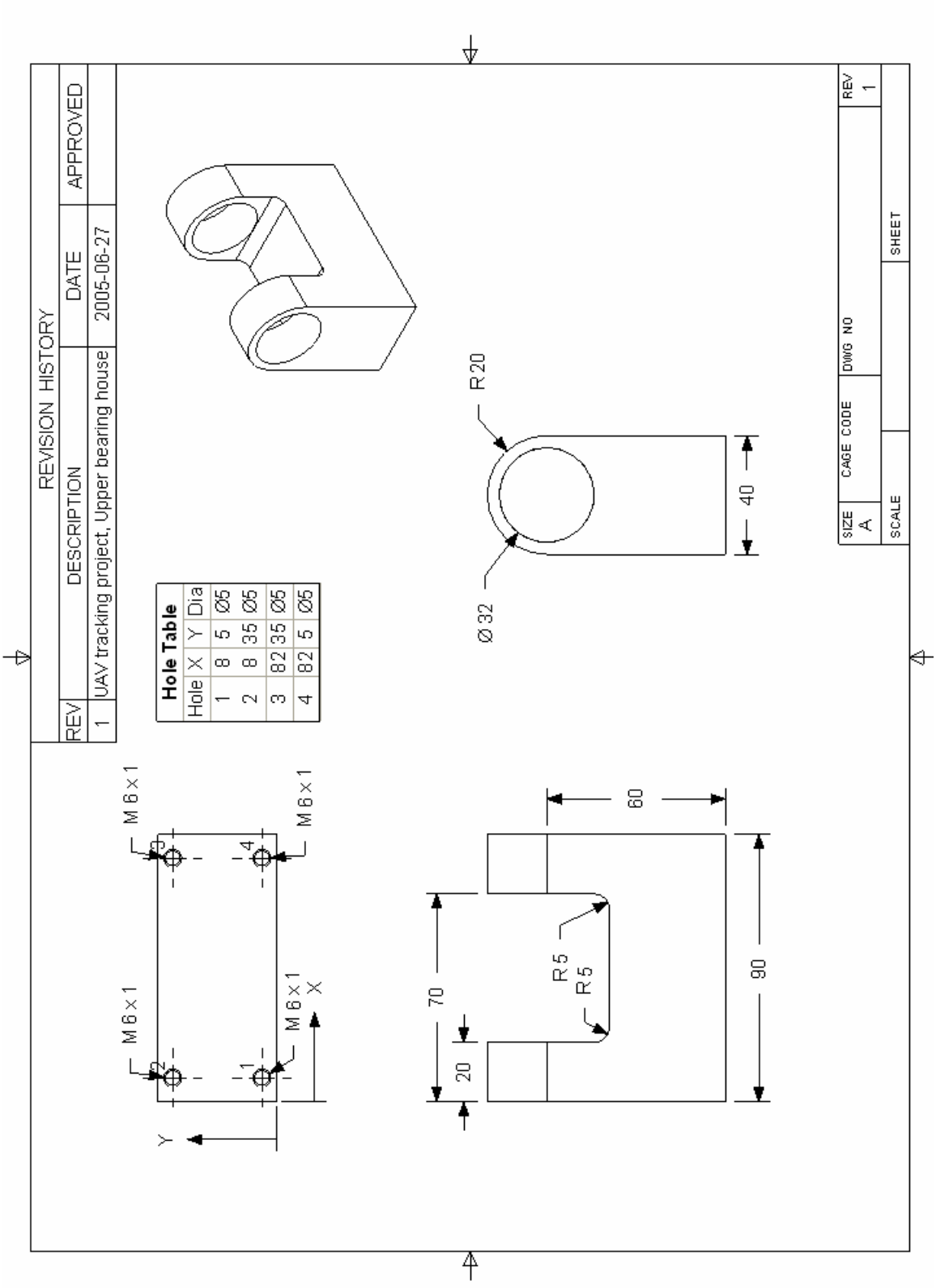

Drawing A1.20 : *Upper main bearing house.*

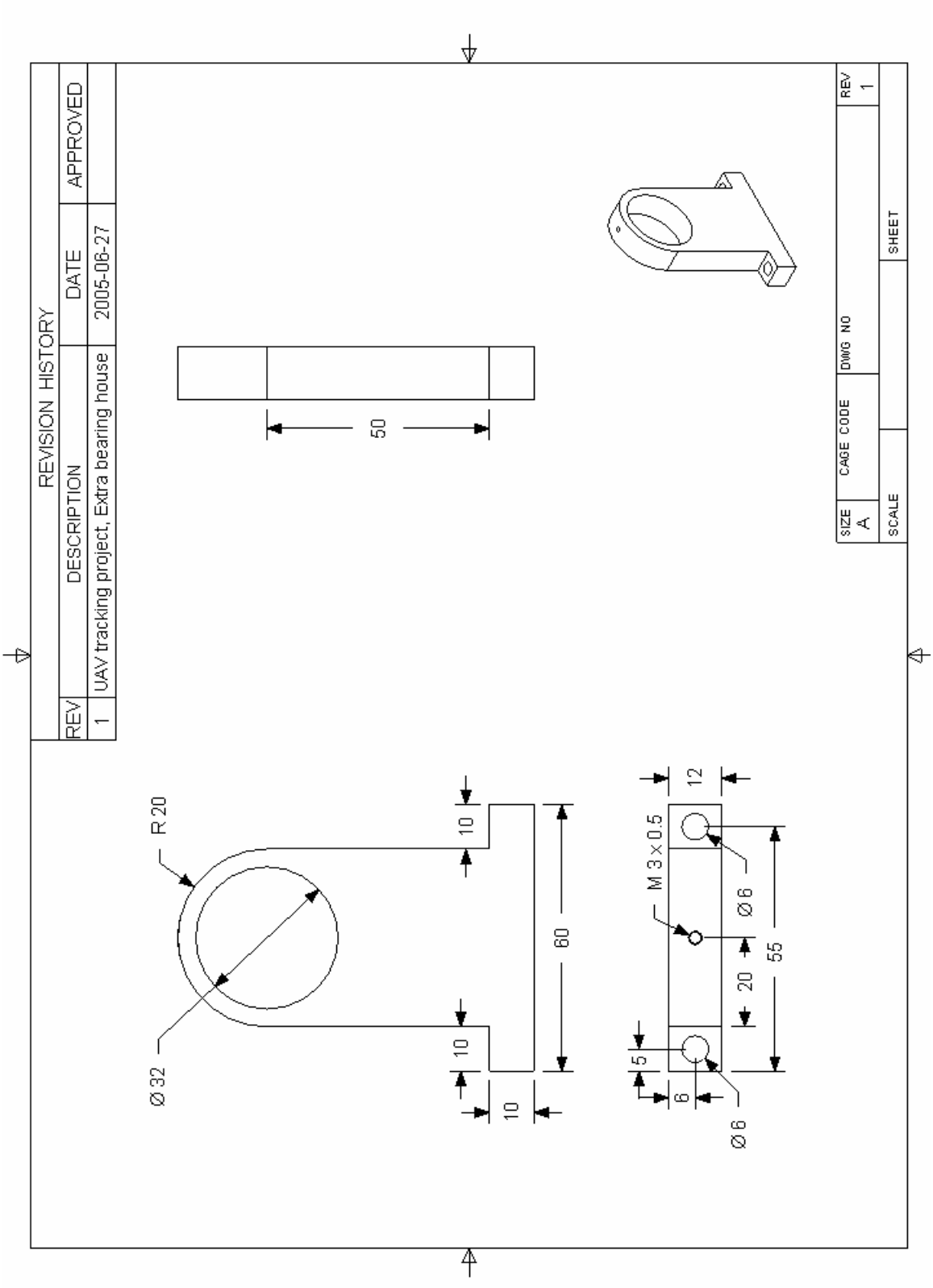

Drawing A1.21 : *Upper extra bearing house.*

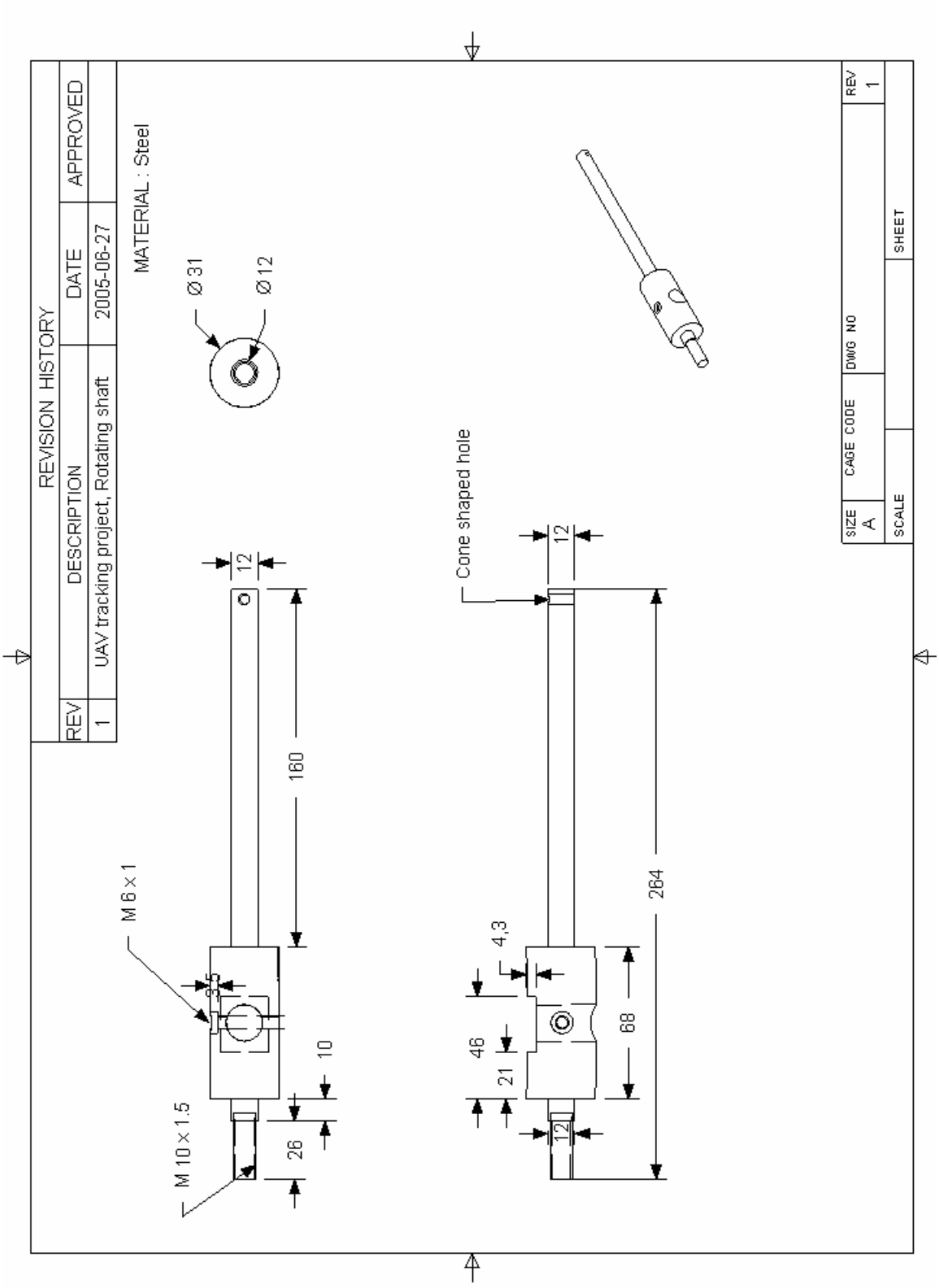

Drawing A1.22 : *Rotating shaft.*

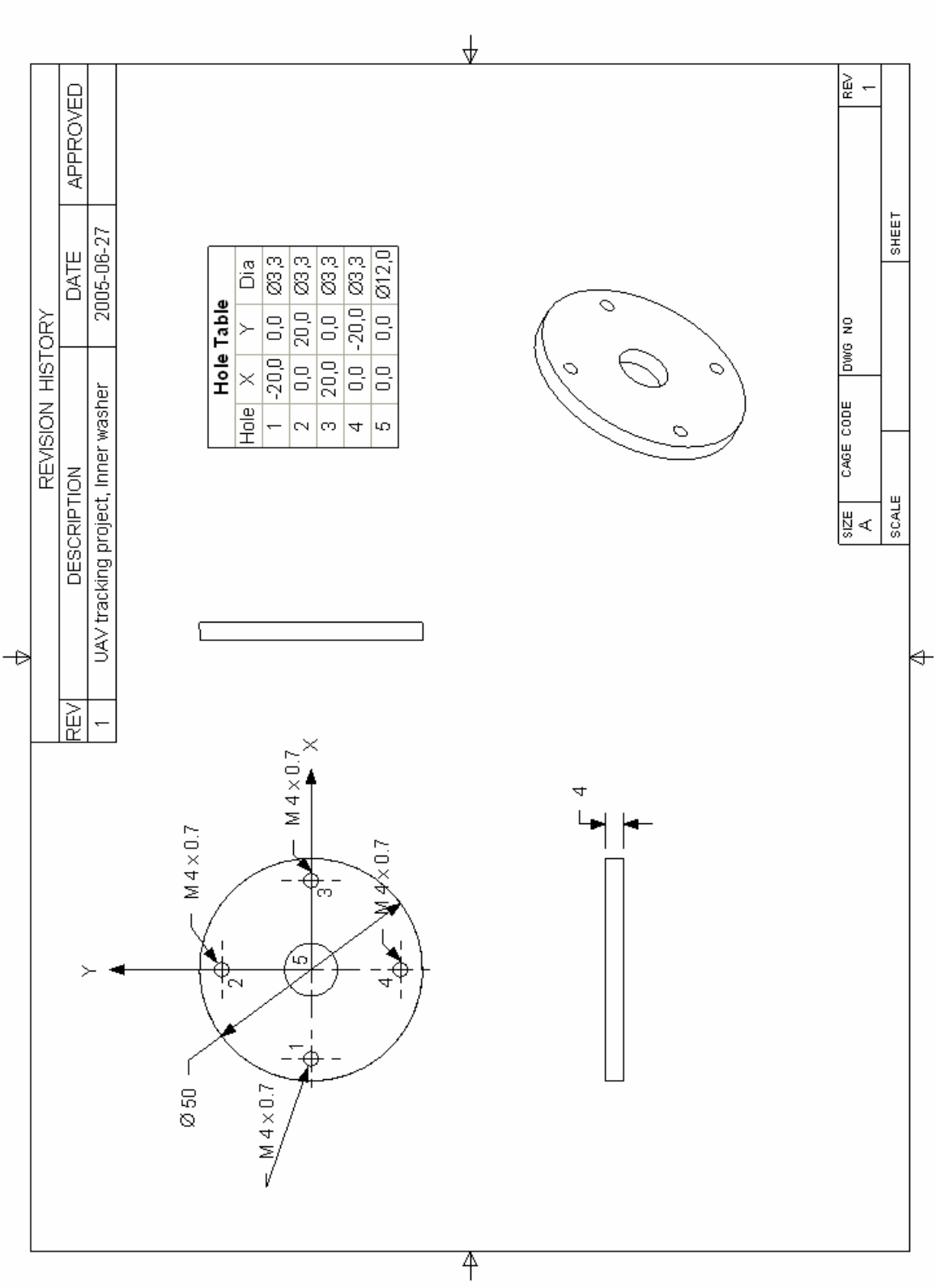

Drawing A1.23 : *Inner gear washer.*

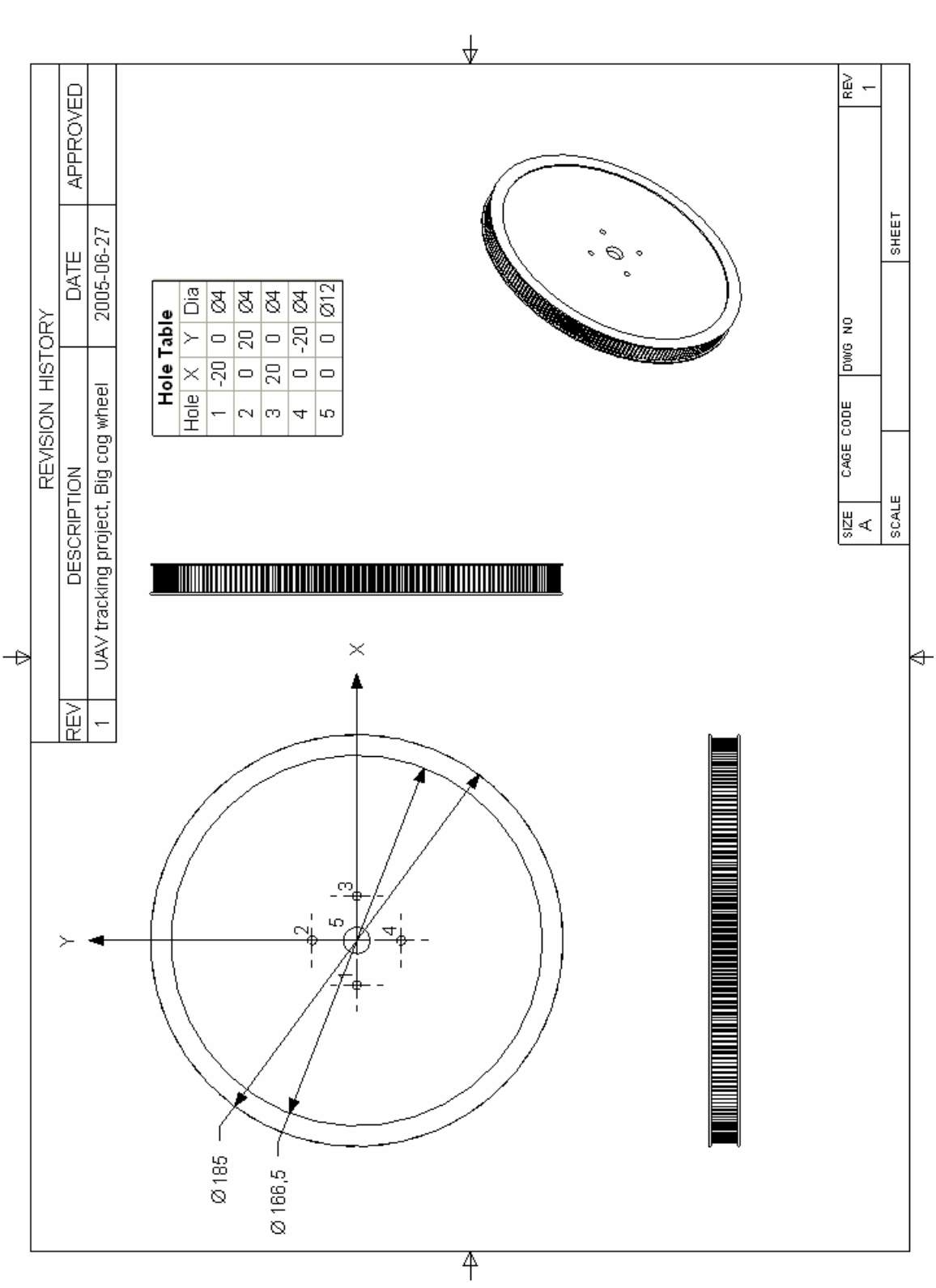

Drawing A1.24 : *Big gear.*

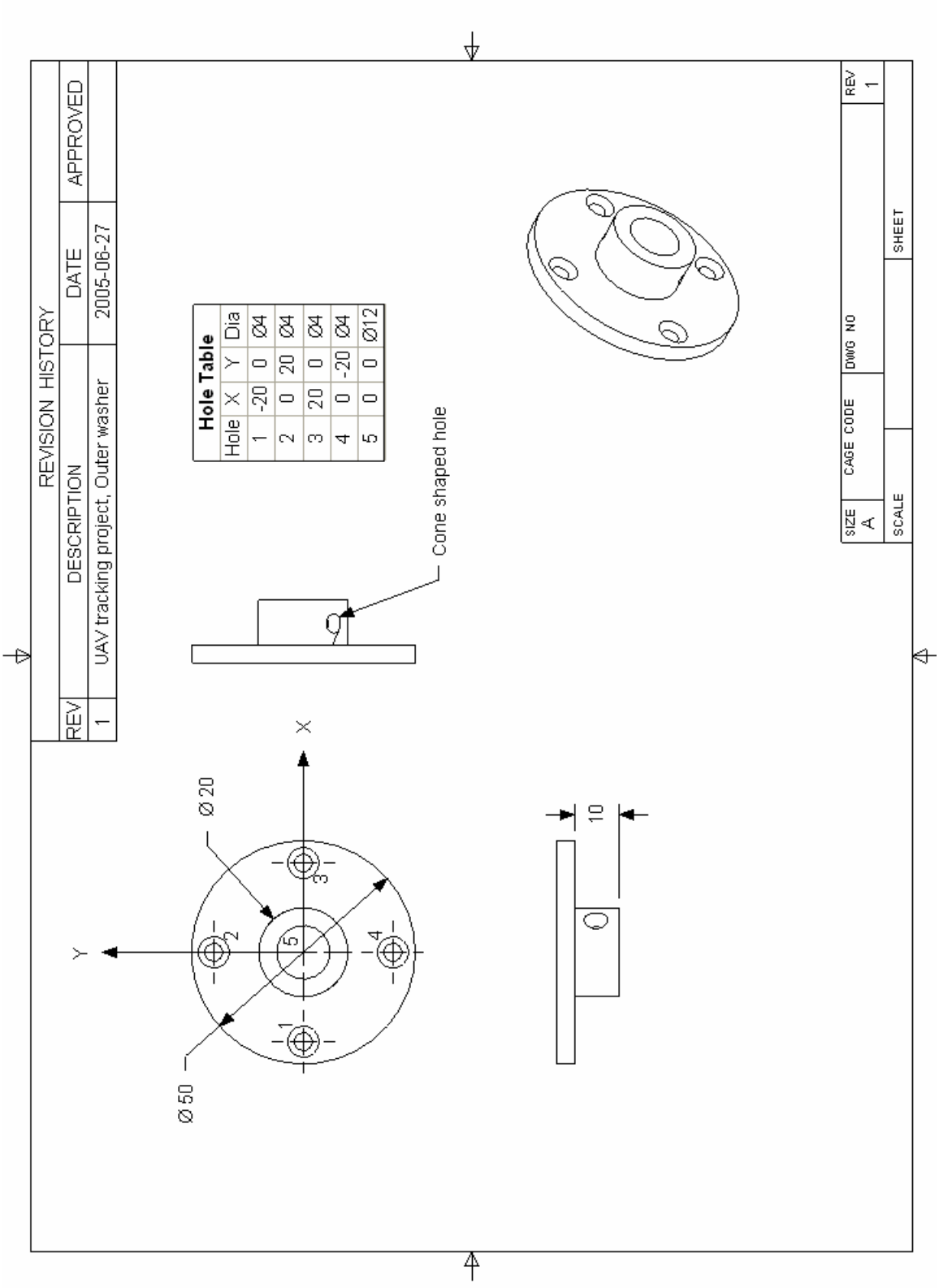

Drawing A1.25 : *Outer gear washer.*

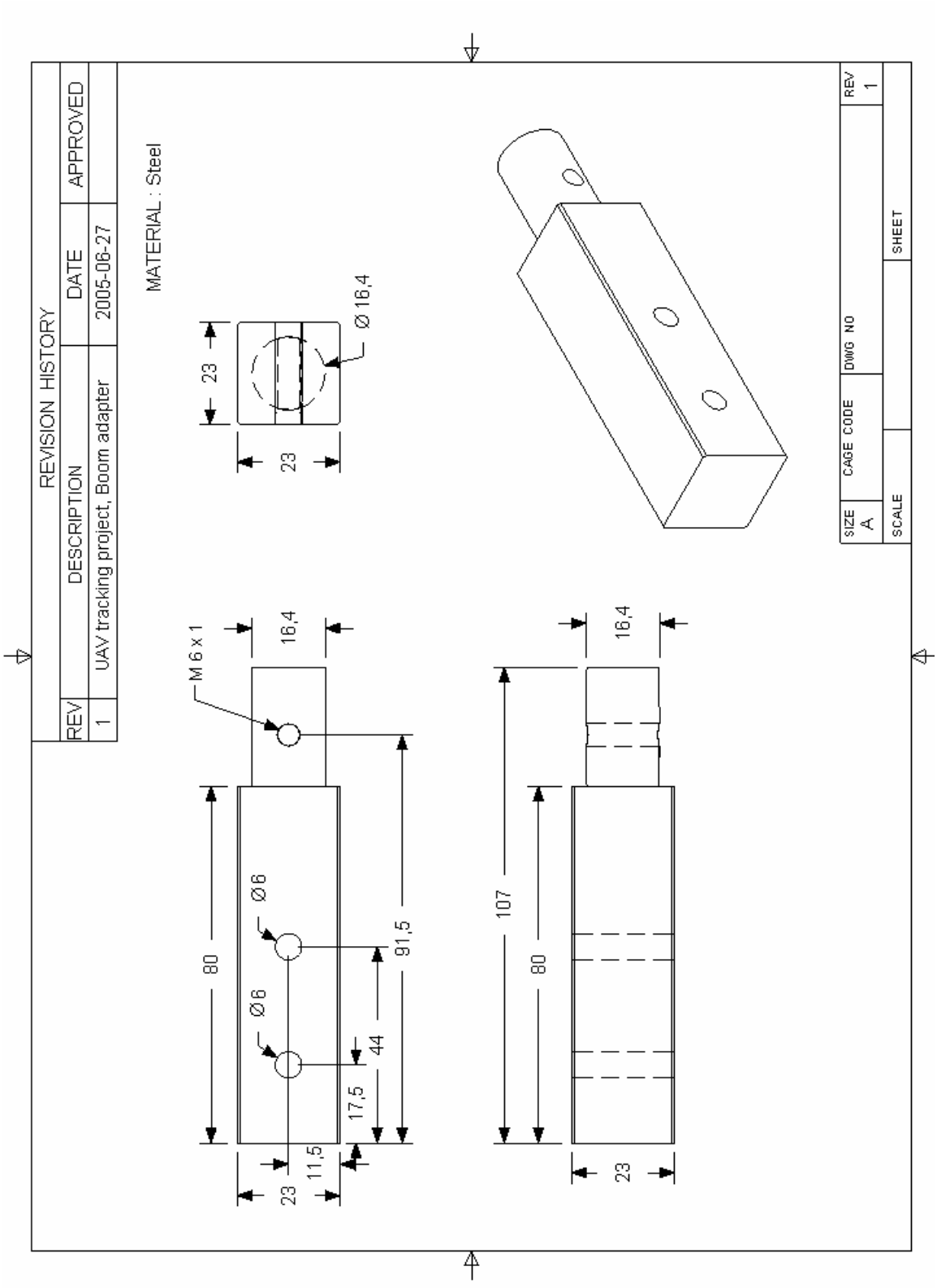

Drawing A1.26 : *Antenna boom adapter.*

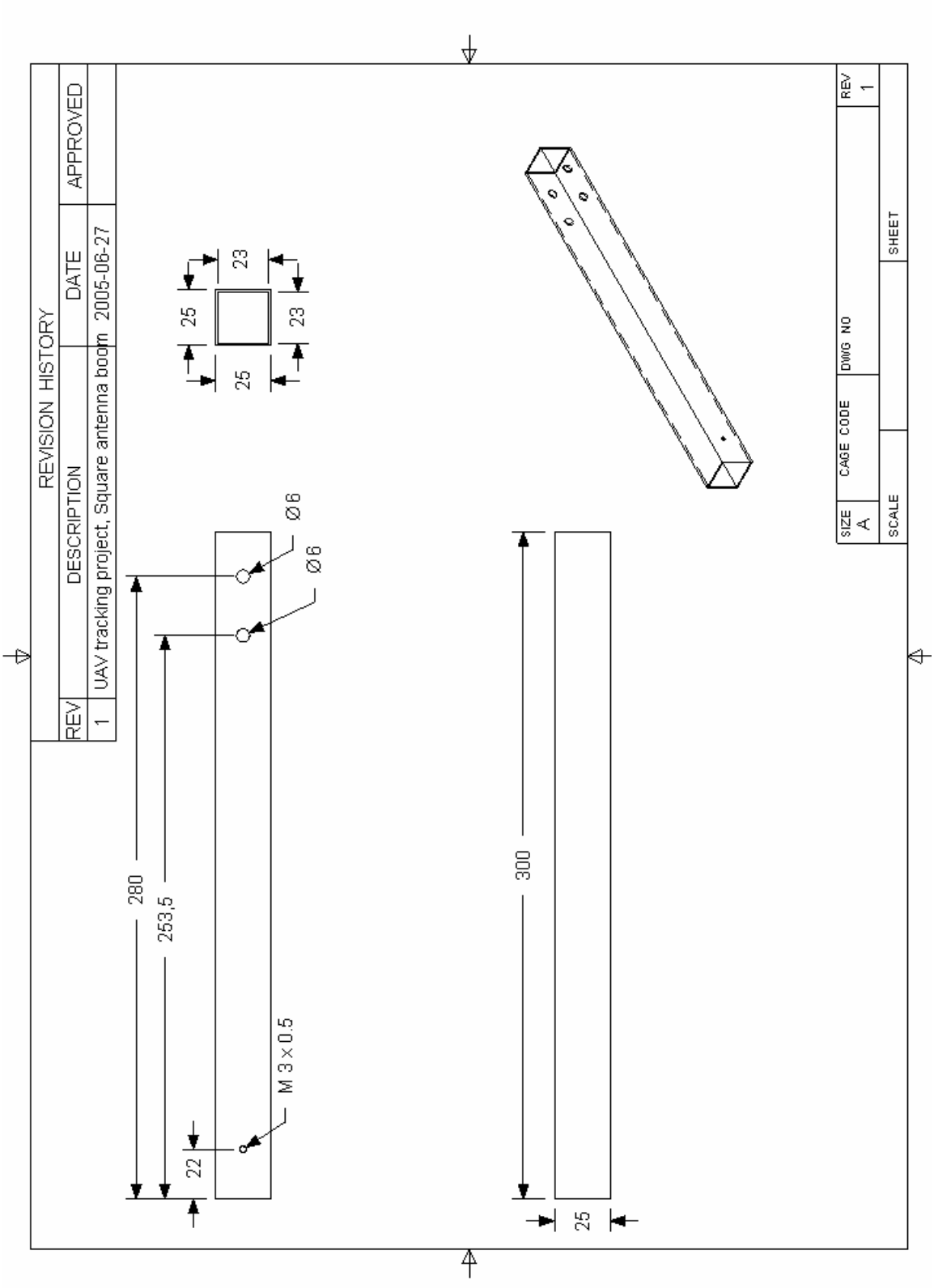

Drawing A1.27 : *Square antenna boom.*

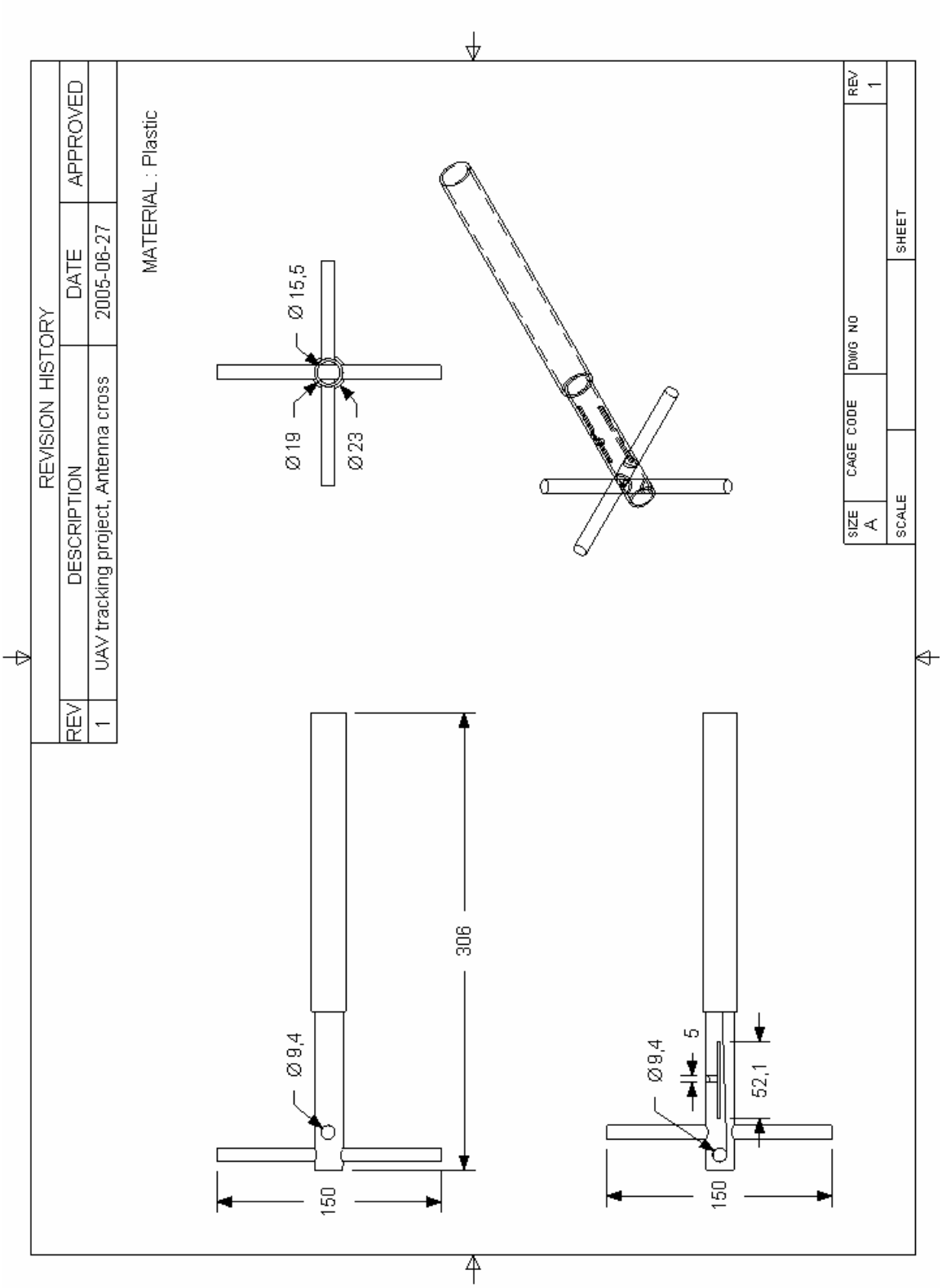

Drawing A1.28 : *Antenna cross (incl. outer part of antenna boom).*

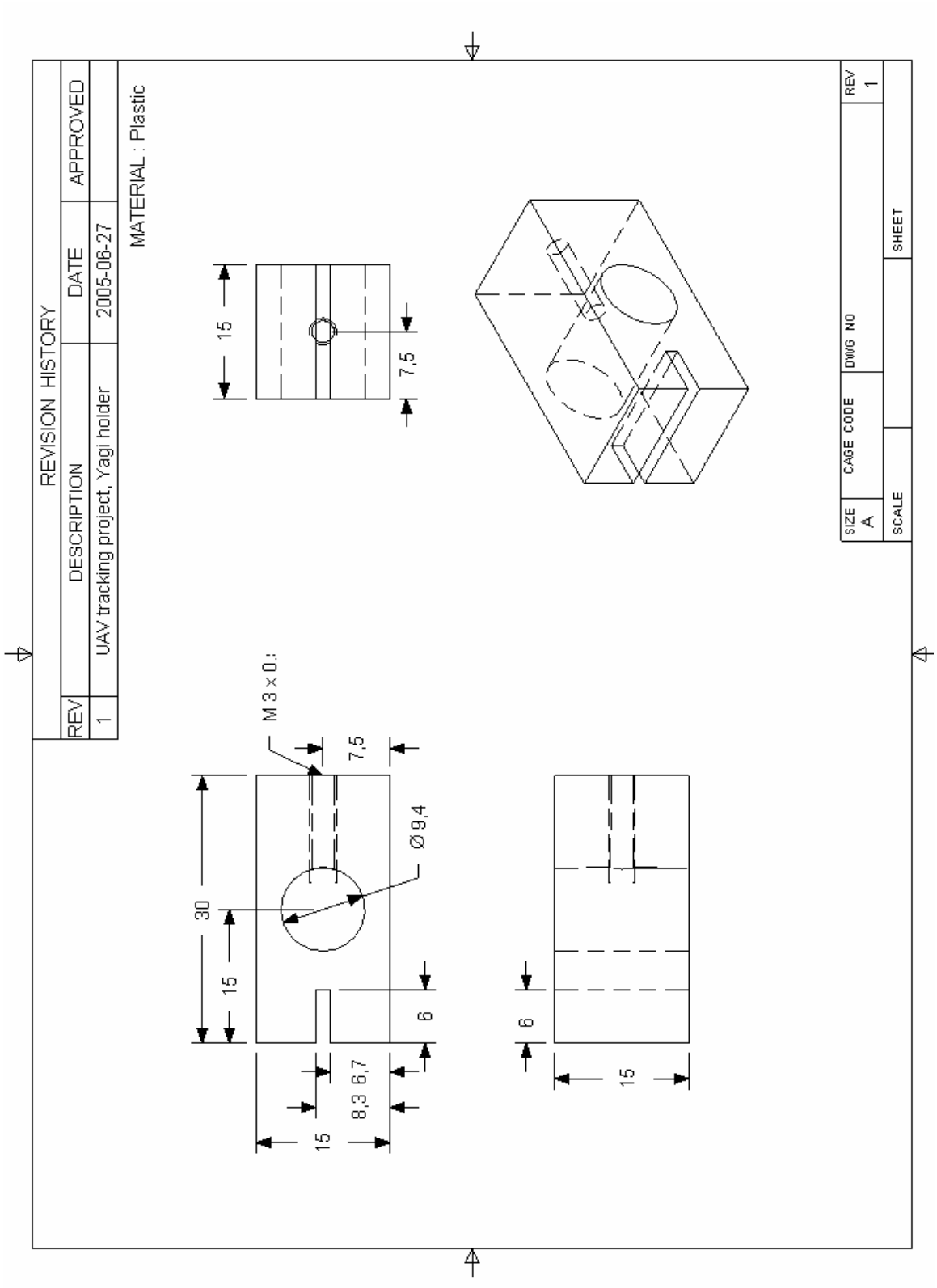

Drawing A1.29 : *Yagi holder.*

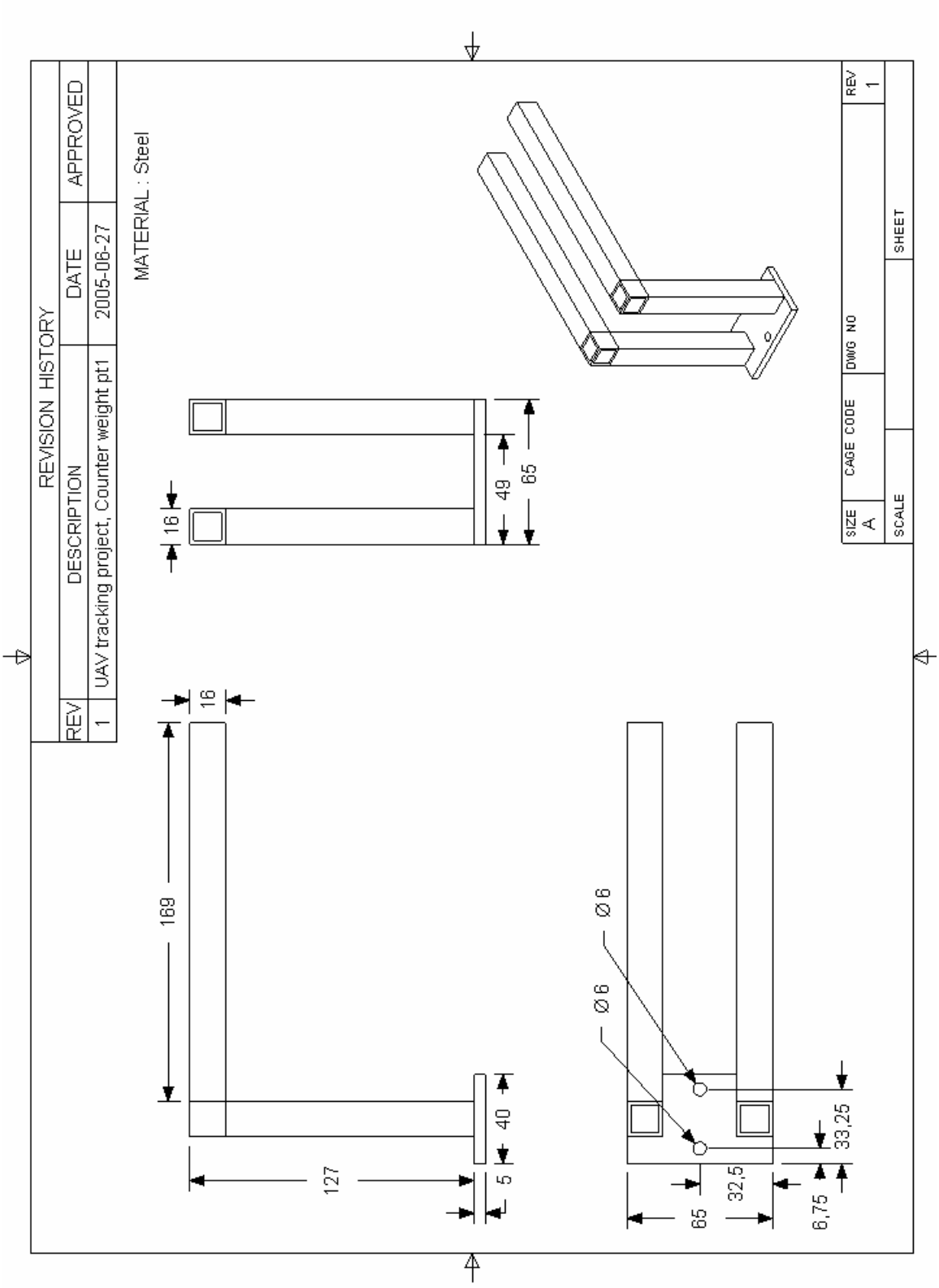

Drawing A1.30 : *Counter weight part 1.*

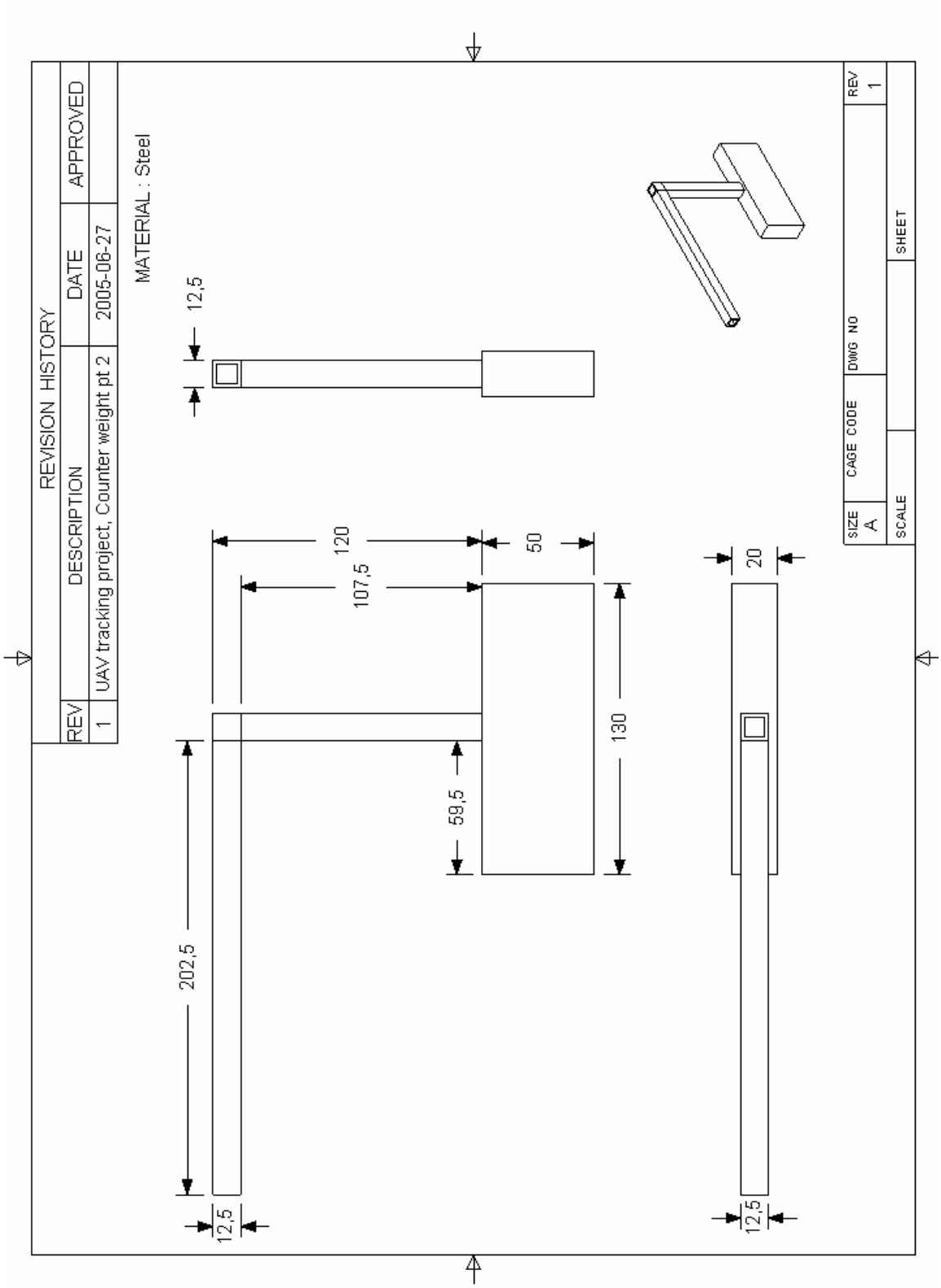

Drawing A1.31 : *Counter weight part 2 & 3.*

A.2 Electric overview

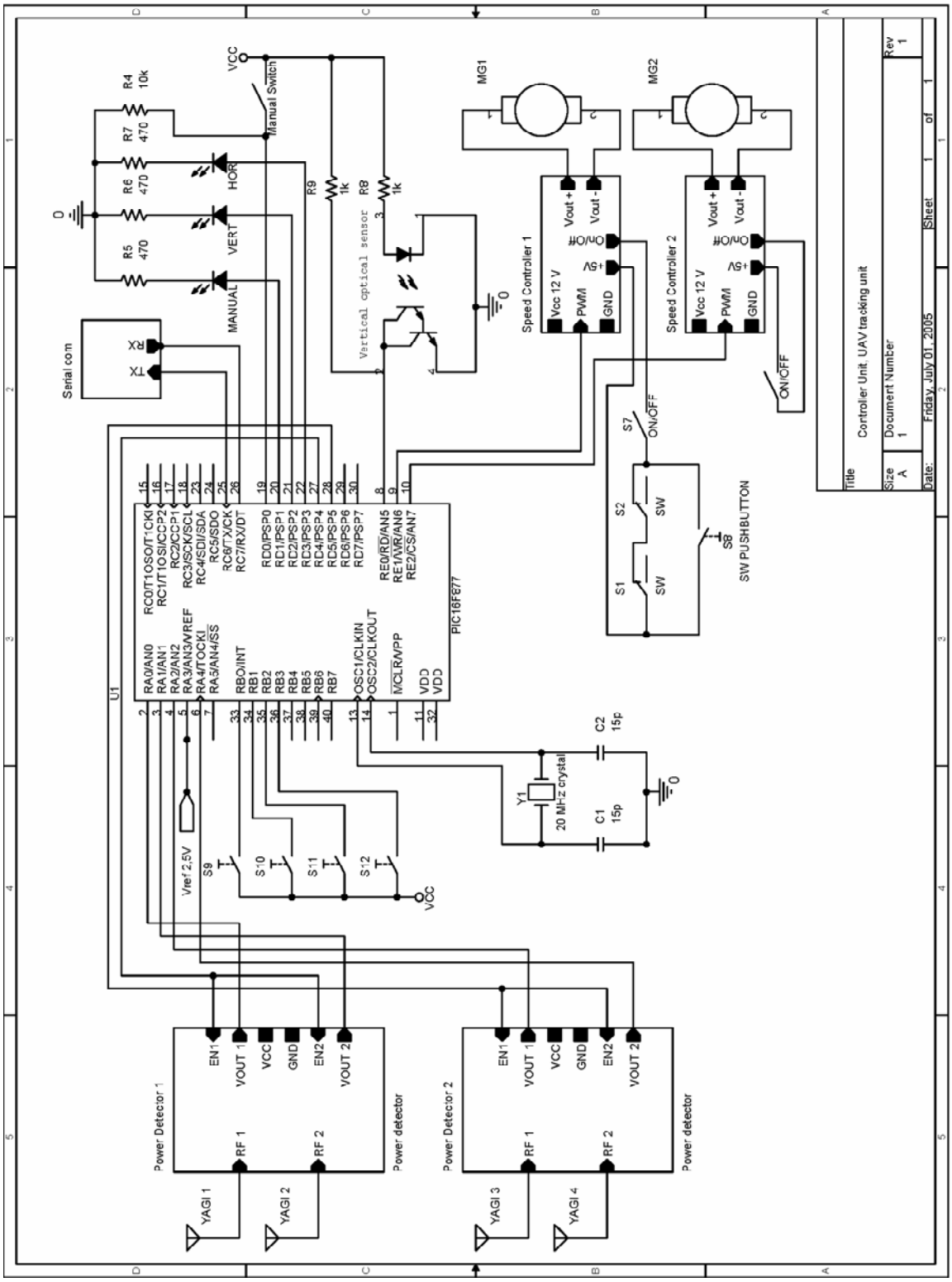

Schematic A2.1 : *Electric overview.*

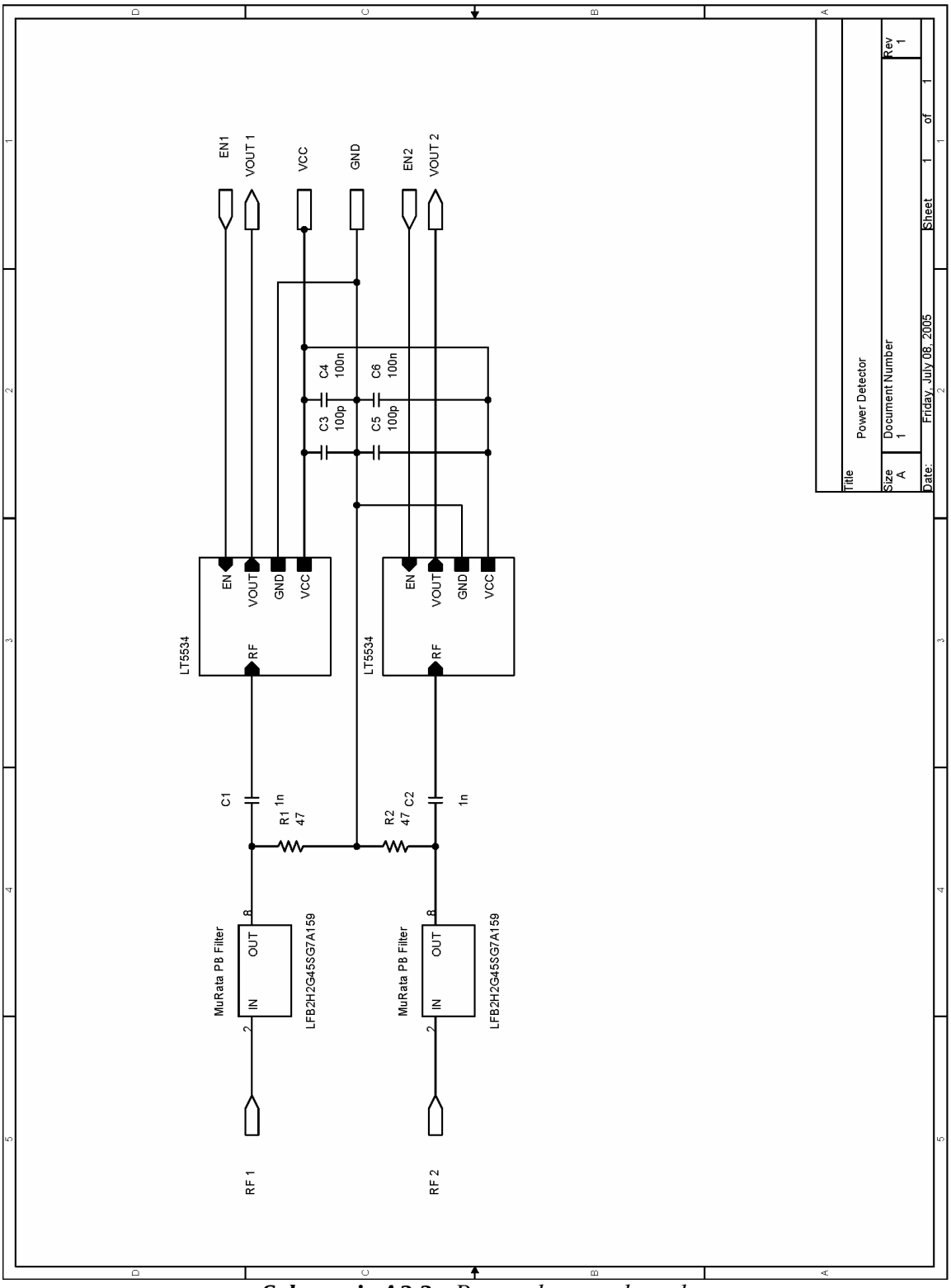

Schematic A2.2 : *Power detector board.*

A.3 Electric speed controller

Marine ESC-50

Electric motor speed control for model boat

The HM-50 esc allows remote control of boat electric motors from an RC System. When connected with motor, it is capable of supplying up to 50 Amps (forward) or 20A(backward) of continuous motor current. Its integrated Battery Eliminator Circuit (BEC) powers the Receiver from the motor battery, with automatic cutoff of the motor power to preserve Receiver power as the battery becomes depleted. It is small and powerful, waterproof, can be used for different type of boat.

Specifications:

Working Voltage	5-10 cells, 6-12V, NiCd or Nimh
Continuous Load Current	50A forward, 20A backward
Weight	82g
BEC	5V/1A
Low Battery Cutoff	5V
Dimension (mm)	42x47x13mm

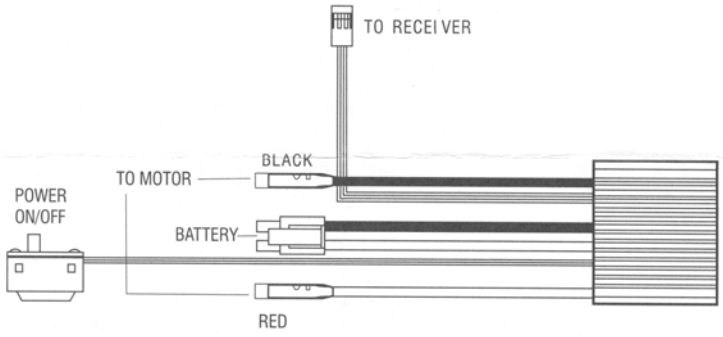

Figure A4.1: *Speed controller data sheet.*

A.4 Network Analyzer plots

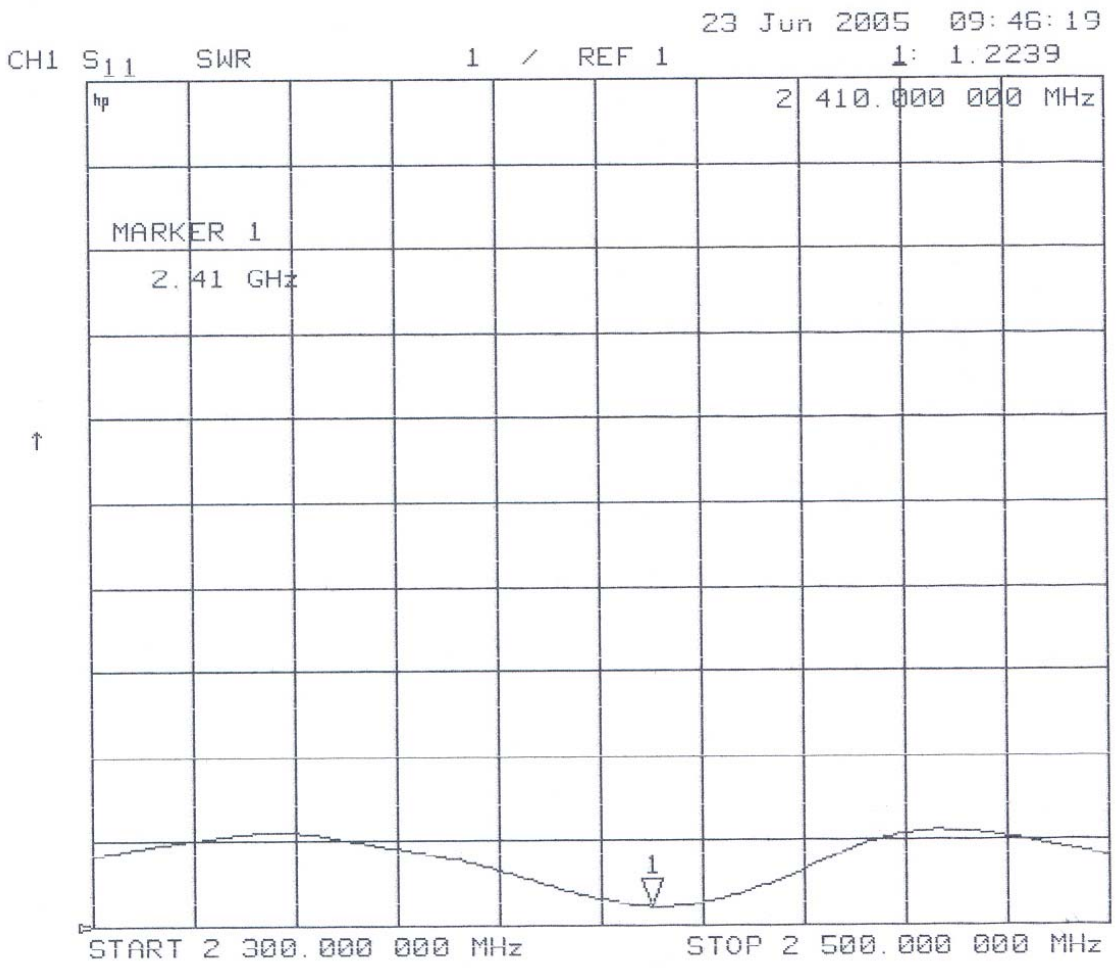

Plot A5.1 : *Antenna 1 Voltage Standing Wave Ratio.*

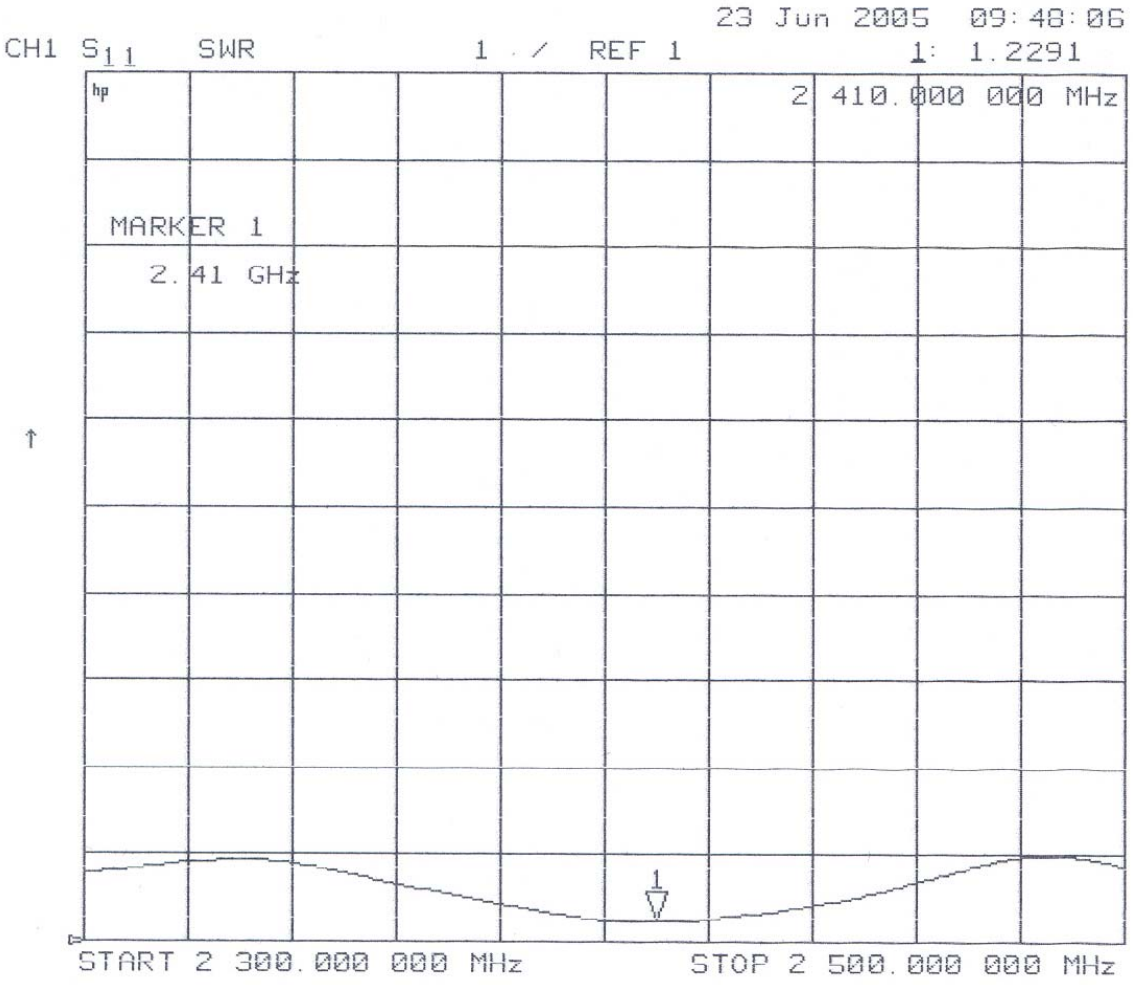

Plot A5.2 : *Antenna 2 Voltage Standing Wave Ratio.*

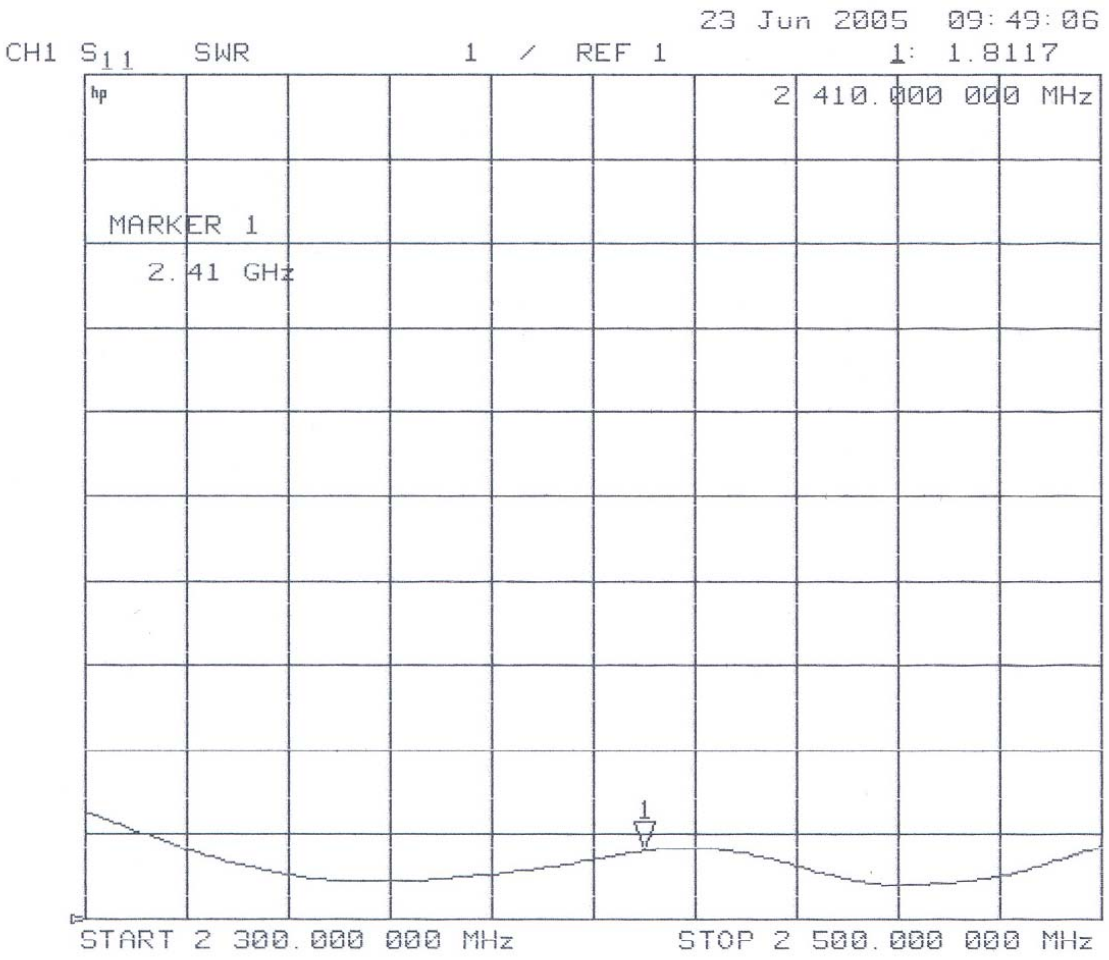

Plot A5.3 : *Antenna 3 Voltage Standing Wave Ratio.*

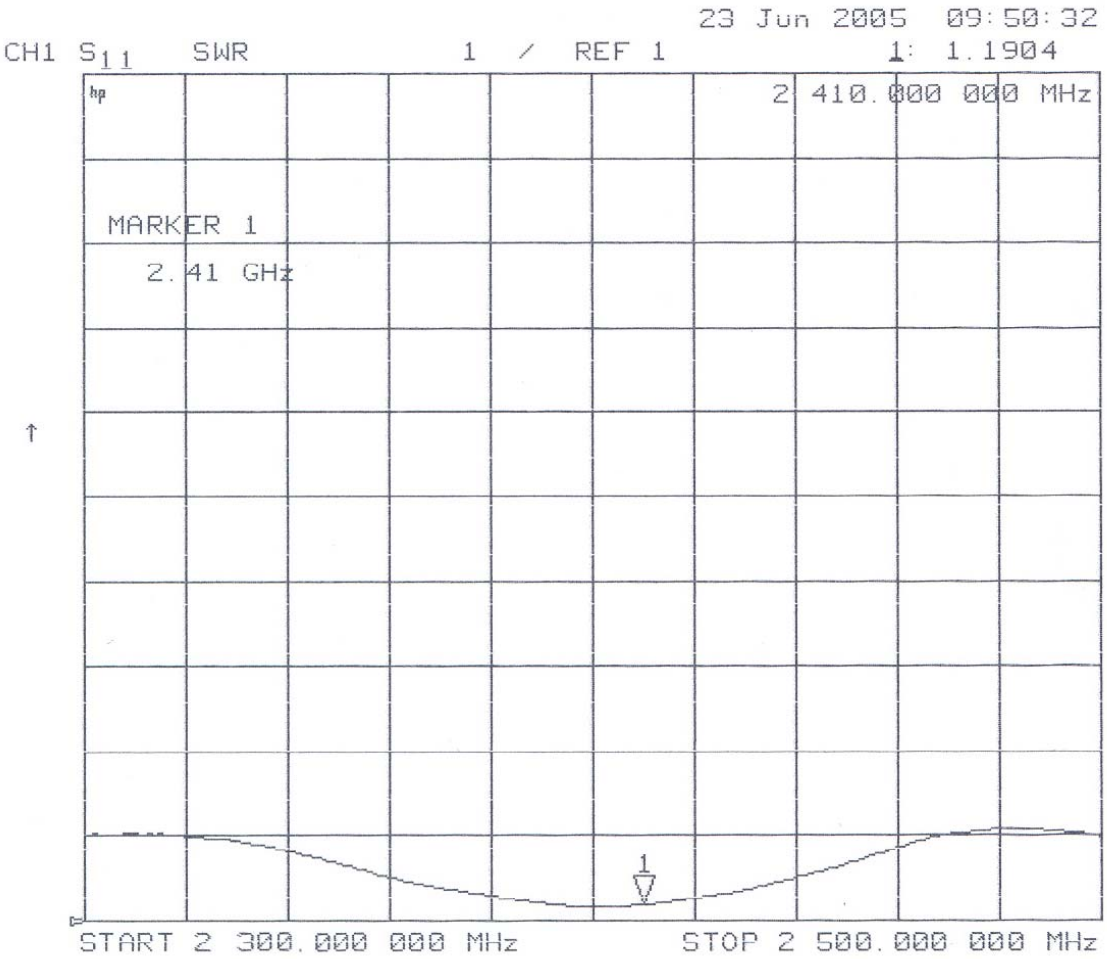

Plot A5.4 : *Antenna 4 Voltage Standing Wave Ratio.*

A.5 Filter specifications

Previous Part Number	LFB2H2G45SG7A159
Global Part Number	LFB2H2G45SG7A159
Nominal Center Frequency (fo)	2450.0MHz
Bandwidth (BW)	fo±50.0MHz
Insertion Loss in BW I)	2.1dB max. (at 25°C)
Insertion Loss in BW II)	2.4dB max. (-40~+85°C)
Attenuation (Absolute Value) I)	45.0dB min. at 880~915MHz
Attenuation (Absolute Value) II)	48.0dB min. at 1710~1990MHz
Attenuation (Absolute Value) III)	20.0dB min. at 2110~2170MHz
Attenuation (Absolute Value) IV)	30.0dB min. at 4800~5000MHz
Ripple in BW	1.2dB max.
VSWR in BW	2.0 max.
Characteristic Impedance (Nom.)	50ohm
Power Capacity	500mW
Min. of Operating Temperature Range	-40°C
Max. of Operating Temperature Range	+85°C

Table A.5.1 :*Murata filter specification.*

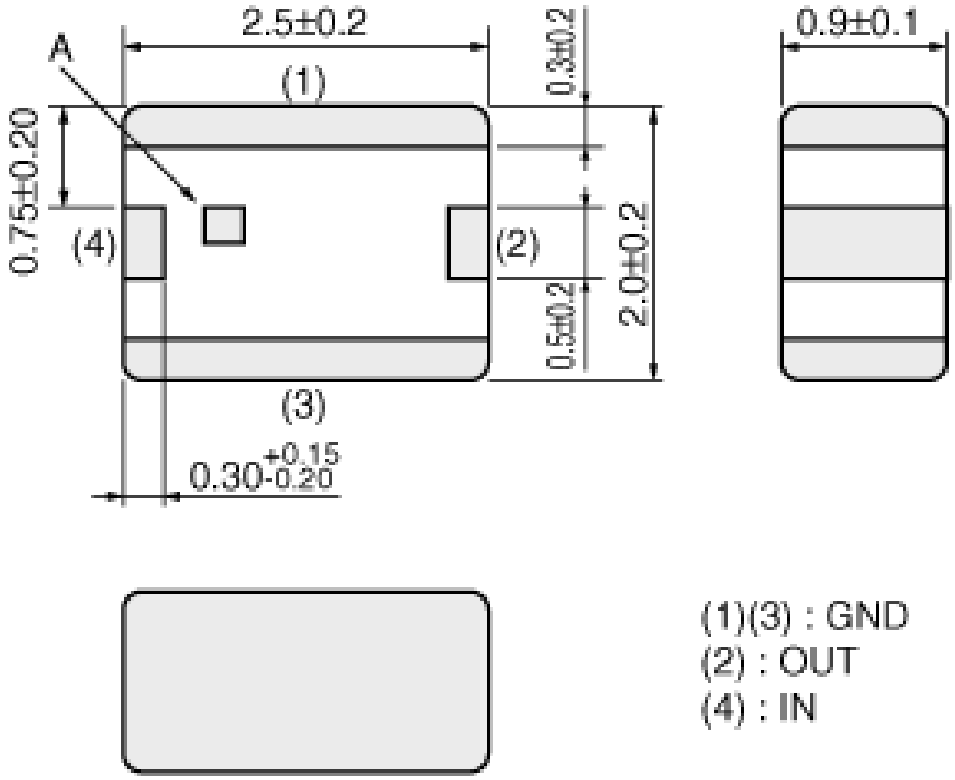

Figure A5.1 : *Murata filter dimensions.*

A.6 Abbreviations

A/D - Analog to Digital
BALUN - BALanced to UNbalanced
BW - Band Width
DC - Direct Current
ECSE - Department of Electrical and Computer System Engineering (Monash University)
ESC - Electronic Speed Controller
GCPW - Grounded Coplanar WaveGuide
GPS - Global Positioning System
LOS - Line Of Sight
LSB - Least Significant Bit
NEC - Numerical Electromagnetic Code
NSW - New South Wales (State in Australia)
I/O - Input / Output
PCB - Printed Circuit Board
RC - Radio Control
RF - Radio Frequency
PWM - Pulse Width Modulation
VHF - Very High Frequency
UAV - Unmanned Aerial Vehicle
USART - Universal Synchrounous/Asynchrounous Receiver/Transmitter
WLAN - Wireless Local Area Network